Supraharmonics in Low Voltage Networks

Daniel Agudelo Martínez

Universidad Nacional de Colombia
Facultad de Ingeniería
Departamento de Ingeniería Eléctrica y Electrónica
Bogotá, Colombia
2020

Supraharmonics in Low Voltage Networks

Daniel Agudelo Martínez

A thesis presented in partial fulfillment to obtain the degree:
Master of Science - Electrical Engineering

Director: Ph.D. Fabio Andrés Pavas Martínez
Universidad Nacional de Colombia Sede Bogotá
Co-Director: Dr-Ing. Ana María Blanco Castañeda
Technische Universität Dresden, Germany

Research Field:
Electromagnetic Compatibility in Low Voltage Networks
Research Group:
Programa de Adquisición y Análisis de Señales
PAAS-UN

Universidad Nacional de Colombia
Facultad de Ingeniería
Departamento de Ingeniería Eléctrica y Electrónica
Bogotá, Colombia
2020

Motivations are stronger than wishes.

Acknowledgements

First I want to thank God, who allowed me to finish this work. Then to my parents, for their support.

This work was developed both in National University of Colombia, (Universiad Nacional de Colombia), Bogotá, Colombia, and in Technical University Dresden (Technische Universität Dresden), Dresden, Germany. Thanks to the help received from the research groups Program of Acquisition and Analysis of Electromagnetic Signals of the National University of Colombia PAAS-UN Group, and the Institute of Electrical Power Systems and High Voltage Engineering Group of Technical University Dresden.

I want to thank my supervisor, Dr. Andrés Pavas, for his long trust and support. I also want to thank Dr. Ana María Blanco and Dr. Jan Meyer, for their kind support and valuable guidance. Many thanks to all my colleagues both in Bogota and Dresden, who helped me with the development of this work.

And finally, many thanks to all people who directly or indirectly helped me achieve this important goal, not only with their technical knowledge, experience or vision about future, but also with their kindness and encouragement through the good and not-so-good times.

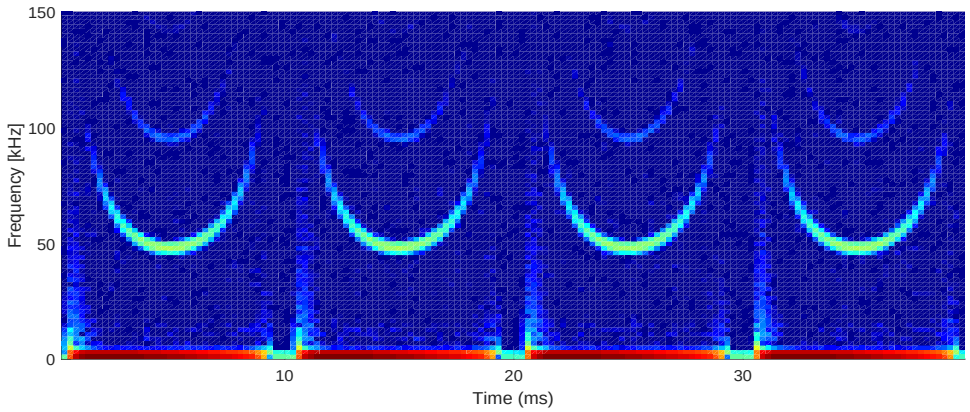

Resumen

Este documento presenta una metodología para la identificación de emisiones supraarmónicas (emisiones conducidas de tensión y corriente entre 2-150 kHz) en el lado del usuario final de la red de distribución, utilizando lámparas LED de baja potencia como Equipo Bajo Prueba (EBP).

El primer capítulo presenta una breve clasificación de las perturbaciones de la calidad de potencia y describe aquellas relacionadas con la distorsión de la forma de onda. El segundo capítulo describe la configuración experimental y de medición utilizada para evaluar las emisiones supraarmónicas de los EBP seleccionados. El tercer capítulo explica la metodología usada para la identificación de las emisiones supraarmónicas cuando los EBP funcionan de manera individual, y el cuarto capítulo muestra la interacción de dichas emisiones en la operación simultánea de los EBP. Junto con un conjunto de combinaciones experimentales, las emisiones supraarmónicas y sus aspectos metrológicos más relevantes se analizan a través del texto.

Los resultados muestran cómo las emisiones supraarmónicas de tensión y corriente se ven (o no) afectadas por diferentes variaciones en la fuente de tensión, la impedancia de red equivalente, el sistema de medición y la topología del circuito del EBP seleccionado.

El objetivo de esta investigación es contribuir a la comprensión y el estudio sistemático de las emisiones supraarmónicas, con especial énfasis en los aspectos metrológicos y los métodos estadísticos para su identificación.

Abstract

This document presents a methodology for the identification of supraharmonic emissions (current and voltage conducted emissions between 2-150 kHz) at the end-user side of the distribution grid, using low power LED lamps as Equipment Under Test (EUT).

First chapter presents a brief classification of power quality disturbances and describes those related to waveform distortion. Second chapter describes the measurement and experimental setups used to assess the supraharmonic emissions from selected EUT. Third chapter explains the methodology for the identification of supraharmonic emissions when EUT perform in single operation, and fourth chapter shows the interaction of such emissions for EUT in simultaneous operation. Along with a set of experimental combinations, supraharmonic emissions and their more relevant metrology aspects are discussed through the text.

Results show how voltage and current supraharmonic emissions are (or not) affected by different variations in voltage source, equivalent network impedance, measurement setup and circuit topology of selected EUT.

This research is aimed to contribute to the understanding and systematic assessment of supraharmonic emissions, with a special emphasis on metrological aspects and statistical methods for their identification.

Glossary

- Emission: Phenomenon by which electromagnetic energy emanates from a source[1]
- Disturbance: Any deviation from the ideal voltage or current [2]
- Interference: Potential consequence of disturbances (power quality issues)[1]
- Harmonics: Conducted emissions at integer multiples of main frequency [1]
- Interharmonics: Conducted emissions at non-integer multiples of main frequency [1]
- Supraharmonics: Harmonics and interharmonics between 2-150 kHz
- EUT: Equipment under test
- FFT: Fast Fourier Transform
- LED: Light emitter diode
- CFL: Compact fluorescent lamp
- PCC: Point of common connection
- Input impedance: Impedance of the input circuit measured between the input terminals under operating conditions [1]
- Threshold: Signal amplitude values above which emissions can be measured with a certain level of confidence

REFERENCES

[1] IEC, " International Electrotechnical Vocabulary (IEV) - Part 161: Electromagnetic compatibility," standard, International Electrotechnical Commission, Geneva, CH, 2017.

[2] M. H. J. Bollen and I. Y. H. Gu, *Signal Processing of Power Quality Disturbances*. Wiley-IEEE Press, 2006.

List of Figures

List of Tables

Table of Contents

1. Introduction

This document presents the methodologies used for the identification of supraharmonic emissions from low power LED lamps and the corresponding results. These current and voltage waveforms distortions between 2-150 kHz are mainly produced by the operation of non-linear loads, i.e. power electronics-based equipment commonly used in the customer side of distribution network.

Emissions between 2–150 kHz and beyond usually appear because of the normal operation of devices such as lighting devices (LED lamps, Compact Fluorescent Lamps), Photo-Voltaic (PV) inverters, Power Line Communication systems (PLC), battery chargers and many other devices based on power electronics circuits. Although some of these appliances comply with strict regulations, supraharmonic emissions are likely to appear when low power, massively-used devices are connected in low voltage installations.

Distortion in voltage and current waveforms between 2-150 kHz is currently a research topic regarding Electromagnetic Compatibility in Low Voltage Networks, among other reasons, because of the incertitude about how realistic the measurements in laboratory setup can reflect the true situation in the grid, as well as how sensible the equipment responds to emissions between 2-150 kHz from the supply side.

Although high-frequency waveform distortions between 2-150 kHz have been already addressed in the literature, there is still a lack of standardization for the complete range between 2-150 kHz. This thesis aims to show that a consistent identification of such emissions can be performed even using a set of low power household appliances. The general objective of this research was the identification of supraharmonic emissions using a low voltage test network under some controlled conditions (main supply, grid topology, loads under measurement), by means of signal spectral analysis, using reproducible methods and adequate measurement systems complying with metrological constraints for these signals. In order to cope with this objective, three specific objectives were successfully developed:

- Establishing an adequate measurement method, an adequate measurement system and their related metrological parameters so as to successfully measure narrowband and broadband supraharmonic emissions in a single-phase, low voltage test network under controlled conditions of main supply, grid topology and loads under measurement.

- Identifying supraharmonic emissions from low power LED lamps in a low voltage test network under controlled conditions of main supply and network topology.
- Describing the interaction between supraharmonic sources in a low voltage test network by means of a previously proposed model.

There are additional research questions not covered in this research regarding supraharmonics, such as how to model and predict supraharmonics in low voltage grids, how equipment may be modified to cope with eventual, future supraharmonic emission limits, and to what extent these emissions would affect the current and future distribution grid operation, considering the latter as an active grid, with distributed generation from renewables, and permanently connected to everyday hardware (Internet of Things).

The identification of supraharmonic emissions required an adequate measurement method, an adequate measurement system and their related metrological parameters so as to successfully measure narrowband and broadband supraharmonic emissions in a single-phase, low voltage test network under controlled conditions of main supply, grid topology and loads under measurement. After this, supraharmonic emissions from a set of selected low power LED lamps were identified in a low voltage test network under controlled conditions of main supply and network topology. Finally, a description of the interaction between supraharmonic sources was presented in a low voltage test network by means of a previously proposed model.

Low power LED lamps were used for the identification of supraharmonic emissions in this research. A set of LED lamps were selected taking into account their previous evidence of supraharmonic emissions under normal operation. The description of supraharmonic emissions is limited only to the conducted emissions. Radiated emissions were not considered through this work. Measurements were mainly performed in the Institute of Electrical Power Systems and High Voltage Engineering, Technical University Dresden (Technische Universität Dresden), Germany, as well as in the laboratory of the Program of Acquisition and Analysis of Electromagnetic Signals (Programa de adquisición y análisis de señales - PAAS) of the National University of Colombia (Universidad Nacional de Colombia), Bogota, Colombia.

This document is organized as follows: Chapter 2 explains the supraharmonic disturbances as well as their relevance in current distribution networks. Chapter 3 describes in detail the measurement and experimental setups used for the assessment of supraharmonic emissions from low power LED lamps. Chapters 4 and 5 show the main results from the assessment of supraharmonic emissions under single and simultaneous operation respectively. Finally, the conclusions and future works about this research are presented.

2. Supraharmonics: Waveform distortion between 2-150 kHz

This chapter presents a background for the understanding of waveform distortions between 2-150 kHz, also known as "supraharmonics". An overview in terms of a general classification, some sources of distortion and their impact in the distribution grid are presented for both conducted emissions below 2 kHz (harmonics, interharmonics) and between 2-150 kHz (supraharmonics). Finally, the current standards related to these emissions are mentioned.

Power quality concerns the interaction between the grid and its customers by means of voltages and currents. The International Electrotechnical Comission (IEC) defines Power Quality in 61000-4-30 [1] as the "characteristics of the electricity at a given point on an electrical system, evaluated against a set of reference technical parameters". Any deviation of voltage or current from the "ideal" waveform is a power quality disturbance, meaning "ideal" a sinusoidal, single frequency waveform with constant amplitude and frequency, without any frequency (or angle) difference between voltage and current. In therms of voltages and currents, power quality is the combination of voltage quality and current quality. As stated in [2], voltage quality is how the network affects the customer or the load, whilst current quality is how the customer or load affects the network.

According to IEC 61000-1-1 [3], Electromagnetic Compatibility (EMC) is "the ability of an equipment or system to function satisfactorily in its electromagnetic environment without introducing intolerable electromagnetic disturbances to anything in that environment". Readers can notice a link between voltage quality and current quality with the definition of Electromagnetic Compatibility, and hence in the international standards power quality is treated as a subtopic of electromagnetic compatibility study field [2][4].

From the definitions of EMC in IEC standards, a "disturbance is a phenomenon which may degrade the performance of a device, equipment or system, or adversely affect living or inert matter". In power quality terms, a disturbance is any deviation from the ideal voltage or current. An interference is defined in EMC standards as the actual degradation of a device, equipment or system caused by a disturbance. In terms of power quality definitions, interferences and power quality issues are synonyms [2][4].

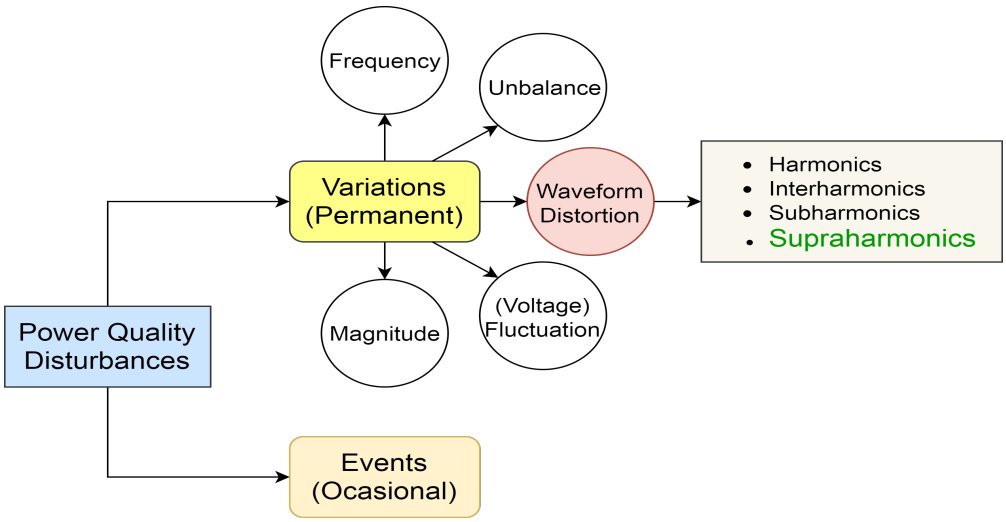

Figure 2-1.: Classification of Power Quality Disturbances

Power quality disturbances can be classified into two main groups according to the way a characteristic of voltage or current signal is measured: [2][3]

- Variations: They are steady-state or quasi-steady state disturbances that can be measured at different moments.
- Events: They are sudden disturbances than can only be measured in a specific moment.

However, it is important to remark that a power quality disturbance is only considered an issue when it causes perceptible degradation either for the customer or the grid operator [2]. Figure **2-1** shows the classification of Power Quality Disturbances and the *supraharmonic* disturbances, which are related to Waveform Distortion.

Power quality monitoring is a term used to describe the whole process, from the measurement of voltages and currents up to the statistical indices computation which describes the initial signals behaviour [2][4]. In this context, signal processing deals with the extraction of features and information from measured signals[2][4]. Power quality keeps therefore its relevance since commonly used equipment (an those expected to be used in the near future) present an increased susceptibility and disturbances emission [4][5][6].

2.1. Emissions below 2 kHz

In most studies, only the harmonic distortion is considered because its dominant behaviour compared to other waveform distortions. This is the main reason why most of the literature refer to harmonics and interharmonics as the main waveform distortion disturbances. However, advances in equipment based on power electronics (i.e. switched-mode power supplies,

lighting devices, photovoltaic inverters, electric vehicle chargers, etc) and communication protocols (e.g. Power Line Communication) have transformed the conducted emissions perceived at electrical grid both below and above 2 kHz.[5][6].

2.1.1. Classification of Distortions below 2 kHz

Using the Fourier Transform, the waveform distortion of a signal can be separated into the following components [4][5][6][7][8]:

- DC component: Zero frequency distortion (signal mean value different from zero)
- Harmonics: Spectral components with frequencies that are integer multiples of the fundamental frequency (60 Hz is the fundamental frequency in Colombian Power System).
- Interharmonics: Spectral components with frequencies that are non-integer multiples of the fundamental frequency.
- Subharmonics: All interharmonics with frequencies below the fundamental frequency.

2.1.2. Sources of Distortions below 2 kHz

Waveform distortion below 2 kHz are due to non-linear loads in the power system, either existing in the grid or in the loads[2][4]. A nonlinear element develops a nonsinusoidal current from a sinusoidal voltage. Even for a non-distorted voltage waveform, the current through a non-linear element can be distorted. In return, the harmonic current components from non-linear loads cause harmonic voltage distortion and thus a non-sinusoidal voltage in the system. Most of the non-linear devices commonly used in the low voltage grid are composed by power-electronics-based circuits.[2][4][9]. Some of them are:

- Energy-saving lamps
- Computers
- Battery chargers
- Appliances (TVs, washing machines, coffee machines, etc)

Some sources of distortion are listed below [2][9]:

- DC Sources: the input voltage leads to a mostly DC voltage output when using a non-controlled, single phase rectifier (non-controlled AC-DC converter). However, because of the operation of such converters, the current has in general a pulsate behaviour at AC side. This pulsate behaviour in time is perceived as the spread of harmonic emissions in frequency domain.

- Notching: This is due to the temporary shorting of two phases of a rectifier during the commutation of current from one phase to another.
- Transformers: When the system voltage exceeds the rated voltage of the transformer, the magnetizing current may become significant (more than 1 % p.u.).
- Synchronous machines: Because of construction constraints, currents from synchronous machines are not fully sinusoidal.

Considering interharmonic waveform distortions, main causes of these emissions are grouped in two main sources: the variations in amplitude and/or phase of the fundamental component and/or the harmonic components (i.e. inverter drives), and (same as harmonics) power electronics circuits with switching frequencies not synchronized to the power supply frequency (ac/dc supplies, power factor correctors, etc)[9][2].

2.1.3. Impact of Harmonics and Interharmonics

The main impact of waveform distortions below 2kHz can be divided between voltage and current distortion consequences (interferences). Voltage distortion leads to harmonic currents through linear loads[2]. Extra heating in loads, lifespan reduction due to isolation ageing and additional torque on motors and generators are some of the consequences of voltage waveform distortion. Some consequences of current disturbances below 2 kHz are the overheating in cables and transformers, noise audio in amplifiers, summ currents through the neutral conductor and disturbed zero-crossing detectors[4][2].

2.2. Emissions between 2-150 kHz

Current and voltage distortion in the range between 2 kHz and 150 kHz has recently become a well-defined Power Quality research topic. This is mainly because of both non-negligible amplitudes within this frequency range and the lack of standards for these emissions [4][10][11][12][8]. Waveform Distortion of current and voltage signals between 2 kHz and 150 kHz have been recently named as Supraharmonics [13][14]. Supraharmonics are also known as high frequency waveform distortions [15][16].

The term “low frequency emission” is used in IEEE standards to refer to frequencies below 150 kHz, whilst in IEC standards the term “low frequency” refers to frequencies below 9 kHz[17]. The recent standard development was mainly triggered by several reasons. First, the use of Power Line Communication technology at this frequency range, as part of smart metering infrastructure. Second, the increasing amount of equipment with active switching (i.e. converters, electronic ballasts, active power factor corrector, variable-speed drives, etc).

2.2.1. Classification

Supraharmonic emissions are related not only to the switching frequency of electronic devices circuits, but also to several capacitive elements that these non-linear devices introduce in typical, passive low voltage grids [5][6][18]. Moreover, in the last years these signal distortions ("emissions" from an Electromagnetic Compatibility Analysis point of view [7]) have increased in amplitude and bandwidth [5][6][13][18]. Electronic devices (non-linear loads) are considered the most common sources of conducted distortion in current and voltage above 2 kHz [5][6][13][18][19][20][21]. This set of electronic devices is mainly composed by LED lamps, monitors and TVs, battery chargers (electric vehicle chargers, low power chargers), power inverters and converters (Inverters for PV systems, wind turbine systems, etc), switched-mode power supplies and other energy-efficient devices currently and widely used [18][14][19].

2.2.1.1. Intentional and Unintentional Emissions

Along supraharmonic emissions from non-linear loads (unintentional emissions), PLC signals (Power Line Communication) have increased supraharmonic emissions in low voltage networks (intentional emissions)[6]. Researchers have even reported electric resonances when domestic appliances and power converters/inverters are connected together [5][6]. On the one hand, although current and voltage from some power inverters/converters show negligible emissions up to 2 kHz, emissions above 2 kHz have increased with the massive use of power electronics circuits of this kind (e.g. active power converters)[5][6]. On the other hand, voltage at a Point of Common Connection (PCC) might be distorted because of unintentional emissions (i.e. from non-linear loads) and intentional emissions (Communication Systems using Power Grids). Some of the Power Line Communication -PLC- protocols in current Low Voltage Networks use voltage signals typically lying between 9-95 kHz, therefore can be also considered as supraharmonic emissions [5][6].

2.2.1.2. Narrowband and Broadband Emissions

Researchers have defined three kinds of supraharmonic distortions according to their features: narrowband, broadband and zero-crossing distortions [5]. Narrowband and Broadband distortions are classified according to emissions bandwidth in frequency domain, whereas zero-crossing distortions are classified according to the behavior of current signals near zero cross in time domain [10]. Regarding frequency domain, previous works have stated emissions below 2 kHz can even develop harmonic and interharmonic emissions in supraharmonic range [10]. Figure **2-2** shows current signal spectra of a CFL device, rated power below 15 W [14][20][21].

Most of the emissions below 2 kHz are mostly perceived as narrowband, odd harmonic

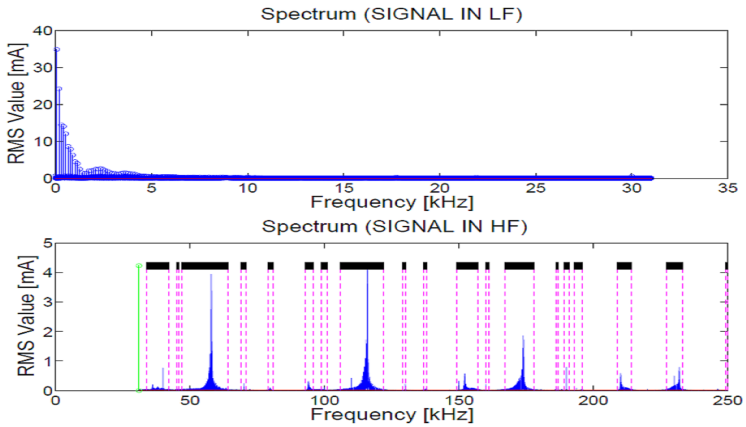

Figure 2-2.: Emissions between 1 Hz-250 kHz from a low power CFL[20]

emissions. However, above 2 kHz emissions usually become more broadband, that to say emissions can be grouped in frequency bands [22][14][20][21].

2.2.1.3. Primary and Secondary Emissions

A commonly used model for harmonic emission simulation and analysis, from single devices or from installations, is an ideal current source at the harmonic frequency of interest. For such model, voltage at device's terminals is assumed not to affect the harmonic current. Although this model has its limitations, the use of such model is preferred because of the lack of knowledge about devices details when performing a harmonic analysis[22].

For the context of waveform distortion between 2-150 kHz, measured emissions can be classified as follows [22]:

- Primary Emission: Emission originating from the assessed device.
- Secondary Emission: Emission originating outside the device.

Primary harmonic emission is the part of the harmonic current at the device terminals that is driven by sources inside the device[22]. The model in Figure **2-3** represents an EUT connected to the grid at a Point of Common Connection (PCC). Using a linearized model and applying the superposition technique, primary emission can be expressed as [22]:

$$I_{primary} = \frac{U_{primary}}{Z_{EUT} + Z_{Grid}} = \frac{Z_{EUT}}{Z_{EUT} + Z_{Grid}} I_{EUT} \tag{2-1}$$

It can be seen that primary emission strongly depends on both EUT and $Grid$ impedances. Hence, primary emission is affected by both grid impedance and voltage at its terminals[22]. An approximate value of primary emission can be obtained using a voltage source with output impedance close to 0 Ω and all other voltages at any other frequencies valued at zero[22].

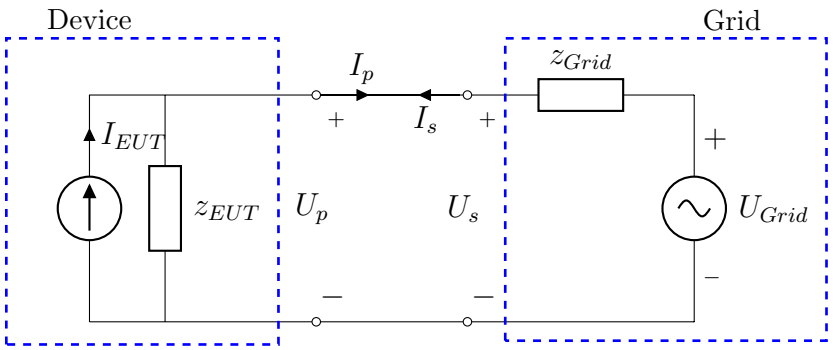

I_{EUT}:	Internal current EUT
Z_{EUT}:	Output impedance EUT
$I_{primary}$:	Primary current emission
$U_{primary}$:	Primary voltage emission
$I_{secondary}$:	Secondary current emission
$U_{secondary}$:	Secondary voltage emission
Z_{Grid}:	Equivalent grid impedance
U_{Grid}:	Background voltage

Figure 2-3.: Linearized model for Primary and Secondary Emissions [23][17][22]

Secondary harmonic emission is the part of the harmonic current at the device terminals that is driven by sources outside the device. Analogous to primary emission, a model for secondary emission can be obtained using a linearized model of circuit depicted in Figure **2-3** and the superposition technique as follows [22]:

$$I_{secondary} = \frac{U_{secondary}}{Z_{Grid} + Z_{EUT}} = \frac{1}{Z_{Grid} + Z_{EUT}} U_{Grid} \tag{2-2}$$

In this sense, a distorted voltage at device terminals could led to distortions in current at same voltage frequencies, at different frequencies and/or modify original device's current emissions[22].

2.2.2. Sources of emission between 2-150 kHz

The two main sources of supraharmonics can be established according to evidence[17]: residues from power-electronic converters and transmitters of Power-Line Communication. Some of the advantages of using active converters is the ability to reduce the emission at lower frequencies and therefore comply with emission limits. Within 2-9 kHz the emission with electromagnetic ballasts is around 2.5 times the emission with electronic ballasts. However, electronic ballasts show higher emissions above 9kHz[17].
according to evidence, devices listed below are examples of supraharmonic emitters[17]:

- Inverters (PV inverters, variable speed drives, etc)
- Switched Mode Power Supplies (LED lamps, computers, etc)

- Converters (Electric vehicle chargers)
- Power Line Communication devices

In the undergraduate thesis "Identificación de emisión de supraarmónicos asociada con algunos dispositivos de baja tensión (Supraharmonics emission identification related to some low voltage devices)" [21] supraharmonic emissions were identified in some devices such as LED, CFL, and some computer monitors. The basic statistical techniques used allowed authors to visualize and compare emissions from electronic loads. However, only emissions from appliances in single operation were considered in this undergraduate thesis [21]. From that research it was stated, among others, that current and voltage supraharmonics do not have a linear relationship when observed in frequency domain (current emissions do not strictly match with voltage emissions). Additionally, results showed supraharmonics emission in some low voltage devices is not dependent on devices rated power [21].

2.2.3. Impact of Emissions between 2-150 kHz

Different researchers worldwide have reported results about the origin, measurement and interaction of supraharmonics emission. Indeed, researchers have identified some of the potential consequences of supraharmonics emission: increase of current and voltage distortion, low power factors, interferences with Power Line Communication signals(PLC), lifespan reduction in electrical devices, and resonances in low voltage grids, among others [13][18][5][6][24][21]. However, the eventual differences between emissions in real and artificial (controlled) networks, as well as the detailed behavior of these emissions in real networks, are still under study. Moreover, there is a lack of knowledge about the main impact of these emissions in current and future distribution networks. Although some international standards address emissions below, within and beyond 2-150 kHz, a generally accepted consensus about emission limits, immunity limits and compatibility levels in the supraharmonic range is still under development. There is still no evidence of any Colombian standard addressing emission limits, immunity levels or compatibility levels in the supraharmonic range.

2.3. Standards for Supraharmonics

Finally, research about supraharmonic emissions is important for the development of standards about emission, immunity and compatibility levels in Low Voltage Networks. Because of that, assessing the origin, amplitude, interaction, measurement and eventual mitigation of supraharmonics emission is a topic of interest for different fields of the Electrical Engineering.

Except for induction hubs (EN 55011) and lamps (EN 55015) above 9 kHz, no emission limits exist for the frequency range between 2 and 150 kHz. Emission limits for other equipment

are only defined for harmonics up to 2 kHz (EN 61000-3-2) and above 150 kHz (EN 55014-1)[25]. An overview of limits in existing standards is also given in IEC 610000-4-19 Annex A.

Maximum emission related to power line communication is given in the form of voltage limits in EN 50065-1 and IEC 61000-3-8. Note that emission limits are expressed as voltages, there is no reference impedance associated with this limit. EN 50065 does not cover frequencies above 150 kHz. The limit according to EN 50065 and IEC 61000-3-8 is at 134 $db\mu V$ between 3-9 kHz [22].

Emission limits for broadband signals by lighting equipment are given in CISPR 15. These limits are given as voltages against a reference impedance. Among other suggestions, in [22] authors state that setting limits on the total installation (as IEEE 519) would be different than setting limits on individual devices (as in IEC 61000-3-2).

Regarding equipment testing against emission limits, the test should be both reproducible and lead to results similar to those in a real installation. The use of a reference, realistic impedance could help with both aims [22].

2.4. Conclusions

The current and voltage high frequency waveform distortions between 2-150 kHz, also known as supraharmonics, will play a relevant role in the electromagnetic compatibility of the so called "smart grids". In this regard, power quality regulations will also contribute to the satisfactorily integration to the power grid of energy efficient devices, distributed generation, communication protocols, electric mobility, among other technologies exposed to conducted emissions between 2-150 kHz.

Although Distributed Generation, Renewable Energy Sources and Smart Metering scenarios are still under development in Colombia, supraharmonic emissions might eventually impact Colombian Low Voltage Networks in different ways. In spite of non-extensive reported evidence of Power Grid inadequate performance because of suprahamonics emission, Power Quality researchers remain interested in achieving a better understanding of these phenomena and also in developing standards for suitable compatibility levels for Low Voltage Networks. Features and consequences of supraharmonics emission are not discarded to be a potential hazard for electromagnetic compatibility in low voltage grids. The understanding of this phenomenon will be the main argument to evaluate its future relevance.

REFERENCES

[1] IEC. Electromagnetic compatibility (EMC) – Part 4-30: Testing and measurement techniques –Power quality measurement methods. Standard, International Electrotechnical Commission, Geneva, CH, 2003.

[2] M.H.J. Bollen. What is power quality? *Electric Power Systems Research*, 66(1):5 – 14, 2003. ISSN 0378-7796. doi: https://doi.org/10.1016/S0378-7796(03)00067-1. Power Quality.

[3] IEC. Electromagnetic compatibility (EMC) Part 1: General Section 1: Application and interpretation of fundamental definitions and terms. Standard, International Electrotechnical Commission, Geneva, CH, 2017.

[4] Math H. J. Bollen and Irene Y. H. Gu. *Signal Processing of Power Quality Disturbances*. Wiley-IEEE Press, 2006. ISBN 9780471731689.

[5] Anders Larsson. *On High-Frequency Distortion in Low-Voltage Power Systems*. Luleå University of Technology, 2011.

[6] Sarah Rönnberg. *Emission and interaction from domestic installations in the low voltage electricity network, up to 150 kHz*. Luleå University of Technology, Lulea, 2013. ISBN 978-91-7439-800-7.

[7] Clayton Paul. *Introduction to electromagnetic compatibility*. Wiley-Interscience, Hoboken, N.J, 2006. ISBN 978-0-471-75500-5.

[8] NTC. *NTC 5001: Calidad de la Potencia Eléctrica. Límites y metodología de evaluación en Punto de Conexión Común*. Norma Técnica Colombiana, 2008. ISBN -.

[9] IEC. Electromagnetic compatibility (EMC) – Part 4-7: Testing and measurement techniques – General guide on harmonics and interharmonics measurements and instrumentation, for power supply systems and equipment connected thereto. Standard, International Electrotechnical Commission, Geneva, CH, 2002.

[10] E. O. Anders Larsson, Math H. J. Bollen, Mats G. Wahlberg, C. Martin Lundmark, and Sarah K. Ronnberg. Measurements of high-frequency (2–150 kHz) distortion in low-voltage networks. *IEEE Transactions on Power Delivery*, 25(3):1749–1757, jul 2010. doi: 10.1109/tpwrd.2010.2041371.

[11] Sarah Karolina Ronnberg, Math H. J. Bollen, and Mats Wahlberg. Interaction between narrowband power-line communication and end-user equipment. *IEEE Transactions on Power Delivery*, 26(3):2034–2039, jul 2011. doi: 10.1109/tpwrd.2011.2130543.

[12] Math Bollen, Magnus Olofsson, Anders Larsson, Sarah Ronnberg, and Martin Lundmark. Standards for supraharmonics (2 to 150 kHz). *IEEE Electromagnetic Compatibility Magazine*, 3(1):114–119, 2014. doi: 10.1109/memc.2014.6798813.

[13] Math Bollen, Jan Meyer, Hortensia Amaris, Ana Maria Blanco, Aurora Gil de Castro, Jan Desmet, Matthias Klatt, Lukasz Kocewiak, Sarah Ronnberg, and Kai Yang. Future work on harmonics - some expert opinions part i - wind and solar power. In *2014 16th International Conference on Harmonics and Quality of Power (ICHQP)*. IEEE, may 2014. doi: 10.1109/ichqp.2014.6842870.

[14] D. A. Martínez and A. Pavas. Current supraharmonics identification in commonly used low voltage devices. In *2015 IEEE Workshop on Power Electronics and Power Quality Applications (PEPQA)*, pages 1–5, June 2015. doi: http://10.1109/PEPQA.2015.7168230.

[15] L. Paulsson, B. Ekehov, S. Halen, T. Larsson, L. Palmqvist, A. Edris, D. Kidd, A.J.F. Keri, and B. Mehraban. High-frequency impacts in a converter-based back-to-back tie, the eagle pass installation. *IEEE Transactions on Power Delivery*, 18(4):1410–1415, oct 2003. doi: 10.1109/tpwrd.2003.817724.

[16] Hani Vahedi, Abdolreza Sheikholeslami, Mohammad Tavakoli Bina, and Mahmood Vahedi. Review and simulation of fixed and adaptive hysteresis current control considering switching losses and high-frequency harmonics. *Advances in Power Electronics*, 2011: 1–6, 2011. doi: 10.1155/2011/397872.

[17] Sarah K. Rönnberg, Math H.J. Bollen, Hortensia Amaris, Gary W. Chang, Irene Y.H. Gu, Łukasz H. Kocewiak, Jan Meyer, Magnus Olofsson, Paulo F. Ribeiro, and Jan Desmet. On waveform distortion in the frequency range of 2 kHz–150 kHz—review and research challenges. *Electric Power Systems Research*, 150:1–10, sep 2017. doi: 10.1016/j.epsr.2017.04.032.

[18] Sarah Rönnberg, Math Bollen, and Aurora Gil de Castro. *Harmonic Distortion from Energy-Efficient Equipment and Production in the Low-Voltage Network*. Luleå University of Technology, 2014.

[19] Enrique Jácome. *Análisis de Compatibilidad Electromagnética y Calidad de Potencia entre dos tecnologías de lámparas de descarga que presentan bajo factor de potencia y coexisten en una instalación eléctrica*. Universidad Nacional de Colombia, 2014.

[20] Daniel Agudelo-Martínez. *Identificación de emisión de supraarmónicos asociada con algunos dispositivos de baja tensión*. Universidad Nacional de Colombia, 2015.

[21] D. Agudelo-Martínez, M. Limas, A. Pavas, and J. Bacca. Supraharmonic bands detection for low voltage devices. In *2016 17th International Conference on Harmonics and Quality of Power (ICHQP)*, pages 1003–1009, Oct 2016. doi: 10.1109/ICHQP.2016.7783327.

[22] Sarah Rönnberg, Math Bollen. Propagation of Supraharmonics in the Low Voltage Grid. Report, Energiforsk, Stockholm, Sweden, 2017.

[23] Sarah Rönnberg, Anders Larsson, Math Bollen, and Jean-Luc Schanen. A simple model for interaction between equipment at a frequency of some tens of khz. In *International Conference on Electricity Distribution: 06/06/2011-09/06/2011*, 2011.

[24] Matthias Klatt, Jan Meyer, and Peter Schegner. Comparison of measurement methods for the frequency range of 2 kHz to 150 kHz. In *2014 16th International Conference on Harmonics and Quality of Power (ICHQP)*. IEEE, may 2014. doi: 10.1109/ichqp.2014.6842791.

[25] Christian Waniek, Thomas Wohlfahrt, Johanna M.A. Myrzik, Jan Meyer, Matthias Klatt, and Peter Schegner. Supraharmonics: Root causes and interactions between multiple devices and the low voltage grid. In *2017 IEEE PES Innovative Smart Grid Technologies Conference Europe (ISGT-Europe)*. IEEE, sep 2017. doi: 10.1109/isgteurope.2017.8260267.

3. Measurement System for supraharmonics in low voltage networks

Monitoring of power quality disturbances, in this case waveform distortions between 2-150 kHz, requires accurate and reliable measurement systems and procedures. Some standards propose a measurement setup for the assessment of these current and voltage high frequency conducted emissions, named by some researchers as supraharmonic emissions or simply supraharmonics. However, results from laboratory and real grid measurements have shown that measurement of such emissions need to be reviewed. Therefore, a standard measurement system and a set of procedures for studying the supraharmonic emissions are still under research. This chapter describes the influence of a measurement setup on the emission of devices in the frequency range 2-150 kHz. First three sections describe the proposed measurement setup, the experimental setup and the signal processing techniques respectively. After, a summary of the metrology aspects for measurement of supraharmonics is presented. Last two sections show main aspects of the influence of the proposed measurement setup on supraharmonic emissions and some conclusions from these results.

From different previous works it has been concluded that obtaining sufficient measurement accuracy for supraharmonic is not trivial [1][2]. Instruments should have high accuracy for both amplitudes and phase angles over a wide frequency range. In particular, analogue filters should be used for supraharmonic voltages so as to obtain an adequate measurement range and therefore, accuracy. Supraharmonics emission measurement can be addressed from three key perspectives: measurement accuracy, data acquisition and analysis, and reproducible measurement methods [3]. Measurement accuracy is currently a field of study in supraharmonics assessment. Accuracy strongly depends on transducers (amplitude and frequency accuracy) and filters, in order to avoid additional distortion in measured signals and leakage effects [3]. Regarding digital filters, researchers have stated that a 16 bit or higher resolution measurement system is suitable for supraharmonics assessment [3]. Data processing and analysis of supraharmonics take into account: signal filters, transducers bandwidth, aggregation methods in spectrum and aggregation methods in time domain [1][3]. Furthermore, supraharmonics analysis techniques used in previous works mainly include Short Time Fast Fourier Transform (STFFT) y ESPRIT (Estimation of Signal Parameters via Rotational In-

variance) [1]. Further information about standard methods for measurement procedures can be found in [3]: IEC 61000-4-7 describes a measurement method for supraharmonic between 2-9 kHz; IEC 61000-4-30 includes an appendix describing a set of measurement methods between 2-9 kHz and 9-150 kHz.

3.1. Measurement Setup

Emissions at supraharmonic range can be measured and processed taking into account the methods suggested in standards such as IEC 61000-4-7[4] and IEC 61000-4-30 [5]. However, the latter standard provides suggestions for measurements in low voltage networks [5][3], which are not necessarily applicable for measurements on appliances. In any case, there is still a lack of generally accepted normative methods for measuring emissions between 2-150 kHz [6]. Other measurement and processing methods can alternatively be applied, such as those described in standards like CISPR 16 (EN 55016), whose scope are emissions between 9kHz-30MHz [7][8], and CENELEC EN 50065 for devices using narrow band PLC technologies (intentional emissions) [6][7]. According to standard IEC61000-4-7 [4] the emission assessment of harmonics and interharmonics up to 40th harmonic can be carried out using the general measurement setup depicted in Figure **3-1**. u_S and u_L represent the source and load voltages respectively, whilst $Z_{Network}$ is the impedance between voltage source and other stages of the measurement setup.

From evidence and the development of this research, *supraharmonic distortions strongly depend on the voltage source, equivalent network impedance and sensors used in the measurement setup*. In this sense, each of the stages depicted in Fig. **3-1**, as well as the experimental procedure, should be carefully selected in order to obtain accurate, reproducible results.

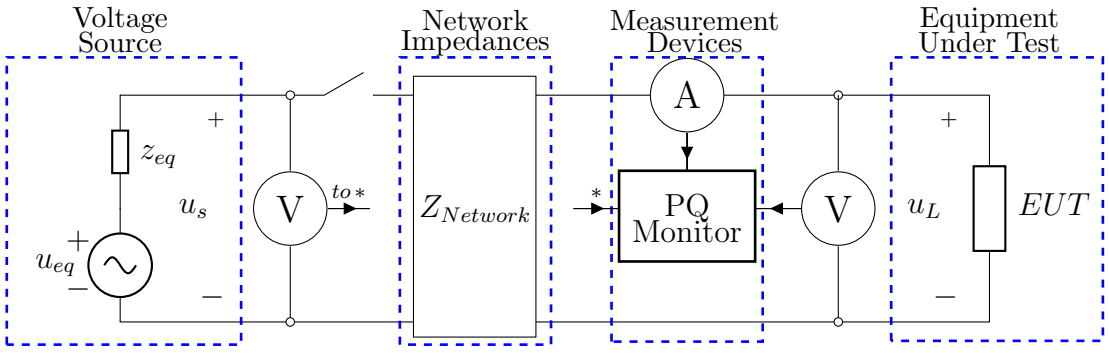

Figure 3-1.: Measurement setup for assessing single-phase emissions between 2-150 kHz.

In laboratory measurements the Power Source, Network Impedance and Current Sensors are expected to remain the same when measuring different Equipment Under Test (EUT). In

real low voltage networks, however, supply voltage (amplitude, waveform distortion) and loads are continuously changing in time[9]. This is one of the most challenging facts about emission assessment between 2-150 kHz, since emissions in laboratory setups could differ from emissions in real grid measurements. The following subsections describe each stage of the measurement setup suggested for the assessment of supraharmonics.

3.1.1. Voltage Source

Waveform distortions between 2-150 kHz are affected by the use of different voltage supplies (see Chapter 2). Some examples of the influence of voltage source over the current and voltage distortion at supraharmonic range are reported in [10][11]. In addition, output impedance of voltage supplies can also influence the behaviour of emissions as reported in [12].

The voltage source stage was composed by a computer (PC), an Digital/Analogue converter, a galvanic isolation module and a linear amplifier 2.25 kW rated power as shown in Fig. **3-2**. Two different linear amplifiers were independently used to supply the EUT.

3.1.1.1. Signal Generation (PC) and Digital/Analogue converter (D/A C)

All synthetic signals used in this thesis were created using the Matlab® scripting environment. After signals are created, they are sent to a Digital/Analogue converter for physical realization. This 16-bits device allows signals to reach analogue values between ± 5 V.

3.1.1.2. Galvanic Isolation

Since the unintentional emissions from supply stage could modify the original emissions from EUT (primary emission), this module allows to block any conducted emission generated at voltage source different from that generated in PC stage (using Matlab), see Fig. **3-2**. Hence the experimental setup composed by Amplifier and other stages depicted in Fig. **3-1** are isolated from the grid.

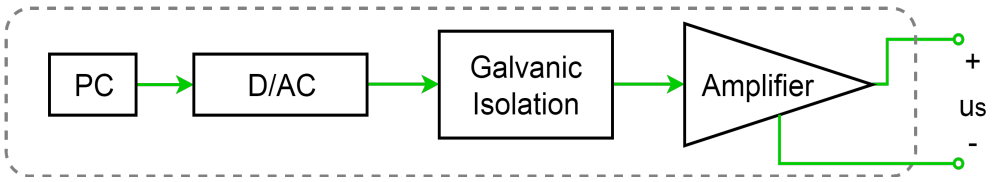

Figure 3-2.: Dashed gray line groups the components of Voltage Source.

3.1.1.3. Amplifier

A 2.5 kW linear amplifier receives the signal between ± 5V from galvanic isolation module and then supplies the EUT through a Network Impedance, see Fig. **3-1**. This amplifier is not expected to produce voltage emissions between 2-150 kHz. However, the current emissions from EUT could lead to voltage distortion through the amplifier's output impedance. Switched-mode amplifiers (e.g. boost converters) are expected to have distorted voltages between 2-150 kHz because of their active switching processes. In this sense, two linear amplifiers were used in this chapter to supply selected EUT. Non-linear amplifiers were avoided in this assessment in order to clearly identify emissions from EUT.

3.1.2. Network Impedances

For reproducibility purposes above harmonic range, standards suggest to include a network impedance between voltage source and EUT, such as an Artificial Mains Network (AMN) or a Line Impedance Stabilizing Network (LISN). Annex B of standard IEC61000-4-7 [4] suggests to use an AMN as a known network impedance, which standardizes the impedance characteristics over the range 2-9 kHz. AMN should be inserted between voltage source and EUT, as depicted in Fig. **3-1**.

However, network impedances such as AMN or LISN may differ from grid impedance above 9kHz. In fact, researchers have shown that grid measurements and laboratory measurements could be different at supraharmonic range, even though the same measurement procedures are carried out [13][14][8]. For instance, the magnitude of some measured grid impedances between 2-150 kHz previously reported in [15] are shown in Fig. **3-3**.

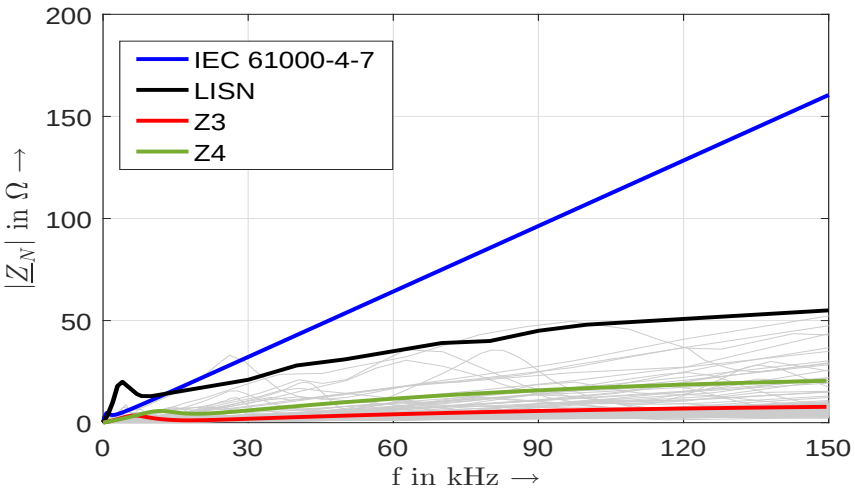

Figure 3-3.: Percentiles of grid impedance measurements between 2-150 kHz[15].

In Figure **3-3**, "IEC 61000-4-7" represents the reference impedance suggested in the standard of the same name, "LISN" is a Line Impedance Stabilization Network , and Z3 and Z4 are impdances based on single loop impedance measurements, resulting from the assessment of 189 representative low voltage networks reported in [15]. Further details about the measurement procedure can be found in [15]. According to Figure **3-3**, the impedance proposed in IEC 61000-4-7 shows a higher magnitude than the LISN impedance and most of the measured low voltage networks between 2-150 kHz.

From the impedances shown in Figure **3-3** and the results reported in [15], four different network impedances were used in this chapter to evaluate their influence on supraharmonic emissions: $Z1$, $Z2$, $Z3$ and $Z4$. $Z1$ corresponds to the case without network impedance between the voltage source and EUT. The Line Stabilisation Network (LISN) is used as the standard network impedance $Z2$ for the frequency range 2-150 kHz, taking into account that LISN is officially designed only for frequencies above 9 kHz; the HM6050-2D device was used as the LISN impedance [16]. Finally, $Z3$ and $Z4$ are impedances based on the analysis of measurements in different public low voltage networks and were also used in [15].

3.1.3. Measurement Devices

It is required to distinguish between emissions from the operation of EUT and from all other sources of emissions between 2-150 kHz, including the sensors operation. Accuracy of the equipment used to digitalize the analogue measured signals (DAQ modules) is also important, taking into account the different amplitude ranges along the assessed frequency range. Estimation of measurement uncertainty considering the whole measurement system is crucial for discerning between true emissions and noise.

3.1.3.1. Current and voltage sensors

A Pearson Current Sensor, a Zero-flux transducer and a shunt resistor were considered in the measurement setup assessment, in order to compare the current measurement and to find eventual differences. Figure **3-4** shows the transfer ratio calibration between 2-150 kHz for current sensors used in this chapter. Dashed lines represent the tolerance band for the estimation of relative error in amplitude measurement.

Supraharmonic voltages are notably lower than voltage at main frequency. In order to decrease uncertainty estimation for such emissions, a filter is used for voltage measurement. This filter, whose design and experimental results are reported in [17], was designed for voltage measurement between 2-150 kHz.

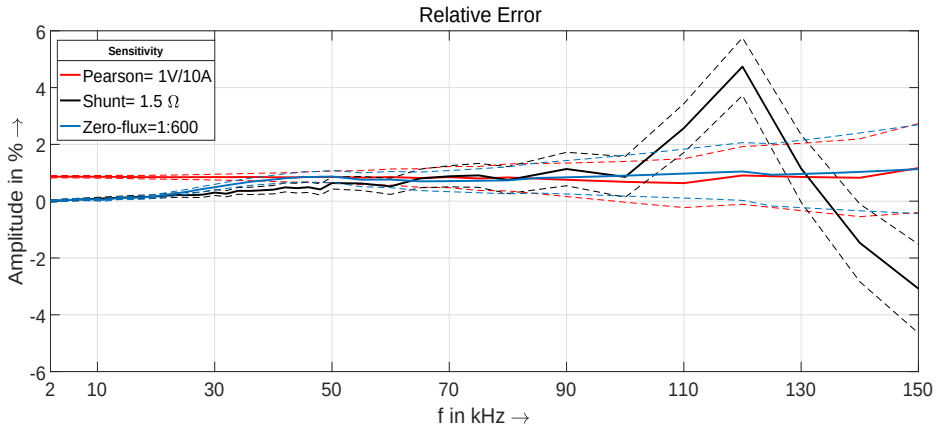

Figure 3-4.: Relative error of current sensors transfer ratio between 2-150 kHz

The most relevant features of filter are listed below:

- Band-pass Elliptic filter, third order
- A damping of 60 dB or more at 50 Hz
- The measured beginning of pass-band filter was at 2 kHz, with an error of -3% above 10 kHz
- The end of pass-band filter was designed at 209 kHz
- Analog implementation, expected to have $230V_{RMS}$ + 15% as maximum input voltage and 10 V_{RMS} as maximum output voltage
- Input impedance of 10 $k\Omega$ in the pass-band frequency range

Further information about this filter can be found in [17]. For the purpose of this research, a digital low-pass filter up to 300 kHz was also used in addition to the voltage analog filter.

3.1.3.2. Data Acquisition Modules (DAQ)

The Power Quality and Energy Analyser DEWETRON-2600 [18] was used as the current and voltage measurement device. Accuracy based on manufacturer specifications for HSI-HV and HSI-LV Acquisition Modules is described in Tables **3-1** and **3-2**.

3.1.4. Equipment Under Test

The measurement of emissions could also be affected when considering different non-linear loads, as well as it is for harmonic emissions [19]. Some non-linear loads are able to produce voltage distortion; current distortion could eventually be different according to the power source used in the assessment [19][12][9].

Table 3-1.: Accuracy for HV Dewetron Module 100V-1400V range (f: Signal frequency in kHz)

Signal Frequency	Accuracy
0.1 Hz to 1kHz	±0.05% reading ±0.01% range
1kHz to 10 kHz	±0.1% reading ±0.05% range
10kHz to 50 kHz	±0.4% reading ±0.05% range
50kHz to 100kHz	$\pm(0.016 * f)$% reading ±0.1% range
100kHz to 1MHz	$\pm(0.010 * f)$% reading ±1% range
1MHz to 2MHz	$\pm(0.014 * f)$% reading ±3% range

Table 3-2.: Accuracy for LV Dewetron Module (f: Signal frequency in kHz)

Range	**Signal Frecuency**	**Accuracy**
10 mV to 100 mV	0.1 Hz to 10kHz	±0.1% reading $\pm 30\mu V$
	10kHz to 50 kHz	±0.4% reading $\pm 30\mu V$
	50kHz to 100kHz	$\pm(0.016 * f)$ % reading ±0.1% range
	100kHz to 1MHz	$\pm(0.010 * f)$ % reading ±1% range
	1MHz to 2MHz	$\pm(0.014 * f)$% reading ±3% range
200 mV to 50V	0.1 Hz to 10kHz	0.05 % reading 0.01% range
	1kHz to 10 kHz	0.1 % reading 0.05 % range
	10kHz to 50 kHz	0.4 % reading 0.05 % range
	50kHz to 100kHz	$\pm(0.016 * f)$ % reading ±0.1 % range
	100kHz to 1MHz	$\pm(0.010 * f)$ % reading ±1 % range
	1MHz to 2MHz	$\pm(0.014 * f)$ % reading ±3 % range

3.1.4.1. EUT Classification from Power Factor Corrector perspective

The diversity of EUT topologies and therefore EUT input impedances can eventually influence emissions between 2-150 kHz [13][9][12]. For instance [20] shows, using simulation tools, how the variation of EMI filter parameters directly modify supraharmonic emissions at the Point of Common Connection.

The assessed devices can be classified according to the Power Factor Corrector circuit they use. A detailed study of such classification is presented in [21]:

- No PFC: Usually consists of a simple power supply (PS) with diode bridge rectifier and smoothing capacitor. The PS provides smooth voltage to the DC load. Usually the power factor is low (PF<0.6).

- No PFC (Capacitive divider): The capacitive divider is a special case of the no PFC topology, where a capacitor is used to lower the input voltage, but it does not improve the power factor (PF<0.6 for capacitive dividers).

- Passive PFC: PS with additional series capacitors or inductors before or after the bridge diode rectifier to increase the power factor (usually 0.6≤PF≤0.9).

- Active PFC: PS with advanced control circuits that shape the input current waveform. This topology has the best performance related to power factor (PF>0.9).

In most of the cases, the devices with no-PFC topology produce the highest distortion ((THDi>80%), except for the capacitive divider (THDi<30%). Usually, passive-PFC devices have a medium distortion (40%≤THDi≤ 80%), and active-PFC devices have the lowest distortion (THDi<40%)[21].

3.1.4.2. EUT Selection

Table **3-3** shows the selected EUT for emission assessment. All of them are low-power LED lamps with rated power equal or below 12 W, typically used as household appliances. The LED lamps are classified according to the Power Factor Correction method implemented in their circuit (see Table **3-3**), following the classification described in [21].

Table 3-3.: Equipment Under Test (EUT)

Device	**Power [W]**	**Voltage [Vrms]**	**Frequency [Hz]**	**PFC**
LED1	12	220-240	50-60	passive
LED2	10	100-240	50	active
LED3	1	230	50	no PFC
LED4	9	230	50	passive
LED5	5	85-265	50-60	passive

3.2. Experimental Setup

The stages of measurement setup and their corresponding equipment described in the latter section were used for assessing their influence on the supraharmonic emissions. Two linear

amplifiers were independently used to supply the EUT. The network impedances $Z1$ to $Z4$ described above were connected between "voltage source" and "measurement devices" stages (recall that $Z1$ means no impedance). The three current sensors were used simultaneously in order to compare measurements. Each EUT was tested at a time using one voltage source and one network impedance. Table **3-4** show the combination proposed for such assessment.

Table 3-4.: Variations of experimental setup base case

Description			
Voltage source	Network impedance	Current sensors	EUT
S1, S2	Z1: No impedance	Pearson, Shunt, Zero-flux	Five different LED devices
	Z2: LISN		
	Z3: Measured		
	Z4: Measured		

3.2.1. Measurements

Voltages and currents were measured during 1 s.Each signal of 1 s duration was divided into 4 windows; then, sub-signals of 200 ms length were processed as suggested in [4]. Power quality monitor might stop the signal record before 1s is completed, therefore, last 200 ms window was neglected. In order to assess emissions up to 150 kHz, the sampling frequency must be at least 300 kHz according to Nyquist theorem. However, effects like aliasing (from sampling process, higher frequencies than those in real signal) and leakage (from truncation process, higher magnitudes than those in real signal) could represent additional, perceptible distortion in the measured signals if Nyquist frequency and measurement duration are not carefully taken into account.

The final selected sampling frequency was 1 Msps, using an antialiasing (low-pass) filter up to 300 kH. Four 200 ms-windows were considered for each measurement, and a total of 5 measurement were performed for each EUT of Table **3-3**. A total of 40 signal blocks of 200 ms duration were obtained for each measurement of voltage and current of EUT under operation.

3.2.2. Stabilization Time

All EUTs had an stabilisation time longer than one hour, in order to decrease measurement variations due to the fluctuation of EUT operation point. This allowed to have a variation in fundamental current lower than 1% during the measurements for all considered EUTs. Figure **3-5** shows the fundamental current variation for all EUT from Table **3-3** after stabilization time.

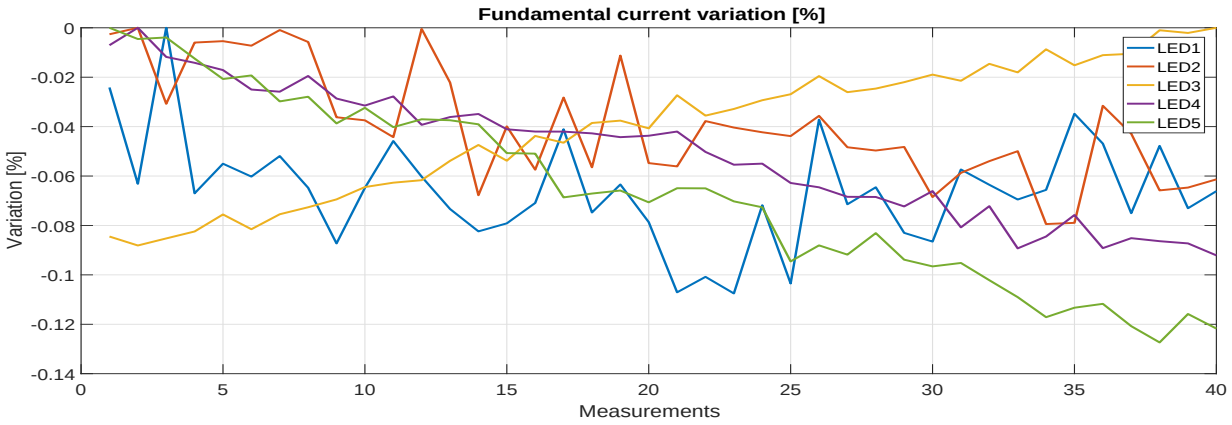

Figure 3-5.: Variation of fundamental current in all measurements

3.2.3. Test Modes

Currents and voltages were measured 5 times from each EUT under operation in two sequential scenarios: "Idle" and "On" modes.

- Idle Mode: Background Emissions:
  Idle mode means that EUT is the only part of the measurement setup depicted in Fig. **3-1** that it is not under operation. Since selected EUT (Table **3-3**) do not have an idle mode by itself, for the context of this paper idle mode implies circuit is open (see Fig. **3-1**) between current sensors and EUT, but power source is turned on though. Because idle mode allows to observe emissions immediately before the EUT start to operate, this can serve as a reference case for measuring background emissions not related to EUT operation.

- On Mode: Emissions under operation
  In contrast, on-mode means EUT and the other stages of measurement setup are operating under rated conditions. In this case, emissions between 2-150 kHz can be seen under EUT operation. This mode, however, could also show emissions from any other part of the measurement setup. Becasue of this, emissions should be compared between idle mode and on-mode rather than assuming on mode show only EUT emissions.

3.3. Signal Processing

All signals were measured and acquired in time domain. However, analysis in frequency domain was used in order to notice the behaviour of emissions from fundamental frequency up to 150 kHz.
The signal processing was developed in three stages:

- FFT: Currents and voltages are processed using Fast Fourier Transform. Since time windows are 200ms long, 5 Hz resolution is obtained. Only magnitude of emissions were analysed in this chapter.

$$\Delta f = \frac{f_s}{N_{tot}}, \qquad N_{tot} = \left(\frac{p}{f_m}\right) f_s$$

  Where:

  - Δf: Frequency bin
  - f_s: Sampling frequency
  - N_{tot}: Total amount of samples
  - p: Total amount of periods
  - f_m: Main frequency

  From this, the frequency bin yields:

$$\Delta f = \frac{f_m}{p} = \frac{50Hz}{10} = 5Hz \tag{3-1}$$

- Mean spectrum: 40 spectra are processed for currents and voltages of selected EUT. An equivalent mean-magnitude FFT is obtained for each considered case, in order to have an aggregated value. The value at any frequency corresponds to the mean magnitude of all spectra at that frequency.

- Grouping: Emissions in frequency domain were grouped in 200 Hz bands as suggested in [4]. The value reported at each frequency band represents the RMS value of currents or voltages using the following index [22]:

$$TSH_{C;V} = \sqrt{\sum_{B=1}^{705} Y_B^2} \tag{3-2}$$

  - Y: RMS value for emissions grouped in 200-Hz bands [4]
  - B: Emissions groups, 200-Hz width (B=1,2,...705 for [2-2.2), [2.2-2.4),...[149.8,150) kHz)
  - $C;V$: Current or voltage signals

- Box Plots: Rectangles were used to represent the maximum, average and minimum Total Supraharmonic Current and Voltage for each of the measurements of each EUT from Table **3-3**. These values are computed using Equation 3-2 between 2-150 kHz.

3.4. Metrological aspects for supraharmonics

Most of the assessments in supraharmonic emissions report magnitude of emissions. However, the metrological properties of measurement system used are not usually reported. Following subsections describe the metrological aspects taken into account for the measurement of supraharmonics, including an emission threshold estimation.

3.4.1. Total accuracy estimation

Figure **3-6** depicts a measurement system regarded as a transfer function. Horizontal and vertical axes represent the quantity subject to measurement (measurand) and the result of the measurement process respectively, regardless measurement units. If the measurement system were to be an ideal one, the transfer function would be a straight line with a slope equal to one. However the stepped, blue line in Figure **3-6** represents the nonlinear behaviour of real measurement systems.

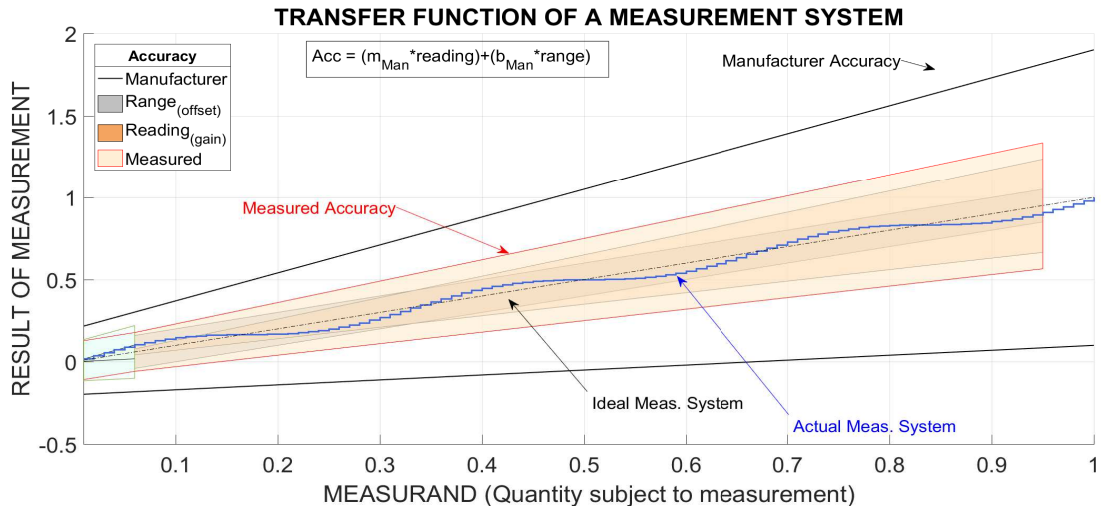

Figure 3-6.: Illustrative explanation of measurement accuracy.

Accuracy is defined as the "closeness of the agreement between the result of a measurement and a true value of the measurand" [23]. The sensors and data acquisition modules are the devices who directly deals with the measurand, in this case, currents and voltages. Therefore, it is required to estimate the accuracy resulting from the combination of sensors and daq modules. These accuracies are influenced by external factors as temperature, devices lifespan and other aspects listed in reference manuals [18] [24]. As an illustrative example, Figure **3-6** shows the accuracy of measurements reported by the manufacturer of a measurement device represented in the two outer black lines. Nevertheless, according to researchers experience accuracy estimation from manufacturer is a rather conservative one. This to say, the actual accuracy of measurement (after a calibration process) might be much better (e.g.

a tighter "error" band) than the manufacturer estimation. This idea is illustrated in Figure **3-6**, where the "offset" (range) and "gain" (reading) components of accuracy are represented by colored bands, as well as their combination for the computation of the total accuracy of measurement.

The estimation of total accuracy from the combination of sensors and daq modules was computed as a summation of both values:

$$Accuracy_{total} = Acc_{Sensors} + Acc_{DAQ} \tag{3-3}$$

Because the results from measurement processes have a central tendency behaviour [25][23], the probability that the true value lies on the borders of the range given by the total (aggregated) accuracy is quite low [23]. However, the total accuracy is estimated in this way in order to have a worst case. The estimation of the measurement uncertainty will take into account the central tendency behaviour of measurements.

As already explained using Figure **3-6**, the accuracy is usually expressed as an equation including two factors: a percentage of the reading and a percentage of the range:

$$Acc = m\,[\%] * reading + b\,[\%] * range \tag{3-4}$$

Notice that when measured values ("reading" in Equation 3-4) are too low (tend to zero), the expression yields:

$$\lim_{reading \to 0} m\,[\%] * reading + b\,[\%] * range = b\,[\%] * range \tag{3-5}$$

This is illustrated in Figure **3-7**, where the low amplitude signals would fall into the blue colored region.

It can be obtained a "limit of error" or "accuracy interval" when the value from Equation 3-4 is summed up to the measured value. In this sense, it is useful to show how the limits of errors in the "accuracy interval" are related to the measured value. Accuracy can be then also expressed as a percentage of the measured value:

$$Acc\,[\%] = \frac{m\,[\%] * reading + b\,[\%] * range}{reading} * 100 \tag{3-6}$$

Accuracy of measurement devices depends on both the amplitude and the frequency of the measured signal as shown in Tables **3-1** and **3-2**. Rated power of selected EUT were different and therefore, different measurement ranges were used in this assessment. The amplitude range is adjusted to fit well with the magnitude of main frequency component, however, the emissions observed between 2-150 kHz have notably lower amplitudes, so the accuracy is not the same for each frequency component. Assuming that a measured, distorted signal can

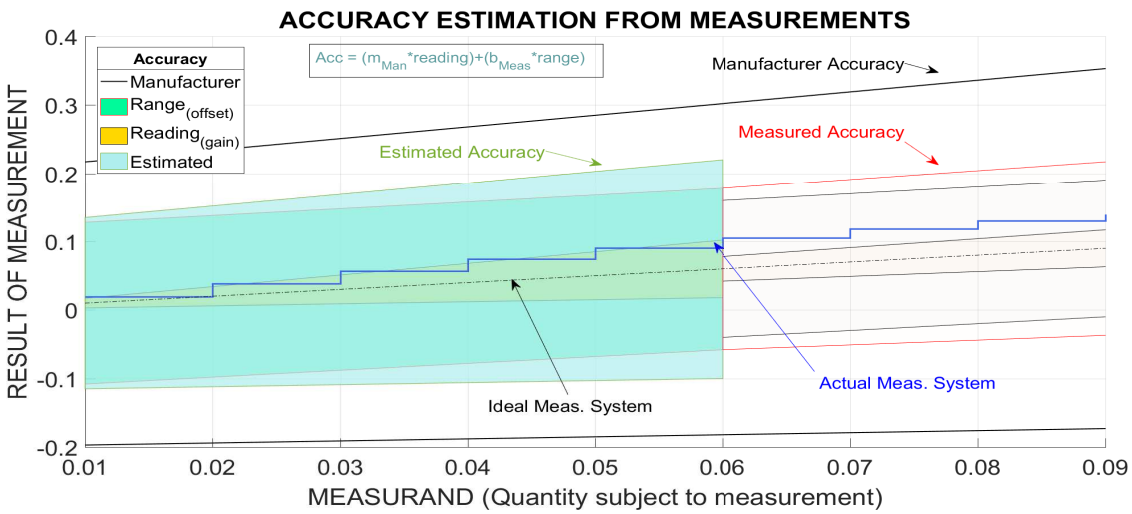

Figure 3-7.: Illustrative explanation of measurement accuracy for low amplitude signals.

be decomposed in the summation of sinusoidal signals according to Fourier Transform, each sinusoidal component of the distorted signal can be used to compute the accuracy defined in Equation 3-6.

In order to observe the behaviour of total accuracy when signals with different amplitude and frequency are used, DAQ and sensor accuracies described in last section were plotted as function of frequency and amplitude. This was performed creating synthetic signals and then computing the accuracy level given by reference manuals; for the purpose of this chapter, this will refered to as "theoretical accuracy". Figures **3-8**a and **3-8**b show two examples of measurement accuracy for current and voltage at 0.1 A (0.01 V DAQ Module and a sensor sensitivity of 0.1V/A) and 400 V ranges respectively, considering different amplitudes within these ranges. Accuracy values are in percentage, where the red and blue colors represent larger and shorter "accuracy intervals" respectively. The wider the "accuracy interval", the wider the range where the true magnitude value lies.

From previous measurements performed by the author and researchers from all over the world, emissions between 2-150 kHz could be lower even than 0.1 % of the magnitude of main frequency component. Hence, it is required to know how accurate is the measurement of emissions between 2-150 kHz when the main component (i.e. emission at main frequency) is higher than 1000 times these emissions. After processing the total accuracy for all sensors and daqs using the methodology shown in Figures **3-8**a and **3-8**b, it could be observed that most of the emissions between 2-150 kHz might lie close to the "red accuracy region". This means that, if the measured amplitude of an emission (e.g. $x \pm \delta x$) was low enough to lie within the red accuracy region, the "accuracy interval" related to such emission (i.e. $2\delta x$) might be equal or even greater than the emissions itself ($2\delta x \geq x$).

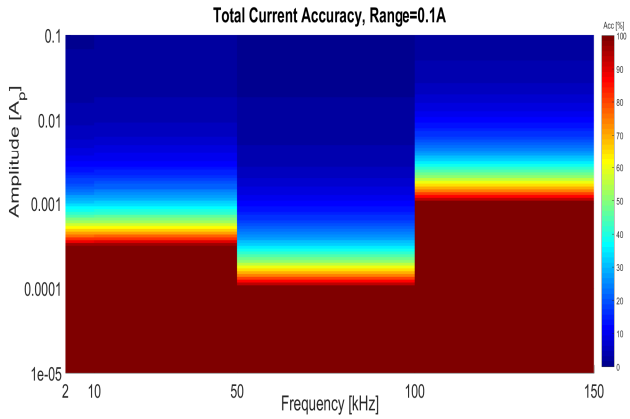

(a) Theoretical current accuracy

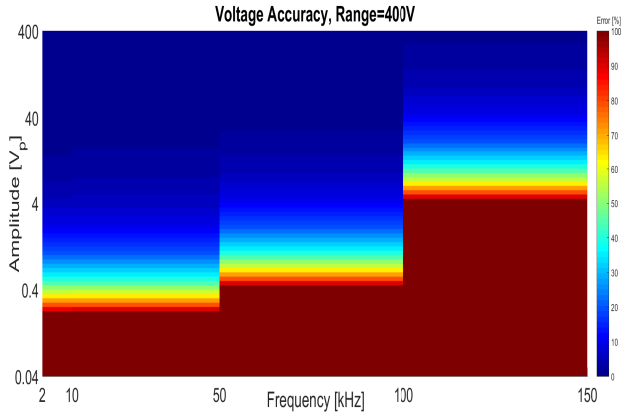

(b) Theoretical voltage accuracy

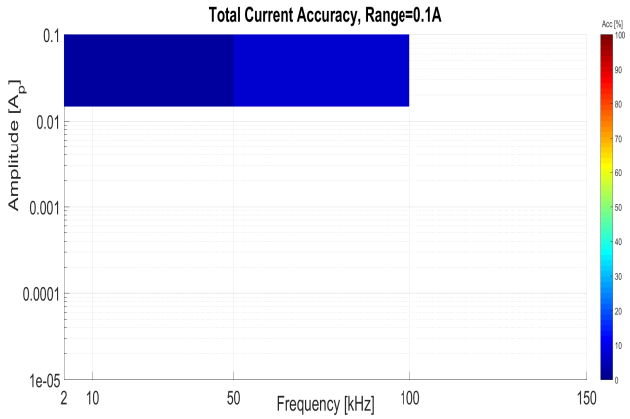

(c) Measured current accuracy

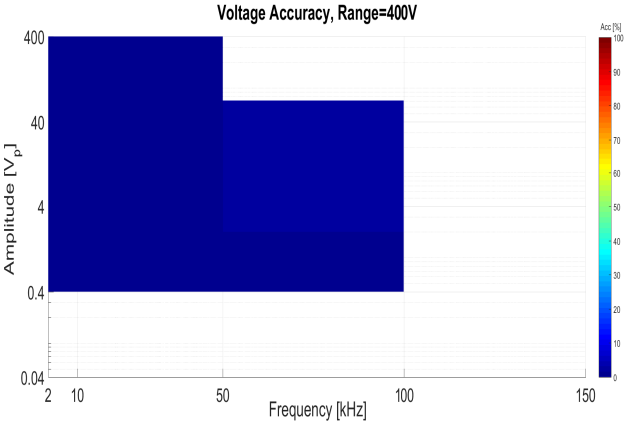

(d) Measured voltage accuracy

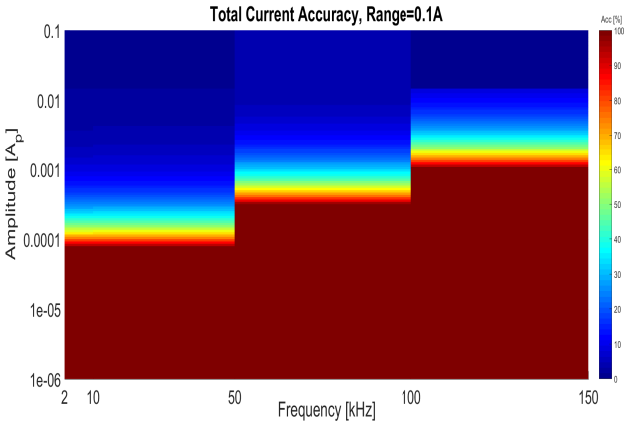

(e) Estimation of current accuracy

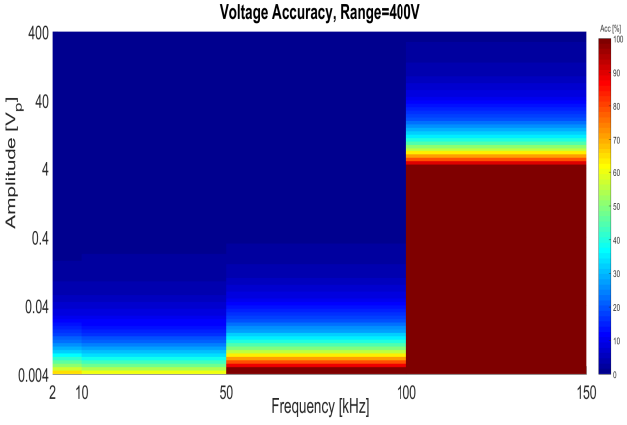

(f) Estimation of voltage accuracy

Figure 3-8.: Total accuracy as a function of frequency and amplitude

Nevertheless, some metrological assessments performed by authors and other researchers in Power Quality have also shown that accuracy values reported by manufacturers actually corresponds to a much better, lower "accuracy interval" values when the measurement device performs under rated conditions and within its expected lifespan. This served as a motivation for calibrating the measurement setup and to identify the real, expected total accuracy values for supraharmonic emissions. The calibration were carried out using the voltage function of Fluke 5730A calibrator from 50 Hz to 100 kHz. However, it was not possible to decrease the calibrating amplitude enough to find the accuracy for amplitudes lower than 0.1% of the full scale amplitude. Calibrator also was not able to produce accurate signals beyond 100 kHz. Blank spaces in Figures **3-8**c and **3-8**d show the lack of information from calibration in the frequency range 2-150 kHz. These "blank" regions are in turn represented by the blue colored region in Figure **3-7**.

From this issue, a combination of the theoretical accuracy given in reference manuals and the measured accuracy is proposed. This estimation was developed using the following criteria:

$$Acc\,[\%] \equiv \begin{cases} Measured & \text{, reading} \geq \text{calibrated amplitude} \quad \text{(3-7a)} \\ \dfrac{m\,[\%] * reading + b_c\,[\%] * range}{reading} * 100 & \text{, reading} < \text{calibrated amplitude} \quad \text{(3-7b)} \end{cases}$$

Accuracy according to Equation 3-7 yields the same measured accuracy values up to the lower calibrated amplitude. From this amplitude down and taking into account Equation 3-5, the accuracy is computed assuming the same behaviour of theoretical accuracy but using the $b_c\,[\%]$ factor obtained in the calibration of the lowest measurement range. Results from such combination are shown in Figures **3-8**e and **3-8**f respectively. Notice that using the approach of Equation 3-7, the relative "accuracy interval" in Figures **3-8**e and **3-8**f is now shorter (lower values) than those obtained in Figures **3-8**a and **3-8**b.

This method is not intended to replace or improve the results from calibration process. Instead of that, the criteria shown in Equation 3-7 relies on the data obtained in calibration process and assumes that the "inaccuracy" obtained with the lowest calibrating amplitude will remain as the factor $b\,[\%] * range$ in Equation 3-5, when very low amplitudes are to be processed.

3.4.2. Threshold estimation

Threshold estimation is required for having knowledge about the minimum amplitude the measurement system is able to accurately measure. The concept of "threshold" is used through this research in the sense of the minimum amplitude that the whole measurement system can accurately measure, given a maximum value of "inaccuracy", supported on the measured difference between manufacturer specifications and noise threshold measurements.

In other words, *threshold is the amplitude above which its corresponding inaccuracy is lower than a given percentage (x%)*, for each measurement range.

Although signals close to this threshold could have a wide "accuracy interval", for the purpose of *emission detection* this assumption allows to make an estimation of what might be or not true emission when considering very low amplitudes. Threshold estimation for supraharmonic magnitudes was based on Figures **3-8**a and **3-8**b. These figures show the theoretical accuracy relative to the measured amplitude: the higher the percentage, the wider the interval containing the true value of the measured magnitude. Figures **3-8**c and **3-8**f show the same concept using measured accuracy (calibration) and Figures **3-8**c and **3-8**f using extrapolated accuracy.

Figures **3-9**a and **3-9**b show the threshold using the 50% criteria for different measurement ranges. This means that the width of "accuracy interval" in percentage is equal or higher than 50% of the measured value using the theoretical accuracy. From previous measurements performed by author using low power appliances, if a percentage lower than 50% is considered for the threshold estimation, many supraharmonic emissions from low power appliances would be detected as "not true signal" and therefore ignored. In contrast, selecting a higher percentage than 50% (for the relation between accuracy and measured value) would lead to detect emissions with a higher "accuracy interval" as true emissions, even those which might be related to noise. The percentage used in this research for threshold estimation (50%) was proposed from experimental measurements using low power appliances, therefore, a holistic and more accurate estimation of such percentage is strongly suggested as future work. This percentage served as a tuning parameter for the measurement system to select only those signals considered as "true emissions".

Figures **3-9**e and **3-9**f show that the "extrapolated" threshold, i.e. the threshold computed as a combination of theoretical and measured accuracies (see Equation 3-7), lay below the theoretical threshold for all considered cases between 2-150 kHz (Figures **3-9**a and **3-9**b). Thresholds shown in Figures **3-9**e and **3-9**f are then used in this research to define the limit above which the spectral components between 2-150 kHz will be considered signals. Emissions below these thresholds cannot be clearly distinguished from noise and therefore are not considered for further analysis.

By the way, the probabilistic behaviour of measurement process is included in the threshold estimation using the uncertainty approach. Further explanation about uncertainty is presented in next subsection. For the purpose of threshold estimation, the following statements should be recalled:

- Accuracy given by Equation 3-4 is a qualitative expression

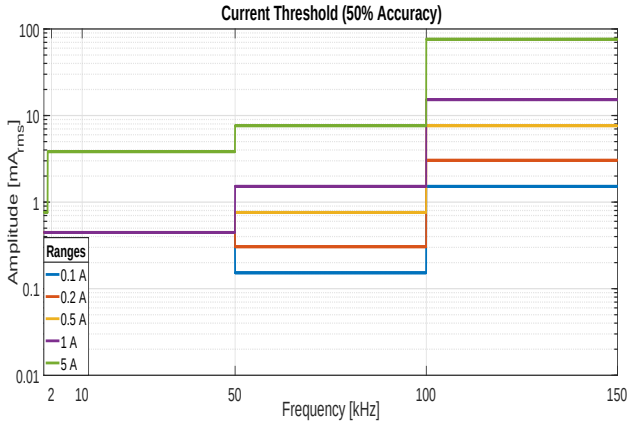

(a) Theoretical current accuracy

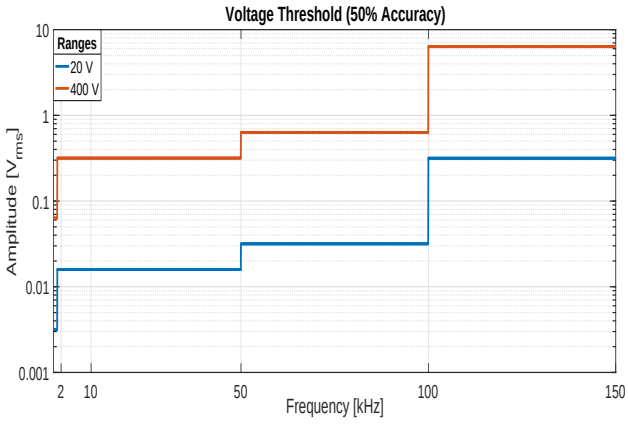

(b) Theoretical voltage accuracy

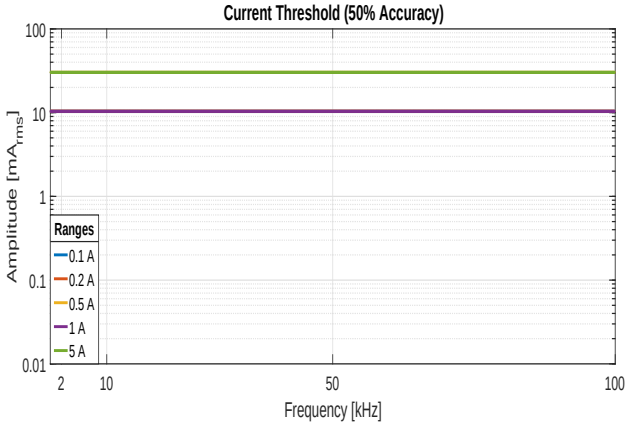

(c) Measured current accuracy

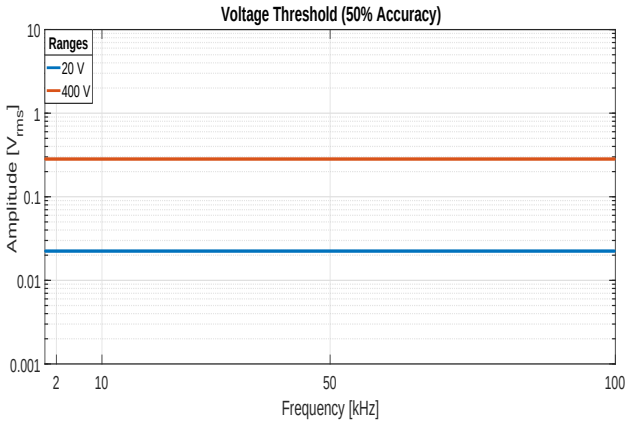

(d) Measured voltage accuracy

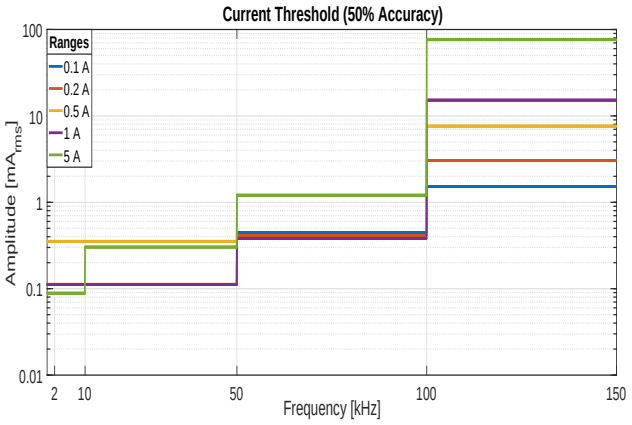

(e) Estimation of current accuracy

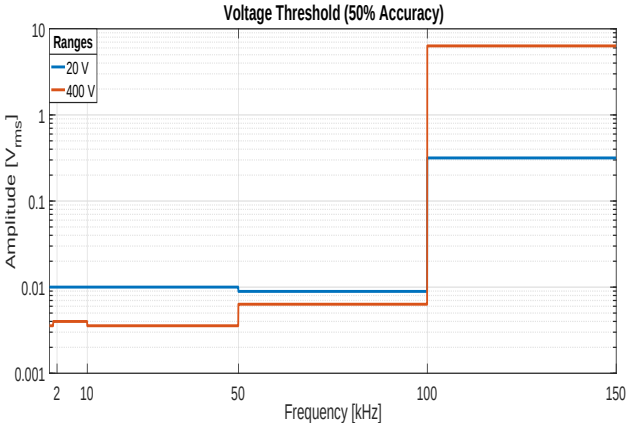

(f) Estimation of voltage accuracy

Figure 3-9.: Threshold for measurement of current and voltages as a function of frequency and amplitude

- When computed, accuracy is a quantitative expression
- Computed accuracy tells about a limit of maximum error for a "measured" (estimated) value
- The limits of error, also known as "accuracy interval", bound a tolerance band where the true value is assumed to lie in
- The tolerance band is assumed to be symmetrical with respect to the "measured" (estimated) value
- The positive half of the tolerance band is used to estimate the threshold for emissions' magnitudes between 2-150 kHz.

The uncertainty of the threshold proposed was computed assuming a rectangular distribution of values inside the tolerance band given by criteria shown in Equation 3-7. A coverage factor of 1.65 is used since it is assumed a rectangular probability distribution. This leads to obtain a 95% level of confidence as suggested in [23], as shown in Equation 3-8:

$$U_{threshold} = +k\sqrt{U_{acc}^2} = +kU_{acc} = 1.65\frac{Accuracy_{total}}{\sqrt{3}} \tag{3-8}$$

The value reported for threshold will vary with amplitude and frequency ranges accordingly. Because of this, the threshold is intended to be compared to the spectra of each current and voltage signals from measurement of EUT listed in Table **3-3**.

Finally, it is important to make clear the difference between "uncertainty of threshold estimation" and "uncertainty of measurement of emissions". Although both estimations aim to take into account the stochastic behaviour of emissions measurement, the "uncertainty of threshold estimation" (explained in this subsection) is related to the estimation of the proposed threshold, whilst the "uncertainty of measurement of emissions" (explained in next subsection) is related to the estimation of the measured value itself.

3.4.3. Uncertainty of measurement for supraharmonic emissions

Uncertainty of measurement is a parameter (it might be multiple of a standard deviation, or the half-width of an interval having a stated level of confidence), associated with the result of a measurement, that characterizes the dispersion of the values that could reasonably be attributed to the measurand [23]. This parameter is by definition related to a Probability Distribution Function (PDF), which represents knowledge about possible values of the measured quantity X in terms of probabilities. When a restricted amount of measurements are available, a t-Student PDF can be used instead of Gaussian (Normal) PDF [23].

Uncertainty of measurement can be generally expressed as a combination of several uncertainties summarized as U_A and U_B and multiplied to a factor k describing the confidence level of such value [23]:

$$U_{total}\,\big|_{\%LC} = k\sqrt{U_A^2 + U_B^2} \tag{3-9}$$

- α: Level of significance related to an acceptable margin of statistical error.
- $\%LC$: Level of confidence related to a level of significance $(1-\alpha)$.
- k: Coverage factor related to a Probability Distribution Function (PDF) to ensure a level of confidence.
- U_A: Type A uncertainty
- U_B: Type B uncertainty
- U_{total}: Total, expanded uncertainty of measurement.

Uncertainty of measurements compromise, in general, many components. Some of these components can be characterized by experimental standard deviations (Type A uncertainty U_A, related to the experiment). The other components are evaluated from probability distributions based on experience or other information (Type B uncertainty U_B, related to the measurement equipment and other influencing factors). Combination of uncertainties has to be done at same level of confidence, otherwise results are meaningless [23]. Prior the combination, all uncertainties considered are therefore converted to "standard uncertainties", i.e. uncertainties with a level of confidence equal to one standard deviation (Gaussian or Normal Distribution), or equivalently, at 68% level of confidence [23]. After this, the coverage factor k is used to declare the total uncertainty value U_{total} at a specific level of confidence, usually equal or higher than the 68% of a standard deviation (Normal Distribution).

3.4.3.1. Uncertainty type A

With n statistically independent observations (n >1), the best estimate of the true value X can be expressed as the arithmetic mean or average of the individual observed values x_i [23]:

$$X \approx \overline{x} = \frac{1}{n}\sum_{i=1}^{n} x_i$$

The experimental variance, i.e the variance of the measured values x_i, from a set of finite experiments n, is given by [23]:

$$s^2(x) = \frac{1}{n-1}\sum_{i=1}^{n}(x_i - \overline{x})^2$$

The experimental variance of the mean value $s_m^2(x)$ is then the best estimate of the variance of the mean value, for a set of measurements x_i:

$$s_m^2(x) = \frac{s^2(x)}{n} = \frac{1}{n}\frac{1}{n-1}\sum_{i=1}^{n}(x_i - \overline{x})^2$$

The corresponding standard deviation of the mean value $\overline{x}$ is finally given by:

$$s_m(x) = +\frac{s(x)}{\sqrt{n}} \tag{3-10}$$

The standard deviation of the mean value $s_m(x)$, shown in Equation 3-10, is the numeric estimation of U_A, the uncertainty type A [23].

In this research U_A is computed using the same Equation 3-10 for all experimental cases. Each signal is recorded during 1 second and after dived into five 200 ms windows. The last window was ignored for ensuring periodicity of signal within each window. Then the process is repeated for 10 measurements. In summary, a total of n =40 spectra are processed for current and voltage from each EUT listed in Table **3-3**. By means of the FFT digital realization, the standard deviation of the mean value of measured values $s_m(x)$ is computed using the set of 40 magnitudes at the same frequency, for all frequencies between 2-150 kHz.

3.4.3.2. Uncertainty type B

The sources of uncertainty different from Type A are the Type B uncertainties. In this assessment signals were measured directly in time domain. The following sources of U_B are considered:

1. DAQs and sensors accuracy (including lifespan correction): According to Tables **3-2**, **3-1** and Figure **3-4** ([18][24])
2. Temperature (thermal drift)

For combination of all Type B uncertainties, each uncertainty component has to be reported at same level of confidence percentage. Using the 68% level of confidence as suggested in [23], the standard uncertainties for the sources of uncertainty above listed are:

$$U_B^2 = U_{acc}^2 + U_{\Delta t}^2$$

$$U_B^2\,\big|_{68\%} = \left(\frac{Acc * y}{\sqrt{3}}\right)^2 + \left(\frac{\Delta t}{\sqrt{3}}\right)^2 \tag{3-11}$$

- 68%: Level of confidence percentage of a standard deviation in Normal Distribution

- *Acc*: Accuracy of measurement. Assumed to be described by a rectangular probability distribution.
- Δt: Offset drift temperature correction. Assumed to be described by a rectangular probability distribution.

Displays or any other indicator from power quality depicted in Figure **3-1** were avoided in this assessment. Hence, it is assumed that the set of accuracies reported in reference manuals [18][24] include the accuracy related to ADC resolution, so this is not explicitly included in Equation 3-11. Resolution from Analogue/Digital Converter is however used for estimate the amount of significant figures the measurand might have, see Appendix A. Calibration certificates for considered instruments/equipment were not available at the moment of measurements. Instead, the lifespan correction for accuracy reported in reference manuals [18] was used.

Other sources of uncertainty can be included, such as the method of measurement, measurements traceability, variation in grid voltage and even the human influence on measurements [23][26]. However, according to authors experience the sources of uncertainty above listed are expected to be the most influential if rated conditions for the selected power quality monitor are kept.

The same as threshold estimation, the value reported for U_B and consequently for U_{total} will vary with amplitudes and frequency ranges accordingly. U_B is therefore computed for each emission between 2-150 kHz. Once the value of U_B is computed at 68% confidence level, it is combined with the value of U_A computed also at 68% level of confidence. Then, the aggregated value of uncertainty is expanded to a higher level of confidence. All this process is explained in detail in next subsection.

3.4.3.3. Total and expanded uncertainty of measurements

U_{total} is expected to be in Amperes for current measurements and in Volts for voltage measurements. In general, the current value is obtained using a current sensor (either a clamp current sensor, a shunt resistor or a current transducer shown in Figure **3-4**). The current sensors used in this thesis convert a current flow to a voltage drop, and the sensitivity/ratio describing this transformation is called s. Current is then obtained as:

$$i = sv$$

- i: Current
- s: Current sensor sensitivity
- v: Measured voltage

According to the law of error expansion (using Taylor Series) the equation for $U_{total,i}$ is computed as [23]:

$$U_{total,c}^2 = k\left(\left(\frac{\partial i}{\partial s}U_s\right)^2 + \left(\frac{\partial i}{\partial v}U_v\right)^2\right) \tag{3-12}$$

- $U_{total,c}$: Total, expanded uncertainty of current emission
- k: Coverage factor
- i: Current
- s: Current sensor sensitivity
- U_s: Uncertainty of current sensor sensitivity
- v: Measured voltage
- U_v: Total uncertainty for voltage

The two terms in Equation 3-12 contains each one the total uncertainty (U_A and U_B) as explained in Equation 3-9. For voltage measurements it is not used any other sensor/transducer different from DAQs. Hence, the counterpart of Equation 3-12 for voltage is [23]:

$$U_{total,v}^2 = k\left(U_v\right)^2 \tag{3-13}$$

- $U_{total,v}$: Total, expanded uncertainty of voltage emission
- k: Coverage factor
- v: Measured voltage
- U_v: Total uncertainty for voltage

Because of the amount of measurements (40 block of signals for each assessed signal) a normal probability distribution was assumed. That to say, the effective freedom degrees were assumed high enough to assume normal probability distribution of measurements. A coverage factor of 2 was therefore used to have a 95% level of confidence according to Annex G in [23]. Finally, taking into account Equation 3-9, the expression used for the estimation of expanded uncertainty for current and voltage emissions was:

$$U_{total_{c;v}}\Big|_{95\%} = 2\sqrt{U_{A_{c;v}|_{68\%}}^2 + U_{B_{c;v}|_{68\%}}^2} \tag{3-14}$$

3.4.3.4. Uncertainty of measurements using an estimation of accuracy

An example of the implementation of uncertainty of measurements is shown in Figure **3-10**. This example shows a narrowband supraharmonic emission from an LED lamp different from those considered in table **3-3**, and it is intended to be a representative example. Black line represents the mean value for a magnitude at specific frequency, blue and cyan lines

represent the interval defined by U_A and U_B respectively. Finally red lines represent the U_{total} of current measurement. Only emissions higher than the set of thresholds estimated in last subsection are shown in Figure **3-10** and considered for further processing.

Using the "theoretical" accuracy reported in reference manuals, the supraharmonic emission in Figure **3-10** is likely not to appear. Because of this, the estimation between theoretical accuracy and measured accuracy allowed to obtain systematically a better accuracy estimation which is however higher than the effective resolution estimated in Appendix A. The same procedure was developed for voltage spectrum.

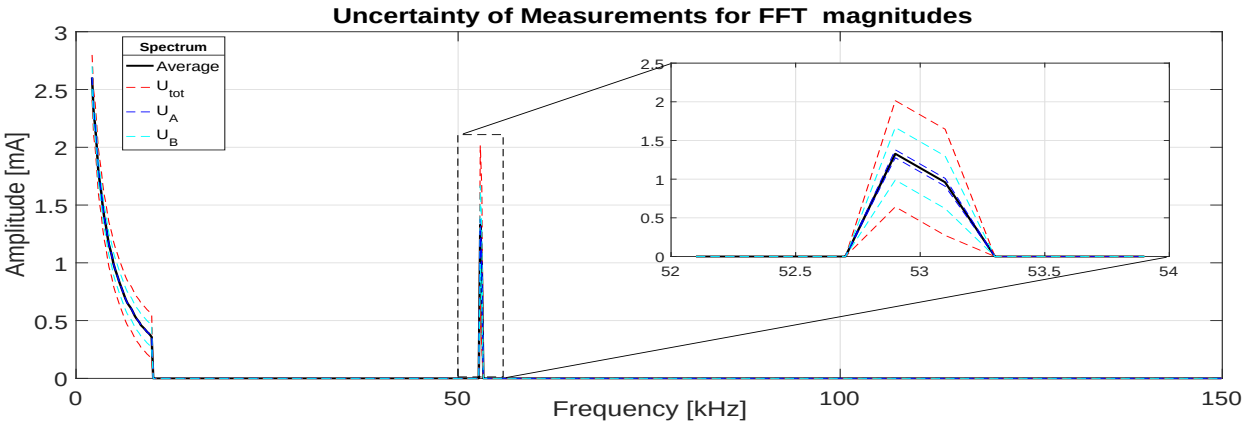

Figure 3-10.: Example of uncertainty of measurement for current spectrum.

3.5. Influence of the measurement setup on supraharmonic emissions

The research in this chapter was intended to show how the measurement setup (voltage source, impedance, sensors and EUT) can influence the waveform distortion between 2-150 kHz. In order to accurately measure the emissions of current and voltage between 2-150 kHz, a metrological assessment was developed in order to clearly distinguish real emissions from noise. In addition, two operation modes were considered for emissions measurement: Idle mode and on-mode. The following paragraphs summarize the results found in this chapter and reported in [27].

According to the results from idle mode, *Zero-flux current sensor used in this assessment emits supraharmonics between 2-150 kHz*, see Figure **3-11**. These emissions are also time-variant, so this kind of sensor could lead to erroneous measurements of EUTs with very low emissions between 2-150 kHz. Therefore, before measuring any emission from EUT under

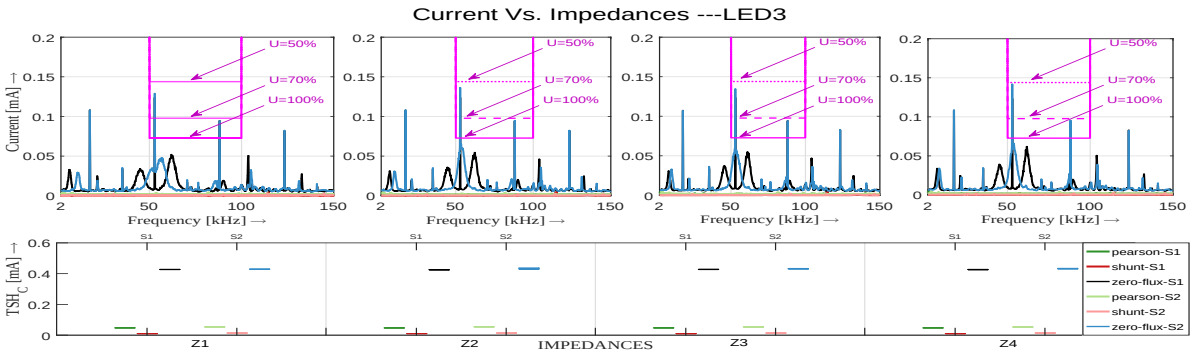

Figure 3-11.: LED3 current emissions between 2-150 kHz in idle mode (similar to LED3 emissions in on-mode). From left to right, emissions are shown using each network impedance ($Z1-Z4$) and each power source ($S1$-$S2$). Dashed lines represent thresholds at different uncertainty values for the 0.1 A measurement range.

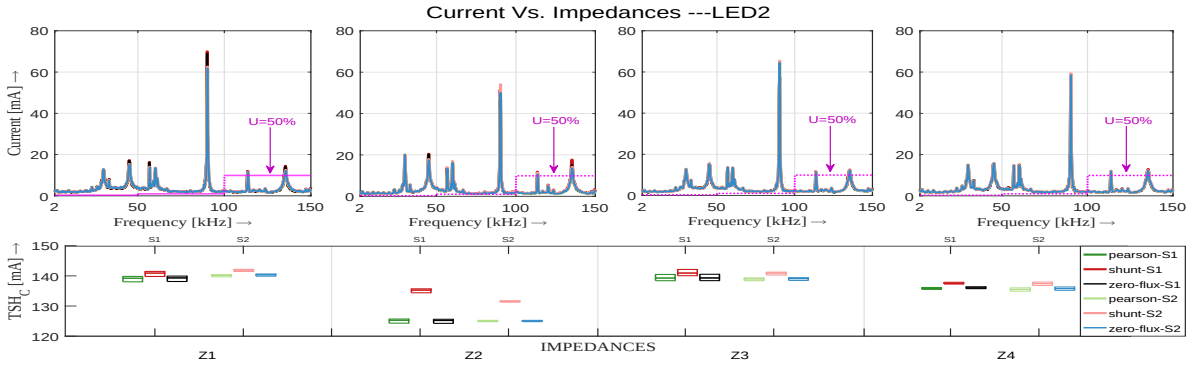

Figure 3-12.: LED 2 current emissions between 2-150 kHz in on-mode. From left to right, emissions are shown using each network impedance ($Z1-Z4$) and each power source ($S1$-$S2$). Legends for current sensors in Fig. **3-11** and **3-12**: $pearson-SX$: Pearson sensor, power source x, $shunt-SX$: Shunt resistor, power source x, $zero-flux-SX$: Zero-flux sensor, power source x

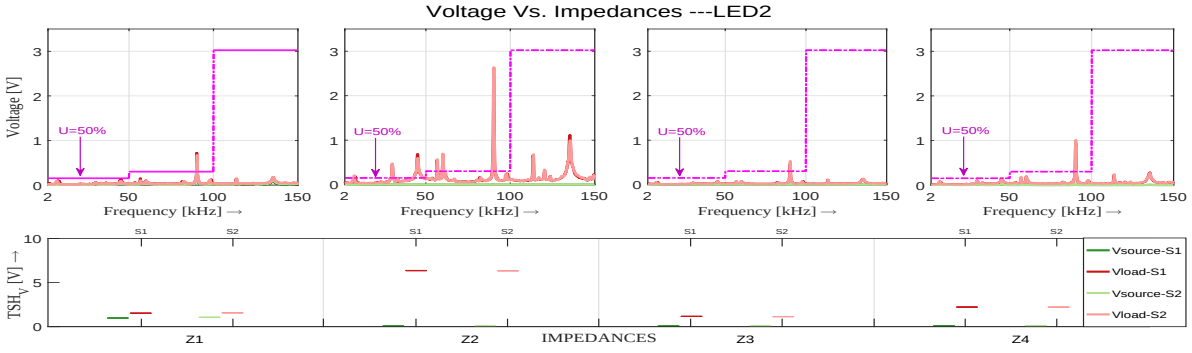

Figure 3-13.: LED2 voltage emissions between 2-150 kHz in on-mode. From left to right, emissions are shown using each network impedance ($Z1-Z4$) and each power source ($S1$-$S2$). Legends for voltages in Fig. **3-13**: $Vsource-SX$: Source voltage, power source x, $Vload-SX$: Voltage at EUT, power source x

rated operation, it is suggested to measure the background emission from measurement setup using the idle mode approach. In general, the supraharmonic components of voltage in idle mode have magnitudes well below the threshold proposed for the measurement system, see Figure **3-13**. Therefore it is assumed that the sources do not emit supraharmonic voltages.

Amplitude of current emissions between 2-150 kHz are reduced in on-mode when EUT are tested using LISN impedance, see Figure **3-12**. The trend observed in all considered cases is a reduction in supraharmonic current. Measured currents using LISN are different from the current emissions using more realistic network impedances, that to say *current emissions between 2-150 kHz tend to be higher in realistic scenarios than those measured using a LISN as network impedance*. In the case of voltage emissions in on-mode, the highest emissions between 2-150 kHz using LED1 and LED2 are not produced by the power sources. This because, when no impedance is used between power sources and EUT, emissions are in both u_S and u_L. However, higher voltage emissions disappear at source (u_S) and persist at load (u_L) when an impedance is used between voltage sources and measurement setup ($Z2, Z3$ and $Z4$). Since these voltage emissions just change in amplitude when using different network impedances but do not disappear completely, these emissions are likely to be attributed to the loads operation (LED1 and LED2).

Finally, when LISN is used as network impedance, authors were able to observe a typical behaviour of low-pass inductive filters: the filtered current is decreased while the corresponding voltage increases. Realistic network impedances used in this assessment did not show such behaviour though. Therefore, *it is suggested to use a realistic network impedance rather than LISN impedances if realistic values of currents and voltages between 2-150 kHz are required, i.e. when EUT are expected to operate under rated conditions and/or directly connected to real low voltage networks*. Otherwise, measurement of current and voltage emissions between 2-150 kHz will lead to different results between experimental and real grid measurements.

Two voltage sources with linear amplifiers were used to supply the EUT, each source at a time. However, each source lead to different variation of emissions for same considered cases. Further research including output impedance of voltage sources is required. In particular, LISN impedance reduces measured current and increases voltage at EUT terminals between 2-150 kHz. The network impedance can have a significant impact on the measurement of supraharmonic emissions. Therefore a comprehensive survey of grid impedances is required in different countries, especially in 230 V and 120 V grids, in order to verify the suitability of the existing LISN/AMN. Current sensors with intrinsic (primary) emissions between 2-150 kHz are not recommended for supraharmonics assessment (i.e. Zero-flux current sensor). EUT input impedance should be also included for a holistic influence and interaction assessments.

3.6. Conclusions

This chapter described the measurement system, experimental setup and metrological aspects used for the identification of supraharmonic emissions. By using a set of sinusoidal voltage sources, network impedances, current sensors and different EUT, it was stated that supraharmonic distortions produced by the operation of different EUT under laboratory conditions strongly depend on the voltage source, equivalent network impedance, sensors used in the measurement setup, and on the input impedance of selected EUT. It was estimated 50% as the maximum percentage of comparison between accuracy estimation and reading (i.e. percentage for metrological threshold), below which supraharmonic emissions were not taken into account for further analysis. Finally, realistic network impedances led to different current and voltage supraharmonic emissions compared to the case with no network impedance and with LISN. Therefore, a discrepancy is expected between supraharmonic emissions measured in laboratory conditions and those measured in real grid.

REFERENCES

[1] Anders Larsson. *On High-Frequency Distortion in Low-Voltage Power Systems*. Luleå University of Technology, 2011.

[2] Sarah Rönnberg, Math Bollen. Propagation of Supraharmonics in the Low Voltage Grid. Report, Energiforsk, Stockholm, Sweden, 2017.

[3] Matthias Klatt, Jan Meyer, and Peter Schegner. Comparison of measurement methods for the frequency range of 2 kHz to 150 kHz. In *2014 16th International Conference on Harmonics and Quality of Power (ICHQP)*. IEEE, may 2014. doi: 10.1109/ichqp.2014.6842791.

[4] IEC. Electromagnetic compatibility (EMC) – Part 4-7: Testing and measurement techniques – General guide on harmonics and interharmonics measurements and instrumentation, for power supply systems and equipment connected thereto. Standard, International Electrotechnical Commission, Geneva, CH, 2002.

[5] IEC. Electromagnetic compatibility (EMC) – Part 4-30: Testing and measurement techniques - Power quality measurement methods. Standard, International Electrotechnical Commission, Geneva, CH, 2014.

[6] Grevener Anne, Meyer Jan, and Ronnberg Sarah. Comparison of measurement methods for the frequency range 2 -150 kHz (supraharmonics). In *2018 IEEE 9th International Workshop on Applied Measurements for Power Systems (AMPS)*. IEEE, sep 2018. doi: 10.1109/amps.2018.8494879.

[7] I. Angulo, A. Arrinda, I. Fernandez, N. Uribe-Perez, I. Arechalde, and L. Hernandez. A review on measurement techniques for non-intentional emissions above 2 kHz. In *2016 IEEE International Energy Conference (ENERGYCON)*. IEEE, apr 2016. doi: 10.1109/energycon.2016.7513893.

[8] S. Subhani, V. Cuk, and J.F.G. Cobben. A literature survey on power quality disturbances in the frequency range of 2-150 kHz. *Renewable Energy and Power Quality Journal*, 1(15):405–410, apr 2017. doi: 10.24084/repqj15.333.

[9] I. Urdea-Marcus, A. Nestor, and P. Clarkson. The influence of the network impedance on the non-sinusoidal (harmonic) network current and flicker measurements. In *CPEM 2010*. IEEE, jun 2010. doi: 10.1109/cpem.2010.5543785.

[10] Daniel Agudelo-Martinez, Camilo Garzon, and Andres Pavas. Interaction of power quality disturbances within 2-150 kHz (supraharmonics): Analytical framework. In *2018 18th International Conference on Harmonics and Quality of Power (ICHQP)*. IEEE, may 2018. doi: 10.1109/ichqp.2018.8378859.

[11] Daniel Agudelo-Martinez, Fabian Rios, and Andres Pavas. Interaction of some low power led lamps within 2–150 khz (supraharmonics). In *2018 18th International Conference on Harmonics and Quality of Power (ICHQP)*. IEEE, may 2018. doi: 10.1109/ichqp.2018.8378815.

[12] D. Zhao and G. Rietveld. The influence of source impedance in electrical characterization of solid state lighting sources. In *2012 Conference on Precision electromagnetic Measurements*. IEEE, jul 2012. doi: 10.1109/cpem.2012.6250921.

[13] Sarah K. Rönnberg, Math H.J. Bollen, Hortensia Amaris, Gary W. Chang, Irene Y.H. Gu, Łukasz H. Kocewiak, Jan Meyer, Magnus Olofsson, Paulo F. Ribeiro, and Jan Desmet. On waveform distortion in the frequency range of 2 khz–150 khz—review and research challenges. *Electric Power Systems Research*, 150:1–10, sep 2017. doi: 10.1016/j.epsr.2017.04.032.

[14] S. Rönnberg and M. Bollen. Measurements of primary and secondary emission in the supraharmonic frequency range 2-150 khz. In -. CIRED, jun 2015.

[15] R Stiegler, J Meyer, J Drapela, T Hanzlik, M Hockel, K Scheida, and S Schory. Survey of network impedance in the frequency range 2-9 khz in public low voltage networks in at/ch/cz/ge. In *(CIRED) 2019, Madrid*. CIRED, jun 2019.

[16] Hameg Instruments Germany. *Line Impedance Stabilization Network, Technical Data*. Rohde & Schwarz Germany, 2019.

[17] Matthias Klatt, Jan Meyer, Peter Schegner, Robert Wolf, and Bernhard Wittenberg. Filter for the measurement of supraharmonics in public low voltage networks. In *2015 IEEE International Symposium on Electromagnetic Compatibility (EMC)*. IEEE, August 2015. doi: 10.1109/isemc.2015.7256141.

[18] Dewetron Inc. *DEWE-3040 Data Acquisition System, Owner's Guide*. Dewetron Inc, 2019.

[19] Ana-Maria Blanco, Ronny Gelleschus, Jan Meyer, and Peter Schegner. Impact of measurement setup and test load on the accuracy of harmonic current emission measurements. In *2015 IEEE International Instrumentation and Measurement Technology Conference (I2MTC) Proceedings*. IEEE, may 2015. doi: 10.1109/i2mtc.2015.7151245.

[20] Daniel Agudelo-Martinez and Andres Pavas. Simulation of supraharmonics: A compact fluorescent lamp (CFL) in single operation. In *2017 IEEE Workshop on Power Electronics and Power Quality Applications (PEPQA)*. IEEE, may 2017. doi: 10.1109/pepqa.2017.7981682.

[21] Ana Maria Blanco, Manish Gupta, Aurora Gil de Castro, Sarah Ronnberg, and Jan Meyer. Impact of flat-top voltage waveform distortion on harmonic current emission and summation of electronic household appliances. *Renewable Energy and Power Quality Journal*, 1:698–703, apr 2018. doi: 10.24084/repqj16.437.

[22] Anne Grevener, Jan Meyer, Sarah Rönnberg, Math Bollen, and Johanna Myrzik. Survey of supraharmonic emission of household appliances. *CIRED - Open Access Proceedings Journal*, 2017(1):870–874, oct 2017. doi: 10.1049/oap-cired.2017.0458.

[23] BIPM. Evaluation of measurement data — Guide to the expression of uncertainty in measurement. Standard, Bureau International des Poids et Mesures - BIPM, 2008.

[24] Pearson Electornics Inc. *Pearson current monitor model 411, datasheet*. Pearson Electronics Inc, 2019.

[25] Semyon G. Rabinovich. *Evaluating Measurement Accuracy*. Springer International Publishing, 2017. doi: 10.1007/978-3-319-60125-0.

[26] ICONTEC. Requisitos generales para la competencia de los laboratorios de ensayo y calibración. Standard, ICONTEC, 2005.

[27] D. Agudelo-Martinez, A.M. Blanco, R. Stiegler, F. Pavas, and J. Meyer. Influence of measurement setup on the emission of devices in the frequency range 2-150 khz. *Power Tech 2019*, 2019(1):to appear, 2019.

4. Identification of supraharmonics in single operation: Emissions

The identification of supraharmonics require to make a clear distinction between those emissions produced by the operation of assessed Equipment Under Test (EUT) and those produced by the measurement setup itself. In fact, different measurement systems might lead to a different perception of supraharmonic emissions, and these might be also different if measurements are carried out in real low voltage grids. Once the measurement system and experimental setup are defined, the waveform distortion related to a specific EUT could be identified. This chapter describes the experimental setup and the results from the assessment of supraharmonic emissions in EUT single operation. First, the three different voltage sources and four network impedance used are described. After, current and voltage supraharmonic emissions from EUT in single operation are graphically presented using spectrograms and mean FFTs. Finally, using the total supraharmonic current or voltage index ($TSH_{C;V}$), as well as the coherence function, it is shown how supraharmonic emissions are different for the selected EUT according to the voltage source and network impedances used.

4.1. Measurement and Experimental setups

The measurement system and experimental procedure presented in previous chapter served as a starting point to the assessment of waveform distortions between 2-150 kHz, also known as supraharmonics. Results from such assessment, however, suggested some changes in the original measurement and experimental setups were required. Main changes were made in the elements used at each stage in Figure **3-1**, depicted here again for reference completeness in Figure **4-1**. Other changes, as the visualization of supraharmonic emissions in time-frequecy domain as well as the aggregation of emissions in frequency and time domain are included in this chapter.

Next subsections describe the similitude and changes made to the measurement and experimental setup presented in Chapter 3: *Measurement System for supraharmonics in low voltage networks*. Since spectral coherence concept is introduced as a tool for assessing the supraharmonic emissions, the signal processing stage is also modified accordingly.

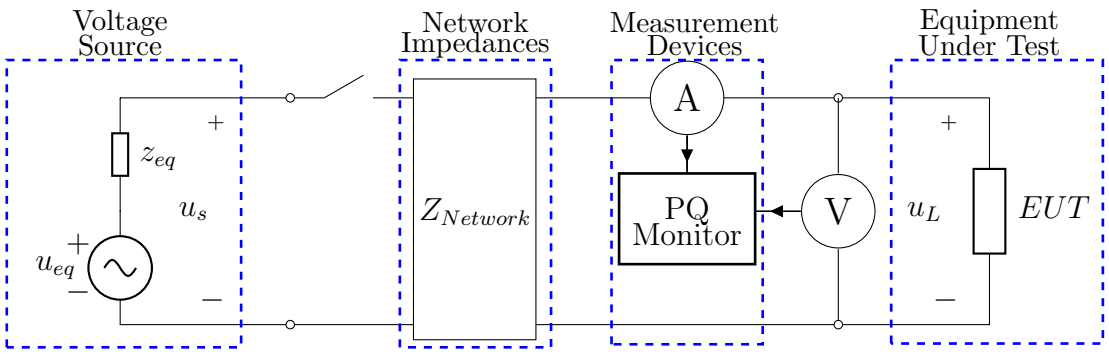

Figure 4-1.: Measurement setup for assessing single-phase emissions between 2-150 kHz.

4.1.1. Measurement Setup

In previous chapter two voltage sources, mainly composed by a signal generator and a linear amplifier, were used (each at a time) for supplying selected EUT. Results showed that different voltage sources might have a different impact over the waveform distortion between 2-150 kHz. This influence seems to strongly depend on the voltage source's output impedance. Nevertheless, only one voltage source acting as both "pure sinusoidal" and "distorted" was used in this chapter for the assessment of the supraharmonics under EUT single operation.

Four network impedances were defined in Chapter 3: *Measurement System for supraharmonics in low voltage networks*, for the measurement setup depicted in Figure **4-1**. Results using Z3 and Z4 were similar, and therefore in this chapter only Z1 (no network impedance), Z2 (LISN impedance) and Z3 (measured grid impedance) are used. The purpose is again to find eventual differences in the emissions between 2-150 kHz when each of this impedances is used.

From results of previous chapter, the zero-flux transducer showed a measurable background emission between 50-100 kHz when no current was expected to be measured. Because of these results, and the relative error of current sensors (shown in Figure **3-4**), the Pearson current sensor was selected for the assessment of current supraharmonics in EUTs single operation.

It was required a bigger amount of devices for assessing supraharmonic emissions than that used in Chapter 3: *Measurement System for supraharmonics in low voltage networks*. Because of this, a total amount of 12 led lamps were measured in both idle and on-mode tests. Taking into account the PFC classification mentioned in Chapter 3 and completely described in [1], at least two devices for no PFC, capacitive, passive PFC and active PFC topologies were selected. Table **4-1** summarizes main features of selected EUT for the assessment in

single operation.

Table 4-1.: Equipment Under Test (EUT) and rated values.

PFC	Power [W]	Voltage [Vrms]	Frequency [Hz]	EUT	Nomenclature
no PFC	12	220-240	50-60	3	n003, n005, n039
Capacitive	10	100-240	50	3	c022, c026, c027
passive PFC	1	230	50	3	p058, p059, p061
active PFC	9	230	50	3	a004, a014, a027

4.1.2. Experimental Setup

The experimental setup described in previous chapter was composed by three items:

- Stabilization time: $\geq$ 60 minutes
- Measurements: 40 signal blocks of 200 ms each one
- Test modes: Idle mode (open circuit) and On-mode (normal operation)

This experimental setup showed a variation of main current magnitude through measurements less than 1%. That to say, the experimental setup presented in Chapter 3: *Measurement System for supraharmonics in low voltage networks*, produced stable, reproducible measurements and showed satisfactorily results. Hence, this experimental setup is kept unchanged.

4.1.3. Signal Processing

Two approaches were selected for the assessment of supraharmonic emissions in EUT single operation: time-frequency domain and frequency domain. Both approaches are presented in the following paragraphs and only one is selected for further analysis of signals.

4.1.3.1. Spectrogram: Discrete STFT

From measurements analyzed in the previous chapter and other measurements performed by researchers all over the world, it is known the time-varying behaviour of the conducted emissions between 2-150 kHz [2][3][4][5]. In order to know how frequency components vary through time, the Short-Time Fourier Transform (fundamental principle of the so called "spectrogram") is implemented. The concept behind STFT is quite similar to the computation of Fourier Transform for periodical signals (infinite energy): just one portion (block) of

the signal in time domain is selected for the transformation into frequency domain. In the case of STFT, the Discrete Fourier Transform DFT is applied to a set of sub-windows of the original measurement window; the windows can be or not overlapped, in order to smooth results between contiguous sub-windows in time domain. Further details about the formulae and digital implementation can be found for example in [6]. In this thesis, the function "spectrogram" from Matlab© was used. Result from the spectrogram function is proportional to the squared magnitude of the Discrete Short-Time Fourier Transform (Discrete STFT)[7]:

$$S_m(f) \propto |X_m(f)|^2, \quad m = 1, 2, ...k \tag{4-1}$$

$$X_m(f) = \sum_{n=-\infty}^{\infty} x\,[n]\, g\,[n - mR]\, e^{-j2\pi fn}, \quad m = 1, 2, ...k \tag{4-2}$$

Where:

- $S_m(f)$ Spectrogram of signal section m.
- $X_m(f)$: Discrete Fourier Transform of windowed data centered about time mR.
- $g(n)$: Window function of length M.
- R: Hop size between successive DFTs.

The frequency resolution of the analysis is expressed using the equation below:

$$df = \frac{1}{T} = \frac{1}{Ndt} = \frac{1}{Nt_s} \tag{4-3}$$

Where N is the amount of samples and t_s the sampling time. In order to analyse signals in Time Domain with enough time resolution (every 2% of one fundamental voltage period) and to obtain a good performance from FFT algorithms the following frequency resolution is obtained:

$$T = \left(\frac{1}{50Hz}\right)\left(\frac{2}{100}\right) = 0,4ms$$

$$N = Tf_s = (0,4ms)(1Msps) = 400\,samples$$

$$df = \frac{f_s}{N} = \frac{1Msps}{2^{nextpow2(400)}} = \frac{1Msps}{512} \approx 2kHz$$

This frequency resolution allowed a trade-off between time and frequency resolution for supraharmonics general identification. This means that the higher the amount of samples, the better the frequency resolution but the worse the time resolution, for a fixed length of analyzed signal. If either a shorter frequency band or a shorter time signal block are selected using this representation for the selected EUT, relevant information about "emissions

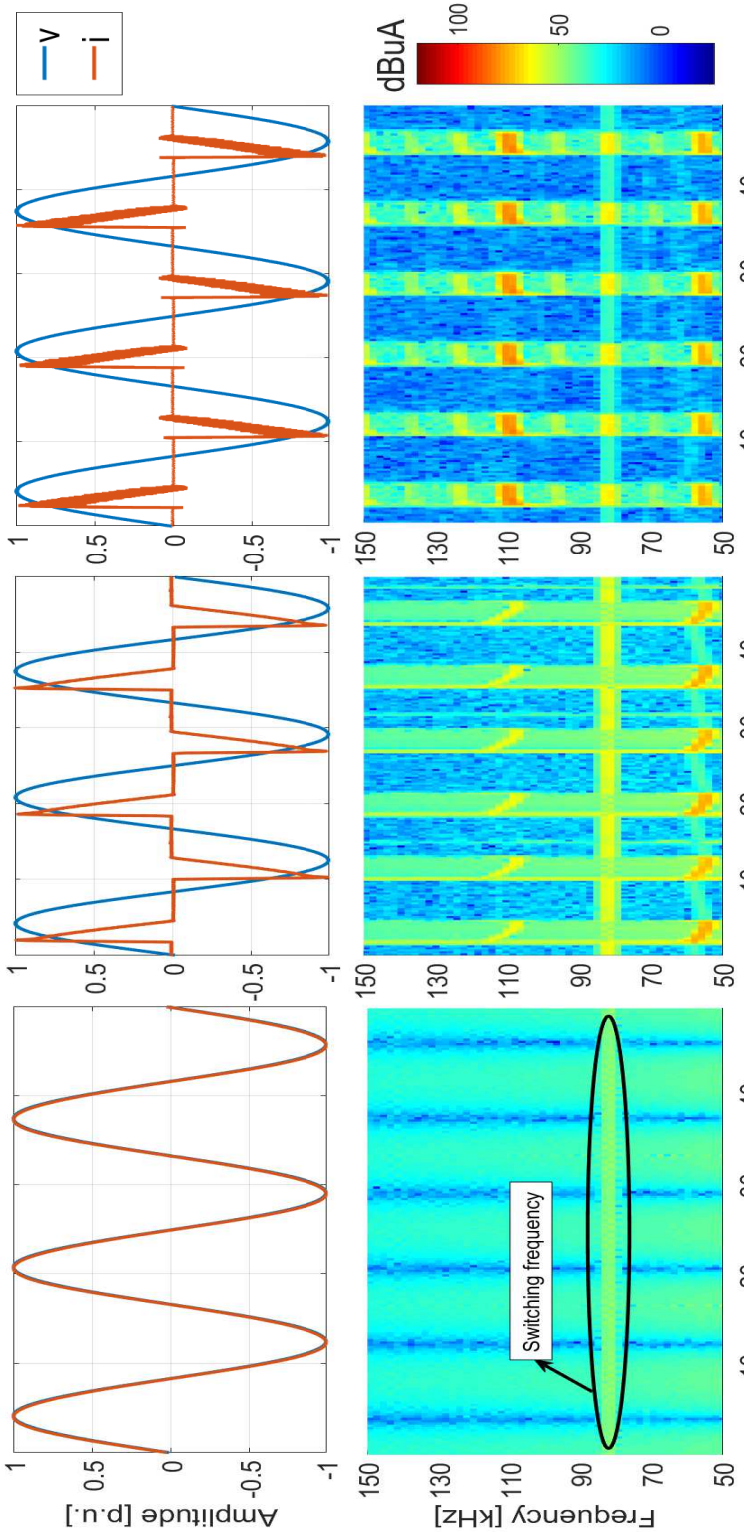

Figure 4-2.: Current emissions from each device under single operation: Fig. 7a) Current emissions from Power Source (using an incandescent lamp); 7b) Current emissions using CFL1; 7c) Current emissions using LED1 [5]

fingerprint" could be lost in time and frequency domains respectively. Therefore, this frequency band of $2kHz$ used in spectrogram representation was a best-effort parameter that also matched the criteria suggested in [8] for visualization purposes. Finally, an overlap of 256 samples was used in the sliding window, as well as a logarithmic scale of spectrograms, so as to improve phenomena visualization.

$$i_{[dBuA]} = 20log_{10}\left(\frac{i_{[A]}}{1\mu A}\right) \tag{4-4}$$

Since the set of analyzed signals included the component at main frequency (50 Hz), Hanning windowing function was used along the analysis (default windowing function of Matlab ©) for better visualization. Figure **4-2** shows an example of spectrogram, whose original amplitude was scaled to obtain logarithmic scale (dbuA, see Equation 4-4) for current or voltage signals respectively. More details about the procedure and EUT used in Figure **4-2** can be found in [5].

4.1.3.2. Mean FFT

The other approach was to process the signal in frequency domain using a mean, grouped FFT. This grouped FFT is based on some procedures suggested in [9] which, among others, suggests a 200-Hz grouping methodology. Although information about emissions behaviour within a fundamental cycle (50 or 60 Hz) is hidden using FFT, the purpose of this assessment is to identify the overall behaviour of supraharmonic emissions using the fundamental period as the time resolution of the analysis. That to say, the purpose is to identify those emissions that in average, are not negligible when analyzing an entire number of signal period. At this point it is important to recall the difference between time resolution, given by the sampling frequency f_s, and the time resolution of the analysis, given in terms of fundamental period (inverse of fundamental frequency). Analysis of disturbances within a time window (signal block) shorter than the fundamental period is then not covered in this thesis.

The stages for signal processing using mean FFT and based to some extent on [9] are listed below:

1. Signal pre-processing in time domain: This stage aims to select an adequate signal block, 200 ms long, according to [9].
    - Signal filtering: 200 ms of signal are selected. After double-sided FFT computation, all frequency components different from main frequency are suppressed. Finally, inverse FFT is performed and now the signal has only main frequency in time domain.
    - Zero-cross detection: Selecting the first suitable sample from which time domain signal should start, that is, when the main component amplitude of signal in time domain is equal or close to zero.

- Amount of samples: Compute the amount of samples that produce a periodical signal and therefore, a minimum leakage effect in FFT.

2. Signal processing in frequency domain:
   - FFT: Single-sided FFT. Adequate factors are used to obtain RMS values of spectrum magnitudes.
   - Aggregation in frequency domain: Emissions between 2-150 kHz are grouped into 200-Hz bands as shown in Equation 4-5 and described in [4],[9]:

$$TSH_{C;V} = \sqrt{\sum_{B=1}^{705} Y_B^2} \tag{4-5}$$

     - Y: RMS value for emissions grouped in 200-Hz bands [9]
     - B: Each of the 200-Hz emission groups between 2-150 kHz
     - $C;V$: Current or voltage signals

     This aggregation highlights the dominant emissions within the 200 Hz bands. For example, smoothing DC filter (after rectification stage) usually leads to rippled voltages at double of main frequency, i.e. 100 or 120 Hz. The side lobes resulting from the modulation between this rippled signal and any other higher frequency signal are included in the 200-Hz aggregation bands. Other features of using a 200-Hz aggregation bands can be found in [9] and [10].

3. Signal processing in time domain: In total 40 signal blocks, 200 ms long each one, are processed in frequency domain as described above. In order to obtain representatives values from these 40 signal blocks, an averaged FFT is computed along each frequency component. This aggregation in time domain shows the predominant emissions, i.e. those which are in average not negligible.

4.2. Supraharmonic emissions in single operation

Identification of supraharmonic emissions was carried out using the measurement system and experimental setups described in last section. This identification aimed to show the supraharmonic emissions attributable to selected EUT and therefore, the emissions under EUT single operation were analyzed. Single operation just means that only one EUT is assessed at a time, and that all eventual interactions registered between measurement system and EUT are mostly attributable only to the operation of EUT supplied by that specific measurement setup. The reasons why the mean FFT methodology is preferred over the spectrogram, as well as the consideration of coherence function for "changes identification", are also described.

4.2.1. Supraharmonic emissions in Base Case: Sinusoidal supply and none network impedance

As mentioned in Chapter 2: *Supraharmonics: Waveform distortion between 2-150 kHz*, primary emissions are the part of the voltage or current at the device terminals that are driven by sources inside the device, whilst secondary emissions are the part of the voltage or current at the device terminals that are driven by sources outside the device. Emissions in base case are assessed using a sinusoidal voltage source and none impedance between voltage source and the experimental setup, see the measurement setup in Figure **4-1**. Because of this, emissions between 2-15 kHz are attributable to the interaction between the selected EUT and the measurement setup, given that no other devices used in Figure **4-1** have conducted emissions within this frequency range.

Two approaches were initially used to assess supraharmonic emissions in base case: Spectrograms (time-frequency domain) and mean FFT (frequency domain). Initially, Spectrograms were intended for the analysis of single blocks of signals, whilst the mean FFT for containing information from several blocks of signals (aggregation in frequency and time domains). Moreover, two different estimations of the minimum measurable amplitudes were considered: the ADC Effective Resolution described in Appendix A and the Threshold estimations described in Chapter 3: *Measurement System for supraharmonics in low voltage networks*. The minimum measurable amplitudes resulting from the computation of ADC Effective Resolution are lower than the thresholds deduced in Chapter 3, since the former one does not include explicitly the estimation of uncertainty of measurements. Hence, the thresholds deduced in Chapter 3 are more rigorous compared with the ADC Effective Resolution for the estimation of the minimum reliable, measurable amplitudes. On the one hand, the mean FFT approach takes into account several blocks of measured signals, so the Type A uncertainty has to be considered. Therefore, the mean FFT approach uses the Threshold estimation for minimum measurable amplitudes. On the other hand, the ADC Effective resolution was used in spectrograms. In summary, the emission of supraharmonics in base case are compared by means of Spectrograms (using minimum measurable amplitudes given by ADC Effective resolution, Appendix A) and mean FFT (using minimum measurable amplitudes given by Threshold estimation, Chapter 3).

Figures **4-3** to **4-6** show the spectrogram of current and voltage signals for each device topology listed in Table **4-1**. The minimum amplitude shown in colorbars were computed using minimum measurable amplitudes given by ADC Effective resolution, Appendix A. 40 ms of signal were selected for the spectrograms (STFT). Amplitude in time domain is in p.u. for visualization purposes. The closer to red color is the spectrogram, the closer to the maximum amplitude the emissions is. Main frequency component is expected to be the predominant emission up to 150 kHz. High amplitude emissions are no expected in voltage

signal, since a linear voltage supply and no additional network impedance were used in the measurement setup depicted in Figure **4-1** and in Chapter 3.

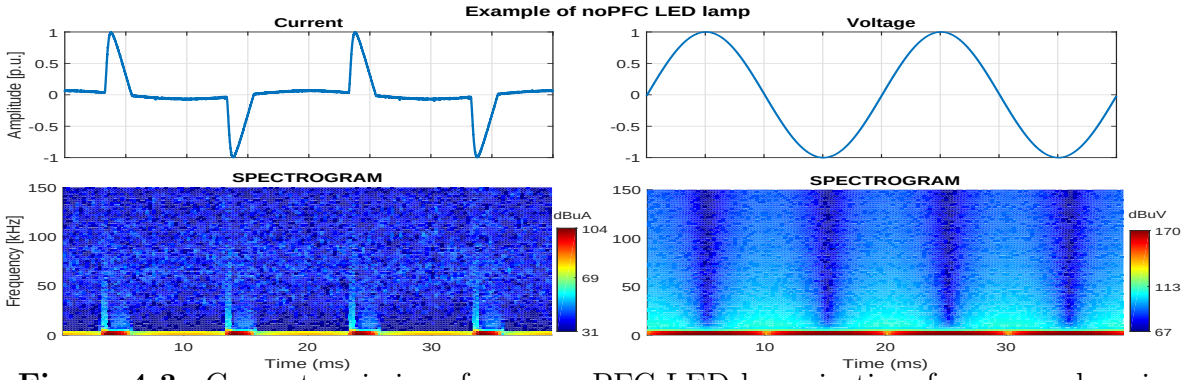

Figure 4-3.: Current emissions from a noPFC LED lamp in time-frequency domain.

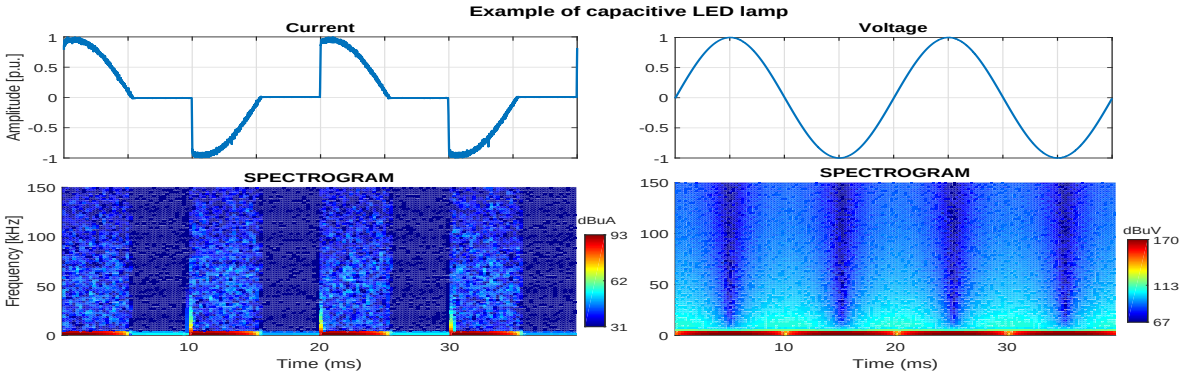

Figure 4-4.: Current emissions from a capacitive LED lamp in time-frequency domain.

Figure **4-3** shows the spectrogram of emissions up to 150 kHz from a noPFC LED lamp. According to the topology classification described in [1], noPFC LED lamps usually have a low power factor ($PF < 0.6$) and a high Total Harmonic Distortion ($THD > 80\%$). However, the predominant emissions are below 2 kHz. These devices consist of a simple power supply with diode bridge rectifier and smoothing capacitor. The capacitive topology for LED lamps is a special case of noPFC topology, where the power factor is also low ($PF < 0.6$) but a Total Harmonic Distortion lower than in the noPFC case ($THD < 30\%$) [1]. Because of the internal circuit, the noPFC and capacitive topologies are not expected to produce waveform distortions between 2-150 kHz. Figures **4-3** and **4-4** show that the emissions at supraharmonic range are very low and mainly produced when current rapidly changes from zero to the maximum or minimum peak values. These emissions can be then related to the high change in current when diodes in rectifier bridge change from non-conduction to conduction state (zero-crossing distortion [1][11]). Because of the measurement setup described in Chapter 3, no emissions between 2-150 kHz are expected in voltage signals depicted in

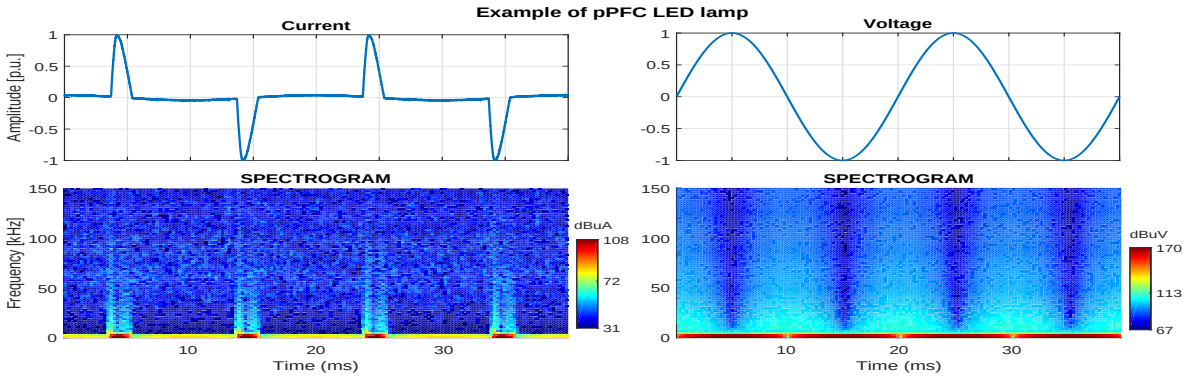

Figure 4-5.: Current emissions from a passive PFC LED lamp in time-frequency domain.

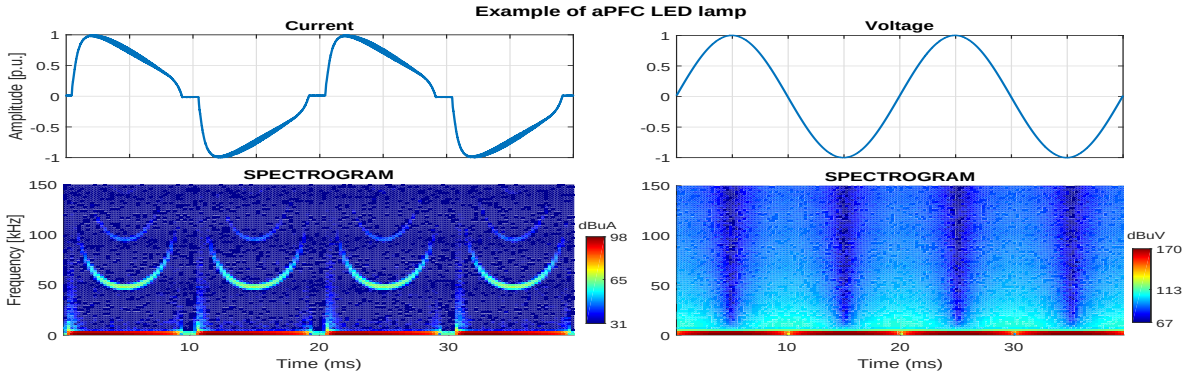

Figure 4-6.: Current emissions from an active PFC LED lamp in time-frequency domain.

Figures **4-3** to **4-6**.

Figure **4-5** and **4-6** show examples of the current and voltage spectrograms for a passive PFC and active PFC from two lamps listed in Table **4-1**. The passive-PFC topology consists on a power supply (diode-based rectifier and smoothing capacitor) with additional inductors and capacitors before or after the rectifier in order to improve the Power Factor. In other words, a passive PFC can be understood as a low-pass filter in order to have an input current which resembles the waveform of the sinusoidal line voltage [1] [11]. In case of Figure **4-5**, the spectrogram of passive PFC LED lamp shows a similar emission pattern between 2-150 kHz than the no-PFC spectrum. However, in Figure **4-5** the emissions might be related to current changes from zero to peak value, and from peak value to zero (zero-crossing distortion [1][11]). Again, this emissions seem to be consequence of the change between non-conduction to conduction state of rectifier bridge.

The active-PFC topology is composed by the power supply (rectifier bridge and smoothing capacitor) with advanced control circuits that modify the current waveform to resemble the voltage waveform. In case of the spectrogram of an active PFC LED lamp, the emission pattern is notably different than the spectrograms from other circuit topologies. Figure **4-6** shows a not negligible emission pattern between 2-150 kHz when current main component

is different from zero. In general terms, the input current signal using active PFC resembles the voltage signal better than in the previous three cases, see Figures **4-3** to **4-6**.

In the case of electric vehicle (EV) chargers, the typical circuit topology for single-phase chargers is the bridge rectifier with a boost converter [12]. Nevertheless, the buck converter is also found in low-power LED lamps as shown in [13]. The first control stage on these converters is a current controller that shapes the input current of converter for obtaining a sinusoidal grid current in phase with voltage grid [12]. Most of the supraharmonic emissions are then related to the ripple on the current measured at the Point of Common Connection (PCC). Two of the common control strategies used for boost converters are continuous conduction mode (CCM) and boundary conduction mode (BCM), the latter having less size and losses than the first one. Each control strategy has a different current waveform in the inductor typically used in buck converters, see [12] for details. The current measured at PCC is then comparable to the current at converters inductor, and this is composed by an averaged current (main frequency) and a rippled current produced by active switching (frequencies between 2-150 kHz) [12].

Additionally, the converters' switching frequency can be also fixed or variable over the time. The spectrum of fixed frequency case is characterized by the highest amplitude at switching frequency and lower, decreasing amplitudes at its harmonics (harmonic supraharmonics). The variable switching frequency case is intended to spread the emissions energy through the spectrum and therefore reducing emissions amplitude at individual spectral components. For the latter case, the switching frequency varies within the power cycle with its minimum and maximum values at grid voltage's peak and zero-cross values respectively. Figure **4-6** shows an example of an LED lamp using a variable switching frequency converter.

The spectrogram methodology allowed authors to observe the behaviour of waveform distortions between 2-150 kHz in time and frequency domains, when EUT listed in Table **4-1** performed in single operation. Using the spectrograms, it was stated that supraharmonic emissions from most of the LED lamps having active PFC vary within the power cycle. However, the identification proposed in this thesis is intended to show the typical emission features (frequencies and amplitudes) using an entire amount of power cycles as suggested for example in [9]. This identification is useful for aggregation purposes when long measurements are carried out, and offers enough information about "average" waveform distortions. Hence, the variation of emission within a single power cycle overflows the purpose of this thesis.

The mean FFT spectrum allowed authors to know the "averaged" waveform distortion between 2-150 kHz using 40 signal blocks of 200 ms each one. Figures **4-7** to **4-10** show examples of emissions between 2-150 kHz using the Threshold estimation deduced in Chap-

ter 3 for each topology listed in Table **4-1**. U_A, U_B and U_{tot} are respectively the type A, type B and total uncertainty values in frequency domain.

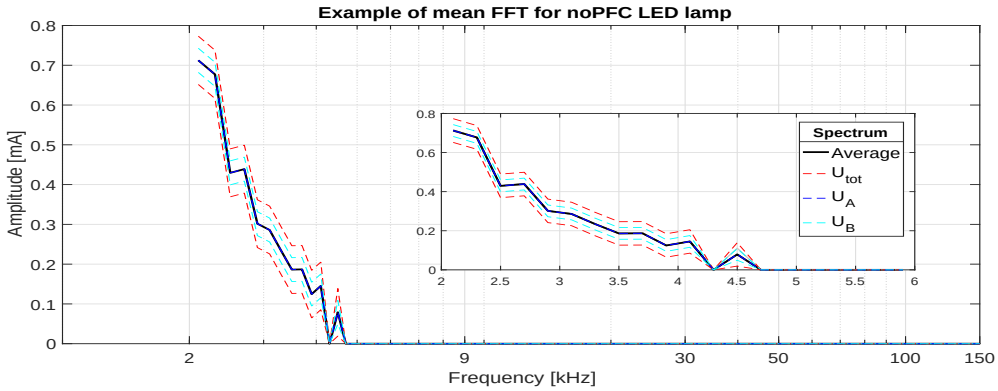

Figure 4-7.: Current emissions from a noPFC LED lamp in frequency domain.

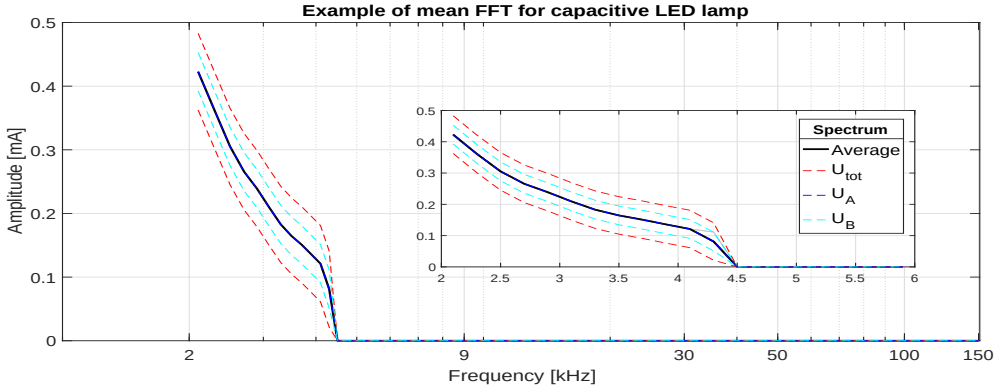

Figure 4-8.: Current emissions from a capacitive LED lamp in frequency domain.

The same as spectrograms shown in Figures **4-3** to **4-6**, the mean FFT spectrum shows that aPFC was the topology having the highest emissions between 2-150 kHz. Devices using other PFC topologies had decreasing emissions up to 5 kHz and were most likely related to residual emissions from harmonic range [9]. Gray lines in Figure **4-10** represents the 40 current measurements performed, and most of them lied within the interval of confidence given by total uncertainty U_{tot}, as expected. Emissions in Figure **4-6** shows time-frequency varying emissions between $\sim$ 50 kHz and $\sim$ 80 kHz as consequence of active-switching circuits. However, because of the application of thresholds estimated in Chapter 3, Figure **4-10** only shows emissions between 46.5 kHz and 50 kHz.

Although spectrograms give more information about waveform distortions behaviour in time-frequency domain, the mean FFT was selected for aggregating several measurements in both frequency and time domains. Spectrograms can be used in future work in assessing waveform

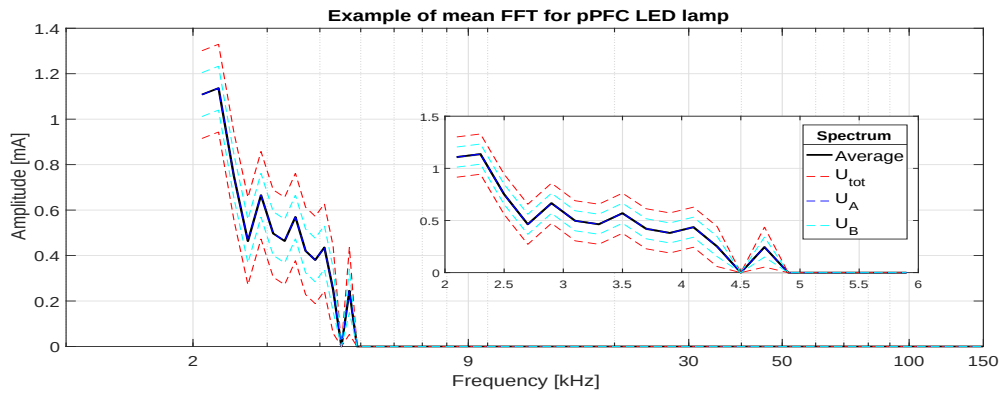

Figure 4-9.: Current emissions from a passive LED lamp in frequency domain.

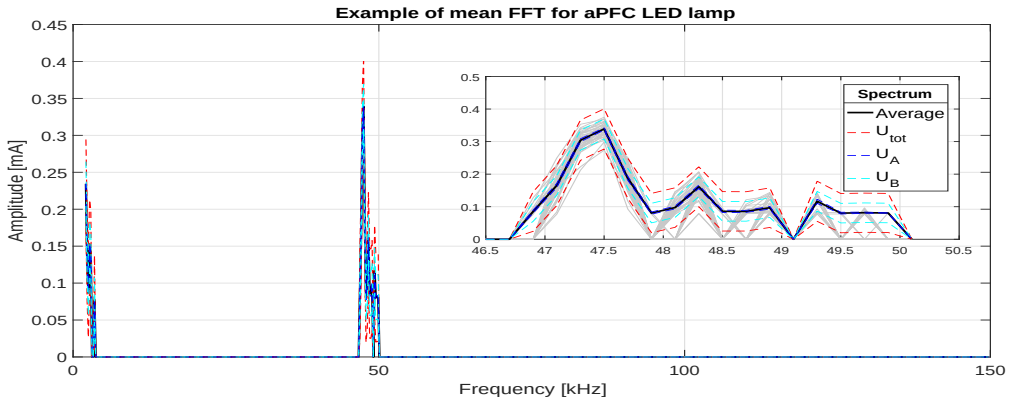

Figure 4-10.: Current emissions from an active LED lamp in frequency domain.

distortion within a power cycle.

4.2.2. Variations in supraharmonic emissions: Distorted supply and different network impedances

The voltage source and network impedance are not under control in real grid measurements. Because of this, it is expected that distortion of voltage source and different network impedances at EUT terminals lead to variation of emissions between 2-150 kHz compared to the emissions in the base case (sinusoidal voltage source, no network impedance at EUT terminals).

In order to know how emissions may vary under EUTs single operation, Table **4-2** lists base case and six deviations from this base case in the experimental setup.
Z2 and Z3 impedances correspond to LISN and a measured network impedance respectively, see Figure **4-1**. Distorted voltage means a superimposed signal of 1V at 20 kHz. This emission can be found for example in street LED lamps, EV chargers, PV Inverters, household devices and Power Line communication [14]. Finally, the real grid case aims to show how

Table 4-2.: Variations of experimental setup base case

Experiment	Description	
	Voltage source	Network impedance
1	Sinusoidal	-
2		LISN (Z2)
3		Measured (Z3)
4	Distorted	-
5		LISN (Z2)
6		Measured (Z3)
7	Grid	

emissions might be different when EUT are supplied directly by the grid in single operation, with an uncontrolled distortion of the voltage source and a real low voltage installation as the network impedance.

Since EUTs listed in Table **4-1** are built with non-linear circuits, emissions from the seven cases listed above could differ in both amplitudes and frequencies. Spectral coherence was then used as a systematic tool for the comparison of base case spectrum and other proposed cases.

The spectral coherence is a complex function in frequency domain that can be used to find common emissions in the spectrum of two different signals. This was used as a "similarity" index which indicates how well at each frequency a function x, in this case the spectrum of emissions in base case, corresponds to y, in this case the spectrum of emissions in other cases proposed. This uses the concept of Cross-Power Spectral Density CPSD. A peak in cross-power spectrum means that there is a common frequency present in both signals. However, peaks may appear at same frequencies but at different times. Because of this, the mean value of CPSD of several signal blocks is used for the computation of spectral coherence function (Welch method). In general terms, the spectral coherence function can be expressed as follows:

$$C_{xy}(f) = \frac{E[S_{xy}]}{\sqrt{E[S_{xx}]E[S_{yy}]}} \tag{4-6}$$

The Magnitude Sqare Coherence MSC is then:

$$C_{xy}^2(f) = \frac{E[S_{xy}]^2}{E[S_{xx}]E[S_{yy}]} = \frac{E[S_{xy}S_{xy}^*]}{E[S_{xx}]E[S_{yy}]} = \frac{E[X(f)Y^*(f)]E[X^*(f)Y(f)]}{E[X(f)X^*(f)]E[Y(f)Y^*(f)]} \tag{4-7}$$

- Pxy: Cross-Power Spectral Density
- Pxx, Pyy: Power Spectral Densities

- $E[]$: Expected value

Note that if no expected (average) value is used for both Power and Cross-Power Spectral Density computation of signals, the equation for Magnitude Square Coherence would always equal 1. Further details about spectral coherence computation can be found in Appendix B.

Supraharmonic emissions are defined as harmonic and interharmonic waveform distortions between 2-150 kHz, therefore, the computation of harmonics and interharmonics angle must be carried out so as to use the spectral coherence function as a comparison index. Angles of harmonics can be estimated from signal in time domain as suggested in [15] and depicted in Figure **4-11**. First, the 200 ms signal block is defined. After that, first zero-cross sample is identified and an entire amount of periods are detected. The relationship between changes in phase angle and samples are expressed by Equation 4-8:

$$\Delta\phi(h) = \frac{2\pi}{N_m} = \frac{2\pi}{\left(\frac{1}{f_g h}\right) f_s} = 2\pi h \left(\frac{f_g}{f_s}\right) \left[\frac{radians}{sample}\right] \tag{4-8}$$

between kHz

- $\Delta\phi$: Radians per sample
- N_m: Samples in signal main period
- h: Harmonic order (h=1,2,...)
- f_g: Power grid frequency
- f_s: Sampling frequency

The value for harmonic angles as a function of samples N is consequently:

$$\phi_h(N) = (\Delta\phi(h))\, N \tag{4-9}$$

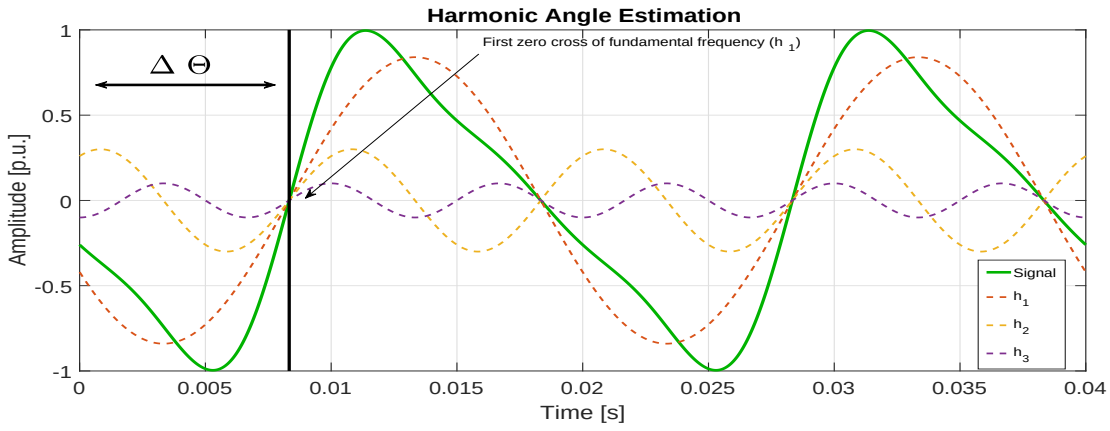

Figure 4-11.: Example of harmonic angle estimation.

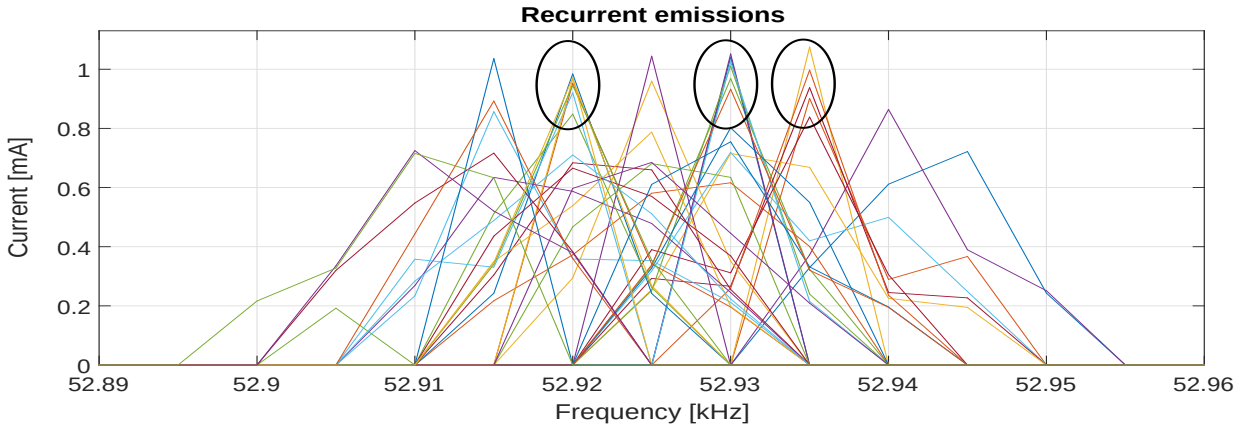

Figure 4-12.: Variation of emissions between 52.8 and 53 kHz

As stated in Equation 4-9, $\Delta\phi$ varies proportionally with harmonic order. Since an entire amount of signal periods are considered for Equation 4-8, the angle computed using Equation 4-9 is by definition only useful to estimate angles of harmonic emissions. Nevertheless, supraharmonics are likely not to be harmonic of the fundamental frequency and therefore, this angle estimation would have limitations.

On the other hand, the angle estimation of interharmonics using Equation 4-9 may vary among different measurements. This because it is unlikely that the starting point of signal matches the same sample among measurements. Moreover, harmonics of supraharmonics may not match an entire multiple of "supraharmonic main frequency" in the spectrum proposed. Again, the estimation of the angle fo interharmonics would have limitations.

Finally, emissions between 2-150 kHz showed a "dynamic" behaviour in terms of amplitude and frequency: Figure **4-12** shows how emissions vary between 52.89 and 60 kHz using 40 block signals, 200 ms each one. Because of the aforementioned reasons, the tradtional approach for the estimation of harmonic angles was not used for the angle estimation of supraharmonic emissions.

Instead of estimating the angles for supraharmonic emissions directly from measurements, a different approach was considered. In order to have a reproducible, frequency aggregated, time aggregated and useful value for the assessment of supraharmonic emissions, it is proposed in this research *an artificial assignment rule for supraharmonic angle values: a linear variation of artificial angles within an emission band*. Since the harmonic angles can be estimated with Equation 4-9, there are two option to apply this artificial assignment rule for emissions angle: the artificial rule can be applied for all interharmonic emissions between two contiguous harmonics, or the artificial assignment rule can be applied within each 200-Hz frequency band defined in frequency aggregation methodology, see Equation 4-5 and Figure

4-13. The latter is rather a relative, artificial angle assignment with respect to the angle of first emission within each emission band. This option is selected as the artificial assignment rule for angles between 2-150 kHz.

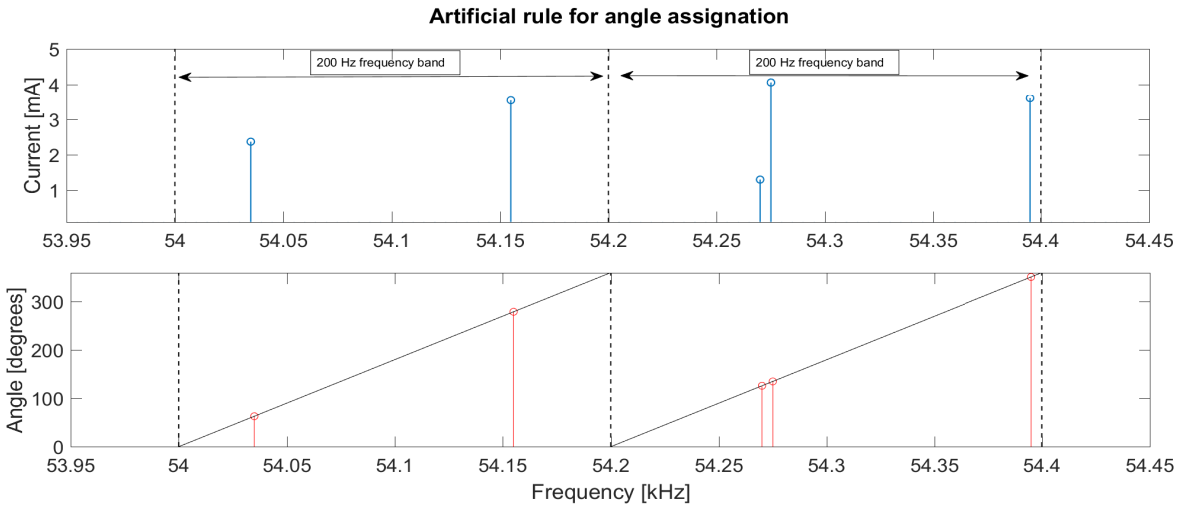

Figure 4-13.: Artificial rule for angle assignation of emissions between 2-150 kHz

In this sense, the artificial angles will vary between 0-2π within each 200 Hz frequency band. In a set of different measurements, a supraharmonic may report the same values for its artificially assigned angles if and only if that emission keeps its frequency as constant in all measurements. In other words, this method allows to detect the variation in emissions' frequency by means of the variation of the artificial angle.

In order to assess how supraharmonic emissions vary between the seven experimental setups listed at the beginning of this section, the coherence function was computed using the magnitude and angle of emissions between 2-150 kHz. Table **4-3** summarizes the signal processing and aggregation methods so as to compute the coherence function.

Table 4-3.: Summary of methodology for assessing supraharmonic emissions in single operation

Parameter	Magnitude	Angle
Spectrum	Scaled single-sided FFT	Artificially assigned
Frequency aggregation	RMS value of each 200 Hz frequency band	The angle of highest emission within each 200 Hz frequency band
Time aggregation	Mean value using 40 signal blocks	Median value using 40 signal blocks

4.3. Results

Results are organized according to *Idle-mode* and *On-mode* tests, each one encompassing the PFC topologies described in Table **4-1**.Results are then described in the following subsections using mean FFT. Additional methodologies for having insights about main results are also explained and applied.

The assessment of supraharmonic emissions was grouped into 4 frequency bands according to previous assessments as those reported in [4][13][16]: 2.1-8.9, 9.1-29.9, 30.1-94.9 and 95.1-149.9 kHz. Using these frequency bands from FFT, the total supraharmonic current or voltage ($TSH_{C;V}$) and the coherence function (C_{xy}) are used to describe the emissions and their variations when measurement setup is modified according to previous section. The total supraharmonic current or voltage is given according to Equation 4-5 [4]:

$$TSH_{C;V} = \sqrt{\sum_{B=1}^{705} Y_B^2}$$

The total supraharmonic current or voltage expressed as function of the four frequency bands is defined as follows:

$$TSH_{C;V} = \sqrt{TSH_{C;V}^2|_{(2.1-8.9)} + TSH_{C;V}^2|_{(9.1-29.9)} + TSH_{C;V}^2|_{(30.1-94.9)} + TSH_{C;V}^2|_{(95.1-149.9)}}$$

The corresponding uncertainty is therefore given by the following equation, given that all uncertainties to be combined are at standard level of confidence:

$$\delta_{TSH_{C;V}}|_{a-b,LC=68\%} = \frac{1}{2}\frac{1}{\sqrt{TSH_{C;V}^2|_{a-b}}}\sqrt{(2Y_a\delta_{Y_a})^2 + (2Y_{a+1}\delta_{Y_{a+1}})^2 + ... + (2Y_b\delta_{Y_b})^2}$$

Where:

- $TSH_{C;V}|_{a-b,LC=68\%}$: RMS value for emissions grouped in 200-Hz bands [9] between frequencies a and b at 68% level of confidence
- $\delta_{TSH_{C;V}}|_{a-b}$: Uncertainty of $TSH_{C;V}$ between frequencies a and b.
- Y_n: Magnitude of spectral component n.
- δ_{Y_n}: Uncertainty of magnitude of spectral component n

Analogous to $TSH_{C;V}$, values from coherence function were grouped into four frequency bands. This was performed using the Equation below:

$$C_{xy|_{band}} = prct_{95}(C_{xy,f_i=[a,b]}) \tag{4-10}$$

Where $prct_{95}$ is the 95th percentile of coherence values between a and b, the limits of one of the four selected frequency bands. These methodologies are used to get insights about the results of the experiments listed in Table **4-2**, for each PFC topology described in Table **4-1**.

4.3.1. Idle-mode

Idle-mode means that EUT is the only part of the measurement setup depicted in Fig. **3-1** that it is not under operation. As explained in Chapter 3: *Measurement System for supraharmonics in low voltage networks*, idle-mode implies circuit in Figure **3-1** is open between current sensors and EUT, but power source is turned on. This was used as a reference case for measuring background emissions not related to EUT operation. Currents and voltages were measured in idle-mode. In Chapter 3 was reported that a certain current transducer virtually measured supraharmonic currents in Idle mode.

Results from measurements showed identifiable supraharmonic voltages in Idle mode (above the metrological threshold deduced in Chapter 3) only when EUT were connected to the grid (experiment number 7 according to Table **4-2**). Figure **4-14** shows background supraharmonic voltages when using grid as voltage source.

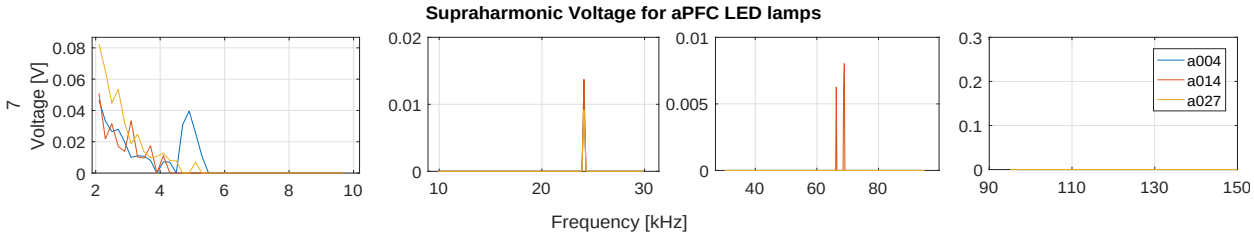

Figure 4-14.: Voltage for aPFC LED lamps in idle mode using grid (experiment 7).

Table **4-4** summarizes the results from supraharmonic voltages in idle-mode. These supraharmonic emissions are close to minimum measurable estimated by ADC Effective Resolution described in Appendix A and therefore, considered as low amplitude voltage emissions. This can also be percevied by the closeness between estimated measured values and their corresponding expanded uncertainty.

Table 4-4.: Supraharmonic voltage from LED lamps with active PFC in idle-mode.

EXPERIMENT	Total Supraharmonic Voltage [V]											
	active PFC											
	a004				a014				a027			
	2.1-8.9	9.1-29.9	30.1-94.9	95.1-149.9	2.1-8.9	9.1-29.9	30.1-94.9	95.1-149.9	2.1-8.9	9.1-29.9	30.1-94.9	95.1-149.9
1	-	-	-	-	-	-	-	-	-	-	-	-
2	-	-	-	-	-	-	-	-	-	-	-	-
3	-	-	-	-	-	-	-	-	-	-	-	-
4	-	-	-	-	-	-	-	-	-	-	-	-
5	-	-	-	-	-	-	-	-	-	-	-	-
6	-	-	-	-	-	-	-	-	-	-	-	-
7	0.09±0.03	0.01±0.01	0.00	0.00	0.07±0.05	0.01±0.01	0.01±0.01	0.00	0.13±0.08	0.01±0.01	0.00	0.00

All measured EUT had supraharmonic voltages in idle-mode when connected to the grid. One of the main difference between laboratory and grid measurements has to do with background noise and network (varying) impedance. Therefore, original emissions attributable to EUT operation could be modified by the presence of background emissions and also by the measurement system itself. It is important to clarify that the EUT considered in this assessment, that is, the set of selected low power LED lamps did not have an idle-mode as an operating mode. Other more complex household appliances as computers, electronic chargers and machines as microwave ovens, coffee machines and washing machines do have one or even several idle-modes. In fact, previous works have shown that some appliances could even produce audible noise between 2-20 kHz in idle-mode [17][18].

4.3.2. On-mode

Figures **4-15**a to **4-16**b show the spectra of measured active PFC LED lamps, for the experiments listed in Table **4-2**. When thresholds deduced in Chapter 3 are applied, current and voltage emissions do not necessarily match. In fact, for the measured active PFC LED lamps there were no identifiable voltage emission in experiments using pure sinusoidal voltage source (experiments 1 to 3, Table **4-2**) but in experiments with distorted voltage source (experiments 4 to 6) and directly connected to grid (experiment 7). Although thresholds applied to spectra magnitude limit the amount of knowledge about the behaviour of current and voltage supraharmonics, they are required for assuring the measured signals are metrologically identifiable.

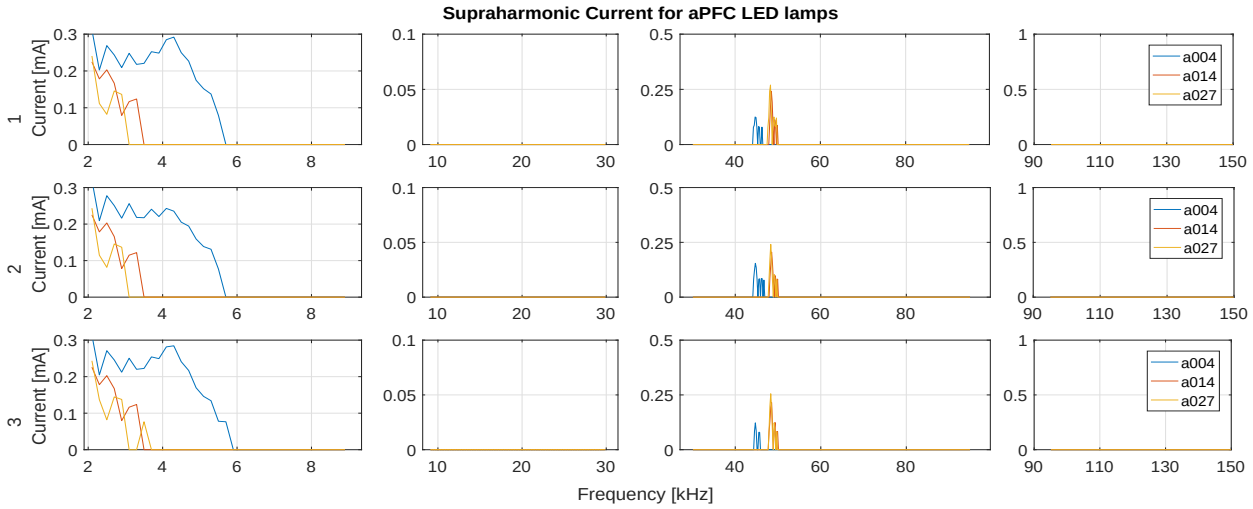

(a) Current using sinusoidal voltage and different network impedances.

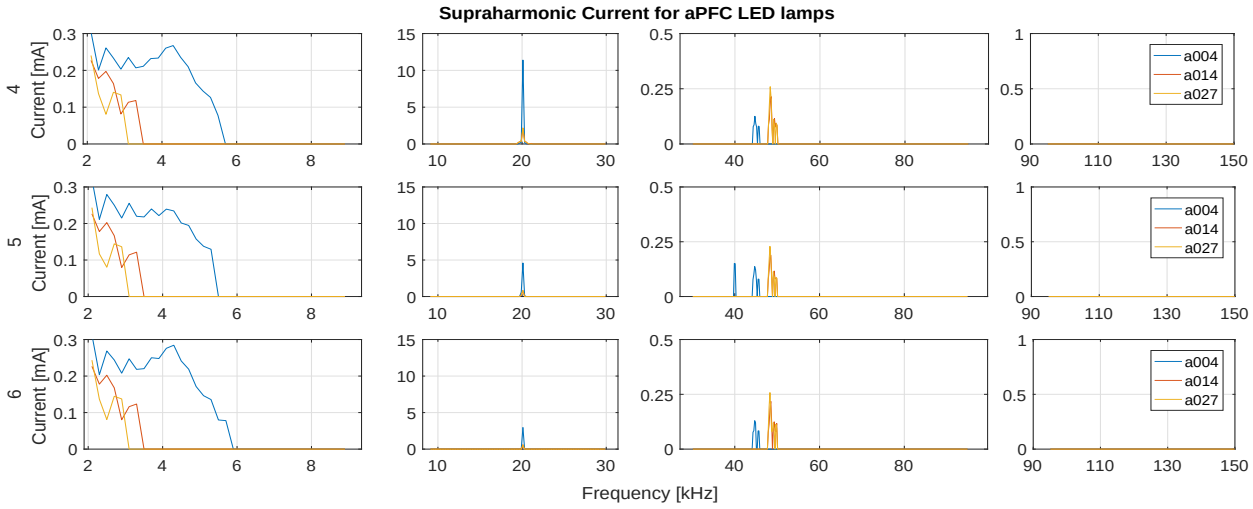

(b) Current using distorted voltage and different network impedances.

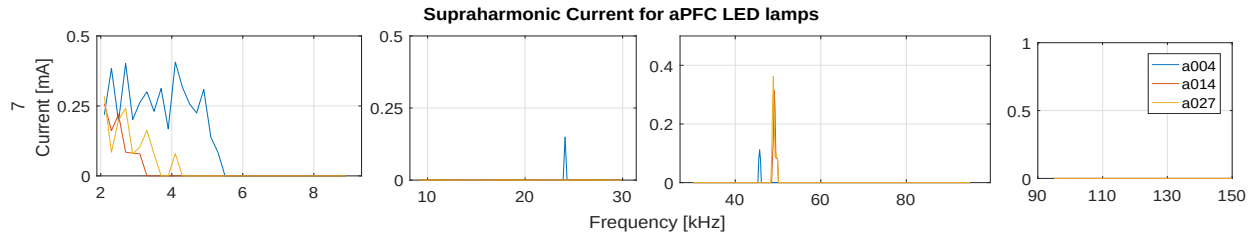

(c) Current from LED lamp directly connected to the grid.

Figure 4-15.: Current emissions between 2-150 kHz from an active PFC LED lamp using different measurement setups.

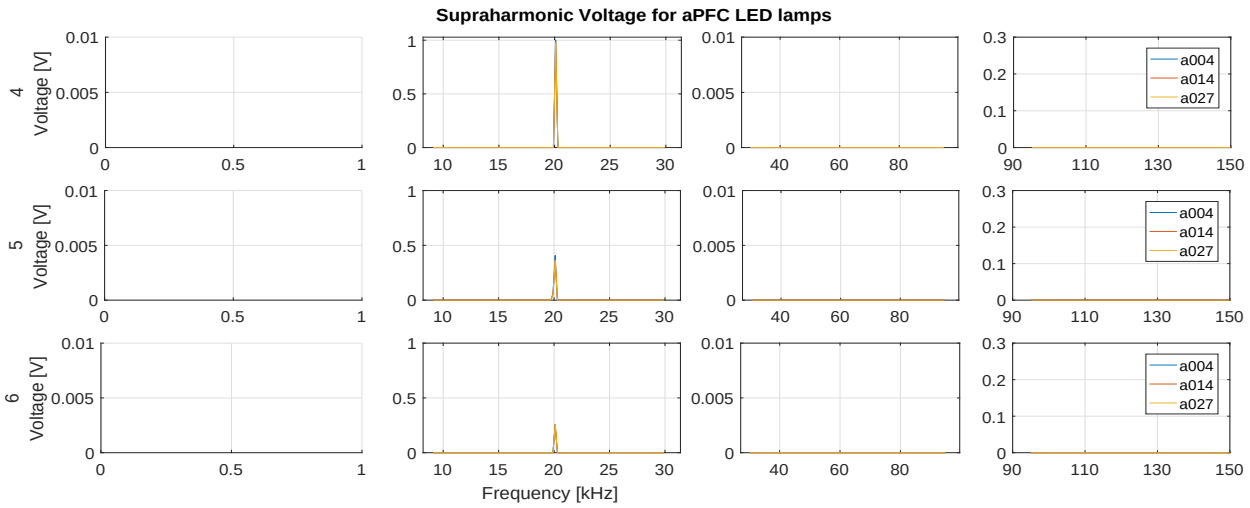

(a) Voltage using distorted voltage source and different network impedances.

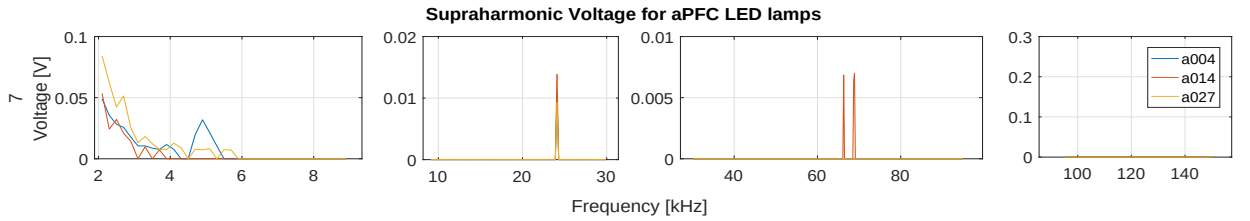

(b) Voltage from LED lamp directly connected to the grid.

Figure 4-16.: Voltage emissions between 2-150 kHz from an active PFC LED lamp using different measurement setups.

The total supraharmonic current and voltage are used as indices of supraharmonic emission magnitude at each of the four proposed frequency bands. This allowed authors to identify which frequency bands the supraharmonic emissions belong to. These indices are computed over the signals resulting from the application of metrological thresholds, therefore, only identifiable emissions are taken into account. However, these indices can hide other relevant information regarding the similarity of emissions when systematic variations in measurement setup are carried out, see Table **4-2**.

The coherence function is then used to quantify how similar are supraharmonic emissions between comparable experiments. In this sense, experiment 1 (sinusoidal voltage, no network impedance) is compared to experiments 2, 3 and 7(sinusoidal voltage, different network impedances and grid). This comparison is also carried out between experiment 4 (distorted voltage, no network impedance) and experiments 5 to 6 (distorted voltage, different network impedance). Figures **4-17**a to **4-18**a show the coherence function for supraharmonic currents and voltages for active PFC LED lamps listed in Table **4-1**. Coherence function compares emissions using the different experimental setups described in Table **4-2**.

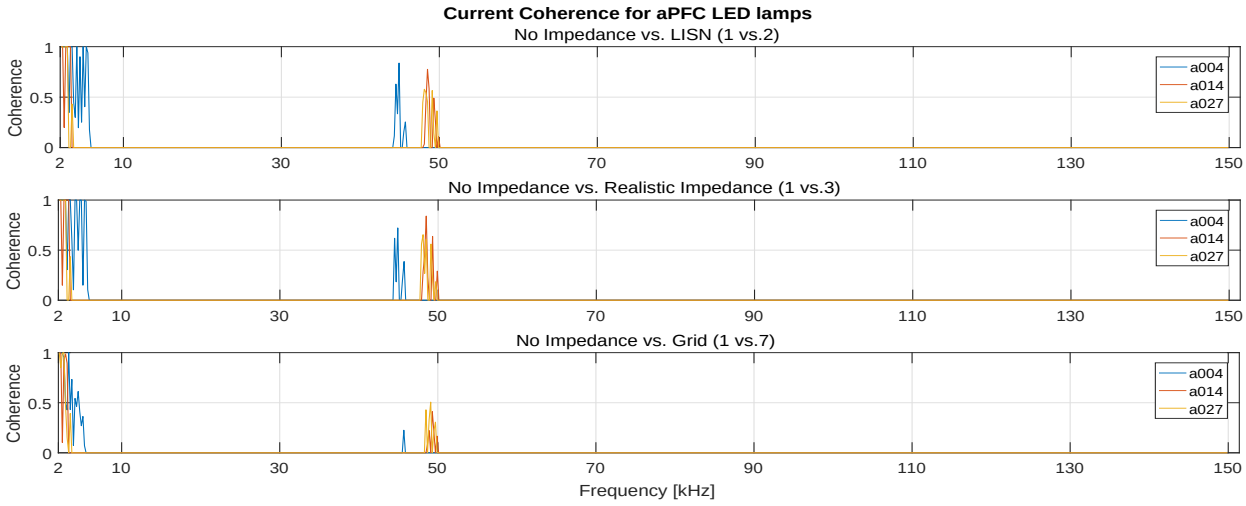

(a) Current coherence using sinusoidal voltage and different network impedances.

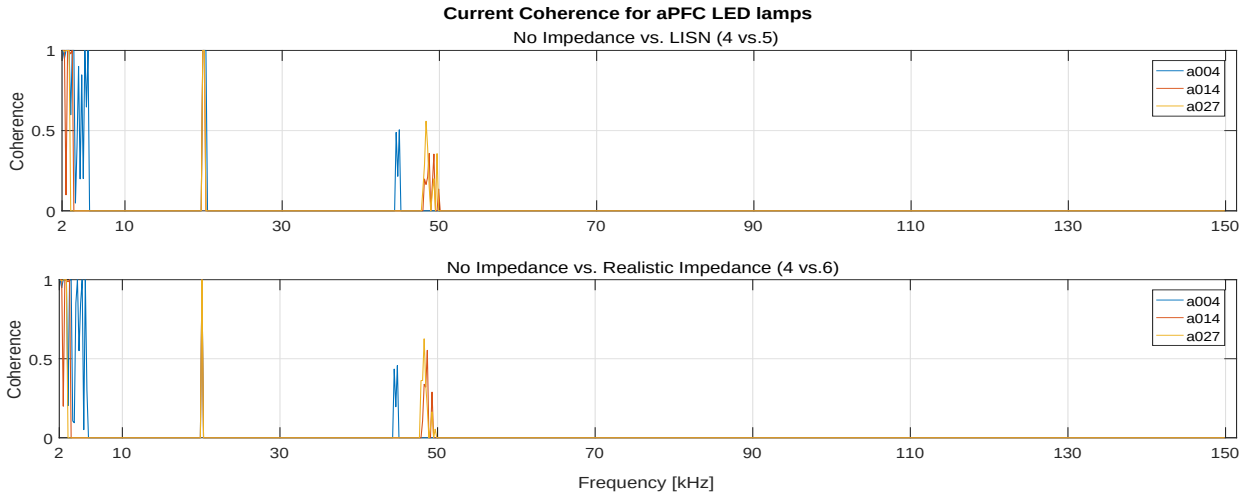

(b) Current coherence using distorted voltage and different network impedances.

Figure 4-17.: Current coherence between 2-150 kHz from an active PFC LED lamp using different measurement setups.

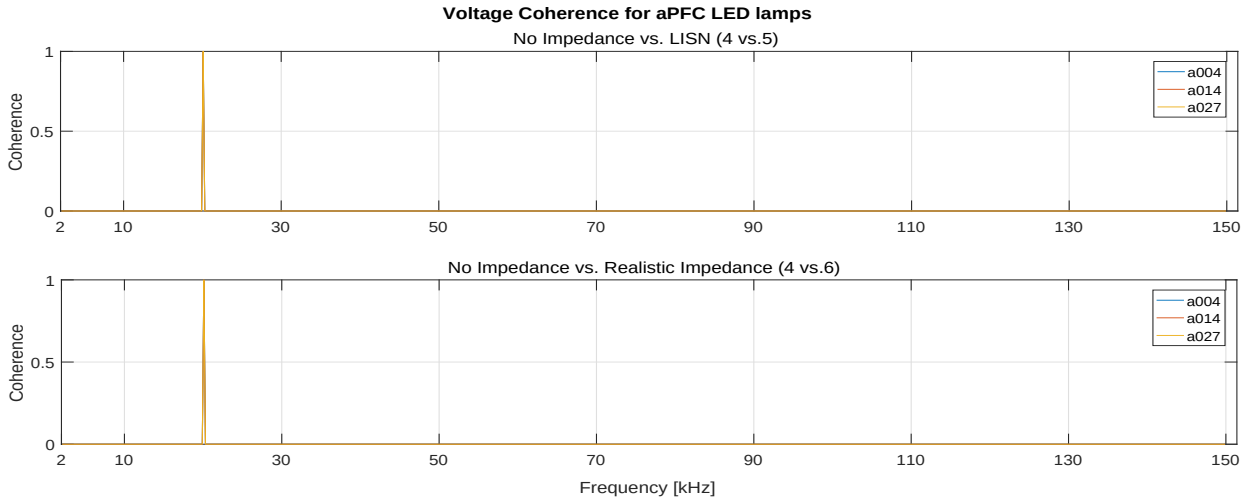

(a) Voltage coherence from LED lamp directly connected to the grid.

Figure 4-18.: Voltage coherence between 2-150 kHz from an active PFC LED lamp using different measurement setups.

The following sections show numerical results from total supraharmonic currents and voltages as well as from the coherence function. Results for other LED lamps listed in Table **4-1** are reported in Appendix C.

4.3.3. Emissions in terms of Total Supraharmonic current and voltage

Tables **4-5** and **4-6** show the TSH index described in Equation 4-5 for current and voltage respectively using the thresholds deduced in Chapter 3. Green color cells are related to emissions originated only from inside the EUT (i.e. primary emissions), whilst yellow color cells are emissions originated outside the EUT (i.e. secondary emissions). Bold data are emissions which cannot be classified only as primary or secondary emissions. All uncertainties were less than measured value. Because of figures rounding process, however, some of them increased.

No supraharmonic emissions were detected using metrological thresholds in the frequency range between 90-150 kHz, fourth frequency band, for any of the measured EUT. This means, there were no clearly distinguishable emissions above the proposed threshold for neither currents nor voltages between 90-150 kHz. It does not mean, however, that emissions did not exist at all: it means the uncertainty of non-detected emissions are higher than 70% and because of metrologycal restrictions, they might be not reported as emissions if any.

Table 4-5.: Supraharmonic current from LED lamps with active PFC. Green color: originated inside the EUT (primary emissions); yellow color: originated outside the EUT (secondary emissions); bold: combination of primary and secondary emissions

Total Supraharmonic Current [mA]												
EXPERIMENT	active PFC											
	a004				a014				a027			
	2.1-8.9	9.1-29.9	30.1-94.9	95.1-149.9	2.1-8.9	9.1-29.9	30.1-94.9	95.1-149.9	2.1-8.9	9.1-29.9	30.1-94.9	95.1-149.9
1	1.0±0.1	0.0	0.3±0.1	0.0	0.4±0.1	0.0	0.4±0.1	0.0	0.3±0.1	0.0	0.5±0.1	0.0
2	0.9±0.1	0.0	0.3±0.1	0.0	0.4±0.1	0.0	0.4±0.1	0.0	0.3±0.1	0.0	0.4±0.1	0.0
3	1.0±0.1	0.0	0.2±0.1	0.0	0.4±0.1	0.0	0.4±0.1	0.0	0.4±0.1	0.0	0.4±0.1	0.0
4	0.9±0.1	11.4±0.1	0.2±0.1	0.0	0.4±0.1	2.3±0.1	0.4±0.1	0.0	0.3±0.1	2.3±0.1	0.4±0.1	0.0
5	0.9±0.1	4.6±0.1	**0.3**±0.1	0.0	0.4±0.1	0.8±0.1	0.4±0.1	0.0	0.3±0.1	0.8±0.1	0.4±0.1	0.0
6	1.0±0.1	2,9±0.1	0.2±0.1	0.0	0.4±0.1	0.6±0.1	0.4±0.1	0.0	0.4±0.1	0.6±0.1	0.4±0.1	0.0
7	**1.1**±0.1	0.1±0.1	0.2±0.1	0.0	**0.4**±0.1	0.0	0.5±0.1	0.0	**0.5**±0.1	0.0	0.5±0.1	0.0

4.3.3.1. Sinusoidal voltage source

For experiments 1 to 3, current emissions are similar for EUT classified in the same topology. Most of the current supraharmonic emissions are located at first and second emission bands, that is between 2-30 kHz. These emissions are mostly related to harmonic emissions below 2 kHz. For the selected active PFC LED lamps, however, current emissions at third frequency band (between 30-95 kHz) were clearly detected. These emissions, depicted in Figures **4-15**a to **4-16**b, are mainly related to the switching frequency typically used in buck and boost converters, see Figures **4-6** and **4-10** and reference [12]. Current emissions were similar when different network impedances were used on each selected active PFC LED lamp. Supraharmonic voltages were detected for no PFC and passive PFC topologies at first frequency band when Z2 was used. No supraharmonic voltages were detected neither for capacitive nor active PFC LED lamps using a sinusoidal voltage source. This means supraharmonic voltages might or not exist , but if any, they were small enough that their magnitudes had an uncertainty higher than 70% from a metrological point of view.

As stated in Chapter 2, primary harmonic emission is the part of the harmonic current at the device terminals that is driven by sources inside the device [19]. It was also stated that an approximate value of primary emission can be obtained using a voltage source with output impedance close to 0 and all other voltages at any other frequencies valued at zero. The set of experiments 1 to 3 were intended to give the approximate behaviour of primary emissions of EUT. As results show from Tables **4-5**, **4-6** and tables in Chapter C, all EUT had identifiable current emissions at firs frequency band (2-9 kHz). Only the selected active PFC LED lamps had current supraharmonics at third frequency band (30-95 kHz). Magnitude of

Table 4-6.: Supraharmonic voltage from LED lamps with active PFC. Green color: originated inside the EUT (primary emissions); yellow color: originated outside the EUT (secondary emissions); bold: combination of primary and secondary emissions

Total Supraharmonic Voltage [V]												
EXPERIMENT	active PFC											
	a004				a014				a027			
	2.1-8.9	9.1-29.9	30.1-94.9	95.1-149.9	2.1-8.9	9.1-29.9	30.1-94.9	95.1-149.9	2.1-8.9	9.1-29.9	30.1-94.9	95.1-149.9
1	0.00	0.00	0.00	0.00	0.00	0.00	0.00	0.00	0.00	0.00	0.00	0.00
2	0.00	0.00	0.00	0.00	0.00	0.00	0.00	0.00	0.00	0.00	0.00	0.00
3	0.00	0.00	0.00	0.00	0.00	0.00	0.00	0.00	0.00	0.00	0.00	0.00
4	0.00	1.00±0.01	0.00	0.00	0.00	0.98±0.01	0.00	0.00	0.00	0.98±0.01	0.00	0.00
5	0.00	0.41±0.05	0.00	0.00	0.00	0.37±0.02	0.00	0.00	0.00	0.36±0.02	0.00	0.00
6	0.00	0.26±0.01	0.00	0.00	0.00	0.26±0.01	0.00	0.00	0.00	0.26±0.01	0.00	0.00
7	**0.09**±0.05	0.01±0.01	0.00	0.00	**0.07**±0.05	0.01±0.01	0.01±0.01	0.00	**0.13**±0.08	0.01±0.01	0.00	0.00

current emissions were similar among considered cases (experiments 1 to 3) when different network impedances were used. Nevertheless, most of the measured current at first frequency band (2-9 kHz) using Z2 (LISN) were smaller or at least equal to the current emissions measured using Z3 (realistic impedance). From results, the selected no PFC and passive PFC devices had identifiable voltage supraharmonics when Z2 (LISN) was used. The assessment of increase of voltage emissions between 2-150 kHz was also reported in [20]. This apparently increase of voltage emissions magnitude is attributable to the inductive behaviour of LISN network impedance acting as low-pass inductive filter.

4.3.3.2. Distorted voltage source

The use of a distorted voltage source (experiments 4 to 6), composed by a pure sinusoidal at main frequency (230 V, 50 Hz) and a superimposed sinusoidal (1 V, 20 kHz) led to different current emissions between different EUT topologies. For EUT classified as no PFC LED lamps, the impact of voltage distortion clearly led to measurable currents at same frequency band of distortion, that is between 9-30 kHz. There was however a subtle but identifiable current emission from one no PFC LED lamp at 40 kHz (harmonic of 20 kHz distortion) when Z2 (LISN) network impedance was used. For two out of three capacitive LED lamps, voltage distortion at 20 kHz led to a clearly perceptible non-linear behaviour when using Z1 and Z2: current emissions at 20 kHz as well as at each of the harmonics of distorted voltage, that is, 40 kHz, 60 kHz, etc (second and third emission bands, 9-95 kHz). EUT classified as passive PFC topology only had current emissions at first (below 9 kHz) and second (between 9-30 kHz) frequency bands. Active PFC topology had a similar behaviour of that of no PFC

topology, that is, distorted voltage led to distorted current at same frequency (20 kHz) and a subtle current emission was detected at 40 kHz when Z2 (LISN) network impedance was used. In terms of supraharmonic voltages, the highest voltage emissions matched with the voltage distortion at 20 kHz for all topologies. The highest voltage magnitude at 20 kHz was measured using Z1 (no network impedance) and the lowest using Z3 (realistic network impedance) for the selected EUT. The same as for pure-sinusoidal voltage source case, supraharmonic voltages were detected for no PFC and passive PFC LED lamps at first emission band (2-9 kHz) when Z2 (LISN) was used as network impedance. Capacitive and active PFC topologies did not report any identifiable voltage supraharmonic emission.

The set of experiments 4-6 were intended to show how an external voltage distortion change the primary emissions of EUT. The combination of selected capacitive EUT and Z1, Z2 network impedances led to the observation of current's non-linear behaviour when distorted voltage is superimposed over main voltage at same phase angle. Indeed, current emissions at harmonics of distorted voltage appeared on grid-side current: 20 kHz and 40 kHz were identifiable from spectra. The EUT with capacitive topology showed to make more visible the non-linear behaviour of current passing through semiconductors like full-wave rectifier and the LED strings themselves. Probably because of PFC and/or EMI filters restrictions of selected EUT, this non-linear behaviour of current can be identified from grid-side current. In the case of no PFC and active PFC, at least one device showed a current emission at both 20 kHz and 40 kHz attributable to the distorted voltage at 20 kHz. This non-linear behaviour of current in no PFC and active PFC topologies was identifiable but more subtle than the emissions when using capacitive topologies. The interaction between Z2 network impedance (LISN) and EUT's input impedance showed to influence the identification of this non-linear behaviour, i.e. the generation of harmonics of distorted voltage source signal. This non-linear behaviour was not clearly identifiable when combining Z3 (realistic network impedance) with selected EUT. Selected passive PFC LED lamps did not have identifiable current emissions at third frequency band (30-95 kHz) for any of the network impedance used in this assessment, that to say the combination of all network impedances and input impedances of passive PFC lamps led to avoid the clear identification of current harmonics of distorted source voltage.

Voltage distortion at 20 kHz produced current emissions at same frequency. In addition, this current emissions were proportional to the voltage at EUT terminals. When no network impedance is used, the 1 V distortion at 20 kHz appears almost the same at EUT terminals. On the other hand, LISN network impedance (Z2) allowed a higher distorted voltage at EUT terminals compared to the realistic network impedance (Z3). Because of this, the current emissions related to the voltage distortion at 20 kHz were higher when using LISN (Z2) and lower when using a realistic grid impedance (Z3). Impedance magnitudes from Figure **3-3**, Chapter 3, show however that Z2 magnitude is in general higher than Z3 magnitude

above 10 kHz. From this, it was expected that voltage drop was higher at Z2 than Z3 and therefore obtain a higher voltage at EUT terminals using Z3 rather than using Z2. Measurement results showed the opposite situation, that is,voltage at EUT terminals is higher when using Z2 (LISN). This can be explained using the angle phase shift when network impedance and EUT's input impedance are combined: the magnitude but also the angle shift of the resultant impedance have to be taken into account. The exact identification of EUT input impedance, however, exceeded the purpose of this thesis.

4.3.3.3. Grid measurements

Finally, the measurements from grid were intended to show how different are measured emissions in-situ compared to emissions measured in laboratory setup. When each EUT were connected to the grid at a time, both current and voltage emissions changed from previous cases. Highest current emissions for all PFC topologies were located at first frequency band (2-9 kHz). Most of the EUT had an identifiable current emission at 24.1 kHz, which matched with a supraharmonic voltage at same frequency. One passive and the three active PFC LED lamps had current emissions at third frequency band (30-95 kHz): the first case matches with a supraharmonic voltage at same frequency, whilst the second case matches with primary emissions of experiments with pure sinusoidal voltage source. In terms of supraharmonic voltages, all EUT spectra showed an emission at 24.1 kHz (second frequency band). None of the capacitive topology devices reported identifiable voltage emissions at third frequency band (30-95 kHz).

In general terms, selected LED lamps have a very different spectrum when comparing laboratory and grid measurements. Only active PFC LED lamps had primary current emissions at same frequencies that those using a pure sinusoidal voltage source (experiments 1-3). Since only selected active PFC lamps have current primary emissions for single operation assessment, most of the current emissions are a combination of primary and secondary emissions or only secondary emissions as a result of voltage secondary emissions from grid. Several supraharmonic secondary voltages were identifiable from grid measurements, as can be seen from Tables **4-5** and **4-6** as well as tables from Appendix C. Nevertheless, not all of the secondary voltage emissions led to the corresponding secondary current emissions: The role of EUT's input impedance seemed again to be crucial for the complete characterization of current and voltage primary emissions of EUT.

Using the index $TSH_{C;V}$ explained in Equation 4-5 was possible to identify the suprahramonic currents and voltages using different combinations of network impedances and EUT. The latter were classified according to their Power Factor Corrector (no PFC, capacitive, passive PFC and active PFC topologies) as suggested in [1]. Results showed that no supra-

harmonic emissions were identified between 95 and 150 kHz neither from laboratory nor grid measurements. Although some different emissions were identified from devices classified as same PFC topology, the classification according to Power Factor Corrector helped to organize some common behaviour of selected EUT. However, from the identification of supraharmonic emissions, EUT's input impedance showed to be determinant for the understanding of emissions generation. Authors suggest the assessment of household aplliances' input impedance as a future work for the assessment of emissions and other power quality phenomena between 2-150 kHz.

4.3.4. Emissions comparison in terms of Coherence function

Tables **4-7**, **4-8** and those in Appendix C show the mean value of the magnitude of coherence function within each of the four defined frequency bands, for all EUT and experiments (variations of basic measurement setup). These coherence functions were computed using spectra after applying the thresholds deduced in Chapter 3. The comparison was performed in five cases, grouped according to voltage distortion: Z1 vs. Z2 (1-2), Z1 vs. Z3 (1-3) and Z1 vs Grid (1-7) using pure sinusoidal source voltage; Z1 vs Z2 (4-5) and Z1 vs Z3 (4-6) using distorted sinusoidal source voltage. Blue color cells in Tables **4-7** to **4-8**and indicate coherence different from zero.

Table 4-7.: Supraharmonic current coherence from LED lamps with active PFC

Supraharmonic current coherence [p.u.]												
COMPARISON	active PFC											
	a004				a014				a027			
	2.1-8.9	9.1-29.9	30.1-94.9	95.1-149.9	2.1-8.9	9.1-29.9	30.1-94.9	95.1-149.9	2.1-8.9	9.1-29.9	30.1-94.9	95.1-149.9
1-2	0.8	0.0	0.4	0.0	0.9	0.0	0.4	0.0	0.8	0.0	0.4	0.0
1-3	0.8	0.0	0.4	0.0	0.9	0.0	0.4	0.0	0.8	0.0	0.4	0.0
1-7	0.6	0.0	0.1	0.0	0.8	0.0	0.2	0.0	0.7	0.0	0.3	0.0
4-5	0.8	0.9	0.3	0.0	0.9	0.5	0.3	0.00	0.9	0.5	0.3	0.0
4-6	0.8	0.5	0.3	0.0	0.9	0.7	0.3	0.0	0.9	0.4	0.3	0.0

Since no emissions were detected between 95-150 kHz, aggregated coherence values in Tables **4-7**, **4-8** and those in Appendix C are zero at this frequency band.

4.3.4.1. Sinusoidal voltage source and Grid

For comparisons 1-2, 1-3 and 1-7 (Z1 vs. Z2, Z1 vs. Z3, Z1 vs. Grid) coherence function was in general terms similar among EUT classified within the same PFC topology. The highest aggregated coherence for current supraharmonics was at first frequency band (2-9

Table 4-8.: Supraharmonic voltage coherence from LED lamps with active PFC

Supraharmonic voltage coherence [p.u.]												
COMPARISON	active PFC											
	a004				a014				a027			
	2.1-8.9	9.1-29.9	30.1-94.9	95.1-149.9	2.1-8.9	9.1-29.9	30.1-94.9	95.1-149.9	2.1-8.9	9.1-29.9	30.1-94.9	95.1-149.9
1-2	0.0	0.0	0.0	0.0	0.0	0.0	0.0	0.0	0.0	0.0	0.0	0.0
1-3	0.0	0.0	0.0	0.0	0.0	0.0	0.0	0.0	0.0	0.0	0.0	0.0
1-7	0.0	0.0	0.0	0.0	0.0	0.0	0.0	0.0	0.0	0.0	0.0	0.0
4-5	0.0	1.0	0.0	0.0	0.0	1.0	0.0	0.0	0.0	1.0	0.0	0.0
4-6	0.0	1.0	0.0	0.0	0.0	1.0	0.0	0.0	0.0	1.0	0.0	0.0

kHz) for all considered EUT. no PFC, passive PFC and active PFC topologies had a high aggregated coherence value at first emission bands (> 0.8). Capacitive LED lamps had a mid-term aggregated coherence between 2-9 kHz (≤ 0.7). The lowest aggregated coherence value was from comparison "Z1 vs. Grid" (1-7). Only active PFC LED lamps had a coherence different from zero at third frequency band (30-95 kHz) using sinusoidal voltage source (because of emissions at same frequency band reported in Table **4-5**). The aggregated value for coherence between 30-95 kHz (third frequency band) using aPFC LED lamps was the same using Z1 and Z2. Again, measurements from grid led to a "less similar spectrum" compared to the base case when no network impedance was used (Z1).

In terms of voltage aggregated coherence, due to the fact that no supraharmonic voltage was higher than proposed threshold, Table **4-8** shows no aggregated coherence for combinations "Z1 vs. Z2" (1-2), "Z1 vs. Z3" (1-3) and "Z1 vs. Grid" (1-7). A high value of aggregated coherence indicates the evaluated set of spectra are rather similar. However, a low coherence value can be originated by several reasons:

- Magnitude variation: Spectral components are increased/reduced
- (Artificial) angle variation: Spectral components changed their emission frequency
- Bandwidth variation: Spectral components disappear / appear

Because of the use of different network impedances, resultant spectra using different EUT are exposed to one or several of the effects listed above.

From this, it can be said that similarity between spectra using Z1 (no-impedance) and Z3 (realistic impedance) was at least equal or higher than similarity between spectra using Z1 and Z2 (LISN) for the assessed cases. Regarding emissions, because of their changing nature

in time domain (see Figure **4-12**), coherence function is higher at low frequencies (first frequency band, 2-9 kHz) than other frequency bands (above 9 kHz.) In other words, some supraharmonic emissions above 9 kHz changed their amplitudes and frequencies through time when different impedances were used. This is the case of comparison 1-7 (no impedance vs. grid), where most EUT had "moving" supraharmonics in both frequency and time. Because of this, the spectrum when EUT were connected to the grid (case 7, Table **4-2**) were mostly "different" in magnitude, artificial angle and bandwidth than the more "stable" spectra using no network impedance (experiment 1, Table **4-2**).

4.3.4.2. Distorted voltage source

The use of a distorted voltage source (comparisons 4-5 and 4-6) intensify the results obtained using sinusoidal voltage source. Spectrum from case 4 (see Table **4-2**) showed high similarity with spectrum from case 5 and 6 between 2-9 kHz. However, most of the EUT had a mid-term aggregated coherence (≤ 0.7). Again, because of the impact of different network impedances and time-variating supraharmonic emissions, the coherence above 9 kHz is lower than coherence below 9 kHz. Once again, aPFC LED lamps were the only ones having an aggregated coherence at third frequency band (30-95 kHz) different from zero. Nevertheless, the value of coherence is lower (≤ 3) than other considered frequency bands. Because of the switching frequency behaviour of boost and buck converters showed in Figures **4-6**, **4-10** and reference [12], it is expected that main emission changes its frequency through time (and consequently the artificially assigned angle).

Regarding voltages, the coherence is complete at second frequency band (9-29 kHz) because the voltage distortion is always present at same frequency and therefore, the artificial angle assigned to this emission remains constant through the different tests.

4.4. Conclusions

This chapter presented the measurement system, experimental setup and results from the assessment of supraharmonic emissions using EUT in single operation. The use of Power Factor Corrector stage as the criteria for EUT classification helped organize some common patterns in supraharmonic emissions. It was perceived the time-varying behaviour of supraharmonic emissions by using the time-frequency domains analysis through spectrograms. Using the measurement system and experimental setup described in this chapter, it was possible to measure current supraharmonics between 2-9 kHz from all selected LED lamps, only between 30-95 kHz from active PFC LED lamps, and no emissions between 95-150 kHz. Because of the metrological restrictions imposed by the measurement system used, most of the voltage supraharmonics presented amplitudes that lied below the proposed metrological thresholds

and therefore an accurate value for such emissions was rather difficult to report. Compared to the other topologies, capacitive topology was more susceptible to have current harmonics as consequence of the intentional, controlled supraharmonic voltage emission. EUT's input impedance (i.e. impedance seen from the Point of Common Connection towards the load) showed to be determinant for the understanding of supraharmonic emissions. It is suggested to also include the input impedance of household appliances in future assessments of waveform distortion between 2-150 kHz.

REFERENCES

[1] Ana Maria Blanco, Manish Gupta, Aurora Gil de Castro, Sarah Ronnberg, and Jan Meyer. Impact of flat-top voltage waveform distortion on harmonic current emission and summation of electronic household appliances. *Renewable Energy and Power Quality Journal*, 1:698–703, apr 2018. doi: 10.24084/repqj16.437.

[2] S. K. Rönnberg, A. G. Castro, M. H. J. Bollen, A. Moreno-Munoz, and E. Romero-Cadaval. Supraharmonics from power electronics converters. In *2015 9th International Conference on Compatibility and Power Electronics (CPE)*, pages 539–544, June 2015. doi: 10.1109/CPE.2015.7231133.

[3] A. Moreno-Munoz, A. Gil-de-Castro, E. Romero-Cavadal, S. Rönnberg, and M. Bollen. Supraharmonics (2 to 150 khz) and multi-level converters. In *2015 IEEE 5th International Conference on Power Engineering, Energy and Electrical Drives (POWERENG)*, pages 37–41, May 2015. doi: 10.1109/PowerEng.2015.7266293.

[4] A. Grevener, J. Meyer, S. Rönnberg, M. Bollen, and J. Myrzik. Survey of supraharmonic emission of household appliances. *CIRED - Open Access Proceedings Journal*, 2017(1): 870–874, 2017. ISSN 2515-0855. doi: 10.1049/oap-cired.2017.0458.

[5] Daniel Agudelo-Martinez, Camilo Garzon, and Andres Pavas. Interaction of power quality disturbances within 2-150 kHz (supraharmonics): Analytical framework. In *2018 18th International Conference on Harmonics and Quality of Power (ICHQP)*. IEEE, may 2018. doi: 10.1109/ichqp.2018.8378859.

[6] Alan V. Oppenheim, Ronald W. Schafer, and John R. Buck. *Discrete-Time Signal Processing (2nd Edition) (Prentice-hall Signal Processing Series)*. Prentice Hall, 1999. ISBN 0137549202.

[7] Matlab. stft: Short-time fourier transform, 2019. Accessed in December 8, 2019.

[8] IEC. Electromagnetic compatibility (EMC) – Part 4-30: Testing and measurement techniques - Power quality measurement methods. Standard, International Electrotechnical Commission, Geneva, CH, 2014.

[9] IEC. Electromagnetic compatibility (EMC) – Part 4-7: Testing and measurement techniques – General guide on harmonics and interharmonics measurements and in-

strumentation, for power supply systems and equipment connected thereto. Standard, International Electrotechnical Commission, Geneva, CH, 2002.

[10] Matthias Klatt, Jan Meyer, and Peter Schegner. Comparison of measurement methods for the frequency range of 2 kHz to 150 kHz. In *2014 16th International Conference on Harmonics and Quality of Power (ICHQP)*. IEEE, may 2014. doi: 10.1109/ichqp.2014.6842791.

[11] Ana Maria Blanco, Sergey Yanchenko, Jan Meyer, and Peter Schegner. Impact of supply voltage distortion on the current harmonic emission of non-linear loads. *DYNA*, 82(192): 150–159, August 2015. doi: 10.15446/dyna.v82n192.48591.

[12] Christian Waniek, Thomas Wohlfahrt, Johanna M.A. Myrzik, Jan Meyer, Matthias Klatt, and Peter Schegner. Supraharmonics: Root causes and interactions between multiple devices and the low voltage grid. In *2017 IEEE PES Innovative Smart Grid Technologies Conference Europe (ISGT-Europe)*. IEEE, sep 2017. doi: 10.1109/isgteurope.2017.8260267.

[13] Daniel Agudelo-Martinez, Fabian Rios, and Andres Pavas. Interaction of some low power led lamps within 2–150 khz (supraharmonics). In *2018 18th International Conference on Harmonics and Quality of Power (ICHQP)*. IEEE, may 2018. doi: 10.1109/ichqp.2018.8378815.

[14] Sarah Rönnberg and Math Bollen. Propagation of Supraharmonics in the Low Voltage Grid. Technical report, Elektra, December 2017.

[15] A. M. Blanco, R. Stiegler, J. Meyer, and M. Schwenke. Implementation of harmonic phase angle measurement for power quality instruments. In *2016 IEEE International Workshop on Applied Measurements for Power Systems (AMPS)*, pages 1–6, Sep. 2016. doi: 10.1109/AMPS.2016.7602811.

[16] Daniel Agudelo-Martinez, Miguel Limas, Andres Pavas, and Jan Bacca. Supraharmonic bands detection for low voltage devices. In *2016 17th International Conference on Harmonics and Quality of Power (ICHQP)*. IEEE, oct 2016. doi: 10.1109/ichqp.2016.7783327.

[17] P. M. Körner, R. Stiegler, J. Meyer, T. Wohlfahrt, C. Waniek, and J. M. A. Myrzik. Acoustic noise of massmarket equipment caused by supraharmonics in the frequency range 2 to 20 khz. In *2018 18th International Conference on Harmonics and Quality of Power (ICHQP)*, pages 1–6, May 2018. doi: 10.1109/ICHQP.2018.8378856.

[18] P. M. KHOKHLOV, J. Meyer, P. SCHEGNER, D. AGUDELO-MARTINEZ, and A. PAVAS. Immunity assessment of household appliances in the frequency range from 2

to 150 khz. In *2019 25th International Conference on Electricity Distribution (CIRED)*, pages 1–5, June 2019.

[19] Sarah Rönnberg, Math Bollen. Propagation of Supraharmonics in the Low Voltage Grid. Report, Energiforsk, Stockholm, Sweden, 2017.

[20] D. Agudelo-Martinez, A.M. Blanco, R. Stiegler, F. Pavas, and J. Meyer. Influence of measurement setup on the emission of devices in the frequency range 2-150 khz. *Power Tech - Milano 2019*, 2019(1):to appear, 2019.

5. Identification of supraharmonics in simultaneous operation: Interactions

The identification of supraharmonic emissions considering EUT in single operation gives an idea about the potential primary sources of emission. However, household appliances are simultaneously supplied by a reference voltage at a common bus, or in the context of this research, at a Point of Common connection (PCC). The main purpose of this chapter is to show how supraharmonic emissions behave when simultaneous operation of different EUT is considered. Firstly, one voltage source and two different network impedances were selected for this assessment; the set of EUT was changed from previous chapter in order to consider a different type of LED lamps under the approach "source" and "sink". Secondly, the interaction of supraharmonic currents is shown graphically using both spectrograms and mean FFTs. Finally, different combination of network impedances and EUT were assessed using the hypothesis test in order to show some of the interactions between supraharmonic emissions from low power LED lamps.

5.1. Measurement and Experimental setups

The measurement and experimental setups for EUT in simultaneous operation kept the main features of that presented in Chapter 4: *Identification of supraharmonics in single operation: Emissions*. Nevertheless, some of the elements depicted in Figure **5-1** and their corresponding combination were redefined. The set of EUT in Chapter 4 showed that the selected noPFC LED lamps mostly had supraharmonic emissions between 2-9 kHz. However, a set of different noPFC LED lamps were selected for the EUT simultaneous operation assessment, whose supraharmonic emissions were also perceptible above 9 kHz. Because of visualization purposes, the interactions in base case were discussed from spectrograms and mean FFT rather than from a computed index. However, the hypothesis test was used as an index to quantify the variations of supraharmonic interactions when the base case is modified through the proposed experiments.

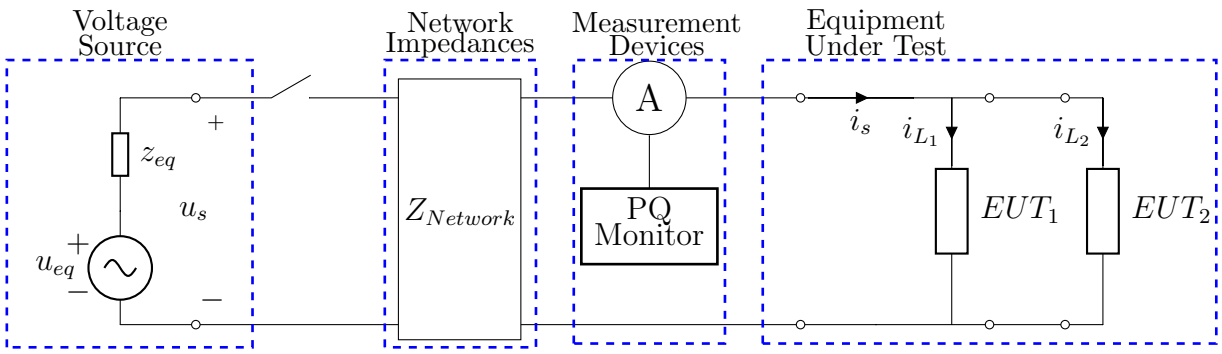

Figure 5-1.: Measurement setup for assessing single-phase emissions between 2-150 kHz in EUT simultaneous operation.

5.1.1. Measurement Setup

From the set of network impedances explained in Chapter 4, the "realistic impedance" (Z3) is in principle not considered for the assessment of supraharmonics in simultaneous operation. This because results from Chapter 4 showed the main difference when using "LISN impedance" (Z2) and "realistic impedance" (Z3) was rather the amplitude of emissions, while the frequencies remained mostly the same. Therefore only "no impedance" (Z1), "LISN" (Z2) and grid were used as network impedances for this assessment.

In order to simultaneously measure the three currents related to the simultaneous operation of EUT (i_s, i_{L1} and i_{L2}, see Figure **5-1**), a different set of current sensors were considered. Table **5-1** shows the accuracy of the integrated current sensors - DAQ modules used for the measurement of currents in EUT simultaneous operation. Procedure for uncertainty estimation explained in Chapter 3 was again used with these accuracy values.

Table 5-1.: Accuracy for DAQP-LA-B module, 300 kHz bandwidth

Range	Accuracy
100 mA and 300 mA	$\pm 0.05\%$(reading) $\pm 300\mu A$(range)
1 A to 30 A	$\pm 0.05\%$(reading) $\pm 0.05\%$(range)

The EUT classification proposed in [1] allowed to group the tested LED lamps according to their PFC topology. Results from Chapter 4 showed the highest supraharmonic emissions related to active PFC LED lamps. However, in [1] it is mentioned that LED lamps (and household appliances in general) effectively do have other components like high frequency elements, protection elements and switching stages after the smoothing capacitor, that are

not expected to highly affect the behaviour of waveform at low frequencies, i.e. below 2 kHz. Indeed, for the purpose of this thesis, authors found out that there are some noPFC LED lamps which effectively do have higher supraharmonic emissions when operate in single mode than those measured from selected active PFC LED lamps.

Hence, a modified set of EUT were selected for the assessment of supraharmonic emissions in simultaneous operation. Three LED lamps classified as no PFC according to [1] were included as EUT, because of their clearly identified supraharmonic emissions. For the capacitive, passive PFC and active PFC the selected EUT remained unchanged. Because of the results from Chapter 4, most of the selected capacitive and passive PFC LED lamps had a similar behaviour in terms of suprahrmonic emissions and therefore, only one device for these categories is considered for the simultaneous operation assessment as shown in Table **5-2**.

Table 5-2.: Equipment Under Test (EUT)

PFC	**Power Range[W]**	**Voltage Range[Vrms]**	**Frequency Range[Hz]**	**Amount of Devices**
no PFC	1-5	220-240	50-60	3*
Capacitive	10	100-240	50	1
passive PFC	1	230	50	1
active PFC	9	230	50	1

*Different from those listed in Chapter 4

5.1.2. Experimental Setup

The experimental setup used in Chapters 3 and 4 is also used with minor modifications for the assessment of emission in simultaneous operation. The three main aspects and the additional one are listed below for completeness:

- Stabilization time: $\geq$ 60 minutes.
- Measurements: 40 signal blocks of 200 ms each one.
- Test modes: Idle mode (open circuit) and On-mode (normal operation).
- Propagation: short and long connection wires between EUT.

This experimental setup was stable with reproducible measurements, since it also showed a variation of main current magnitude less than 1%, see Figure **3-5**.

The additional step included in experimental setup was the comparison among the emissions using short and long connection wires between measurement system and EUT depicted in Figure **5-1**. The "long" wires used in this assessment were the same type of cables previously used in Chapters 3 and 4, but 4 meters longer. The idea behind this was to perceive how a variation in wire lengths might eventually change the emissions and /or the interaction between voltage source and EUT in simultaneous operation.

5.1.3. Signal Processing

As mentioned in Chapter 4, the spectrogram and the mean FFT are used as signal processing tools for assessing the emissions of supraharmonics in simultaneous operation. Nonetheless, the mean FFT allows to directly apply frequency and time aggregation over the measured block signals. Therefore, some spectrograms of EUT in simultaneous operation are shown only for phenomenon visualization purposes whilst mean FFT is used for numerical analysis. All parameters and stages for signal processing using spectrograms and mean FFT remained the same as those described in Chapter 4.

5.2. Supraharmonic emissions in simultaneous operation

Identification of interactions of supraharmonic emissions was performed using the same measurement system and experimental setups described in Chapter 4: *Identification of supraharmonics in single operation: Emissions*. This identification aimed to show the interaction of supraharmonic emissions between voltage source and selected EUT, and also between EUT. Because of this, the emissions under EUT simultaneous operation were analyzed. Simultaneous operation consisted on the operation of two EUT supplied by the same voltage source at the same time, hence all eventual interactions registered are mostly attributable to the operation of the two EUT supplied by that specific measurement setup. Further details about the implementation of hypothesis test for "changes identification" are also presented.

5.2.1. Interaction of supraharmonic emissions in Base Case: Sinusoidal supply and no network impedance

Analogous to the assessment of surpaharmonics in EUT single operation, emissions interaction in base case was assessed using a sinusoidal voltage source and no network impedance between that source and the EUT, see Figure **5-1**. In this sense, the interaction of supraharmonic emissions are mostly attributable to the interaction between EUT and the measure-

ment setup. No additional network impedance is used in the base case experiment. However, the impedance features of both voltage source and the set of EUT will play a significant role in the behaviour of the interactions of supraharmonics.

Figures **5-2**a and **5-2**b show the current emission from single (upper) and simultaneous (lower) operation using one voltage source and two LED lamps as EUT. It can be seen that EUT1 and EUT2 emit supraharmonics in single operation, and that they interact with each other (also with voltage source) in simultaneous operation.

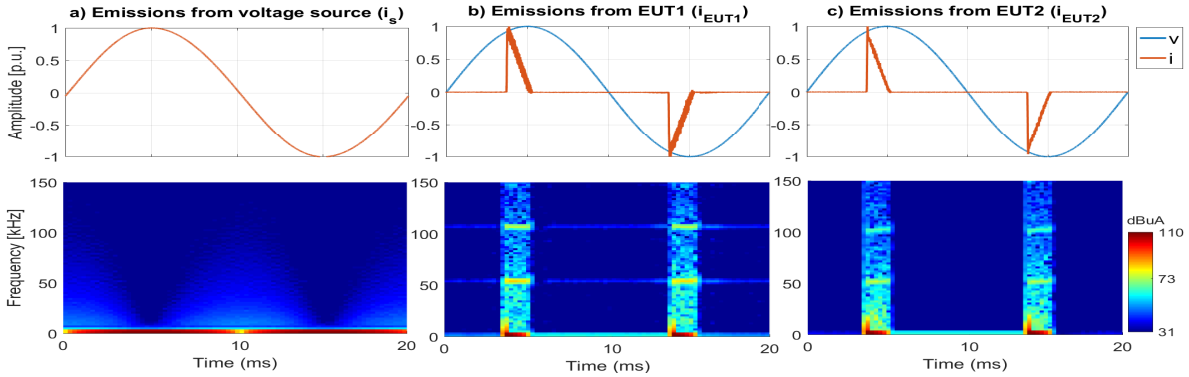

(a) Current emissions from each EUT (voltage source and two no PFC LED lamps) in single operation. a-a) Current emissions from voltage source (i_s, using an incandescent lamp); a-b) and a-c) Current emissions from two noPFC LED lamps (i_{EUT1},i_{EUT2}).

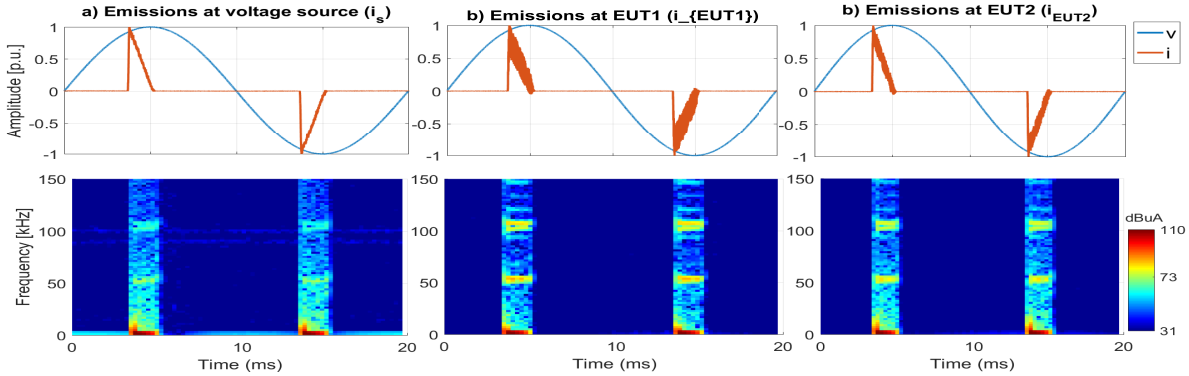

(b) Current emissions from two LED lamp and voltage source in simultaneous operation. b-a) Total current emissions at voltage source (i_s); b-b) and b-c) Current emissions from each of two noPFC LED lamps (i_{EUT1},i_{EUT2}).

Figure 5-2.: Spectrograms for EUT in single (upper) and simultaneous (lower) operation

From heat map colors, it might be deduced that supraharmonic emissions from EUT1 are higher compared to EUT2 for a definite time interval. Indeed, this time interval matches the time the rectifier bridge is on conduction state. Results from Chapter 4 showed, however,

that these emissions are time variant and therefore the whole block signal (200 ms) as well as the whole amount of block signals (40) need to be processed before concluding ordinal differences.

The same as in Chapter 4, information about emissions within a power cycle can be observed from spectrograms. This might lead to the fact that interaction of supraharmonics could eventually be different even within a power cycle time frame. However, for the purpose of this thesis, the mean FFT is used as a tool for visualization of grouped spectra in frequency and time domains. The mean FFT uses the power cycle period as the minimum signal block for signal processing in frequency domain. Figures **5-3**a, **5-3**b and **5-4**a-**5-4**b show the mean FFT for the same cases depicted in Figures **5-2**a and **5-2**b using the threshold estimation deduced in Chapter 3.

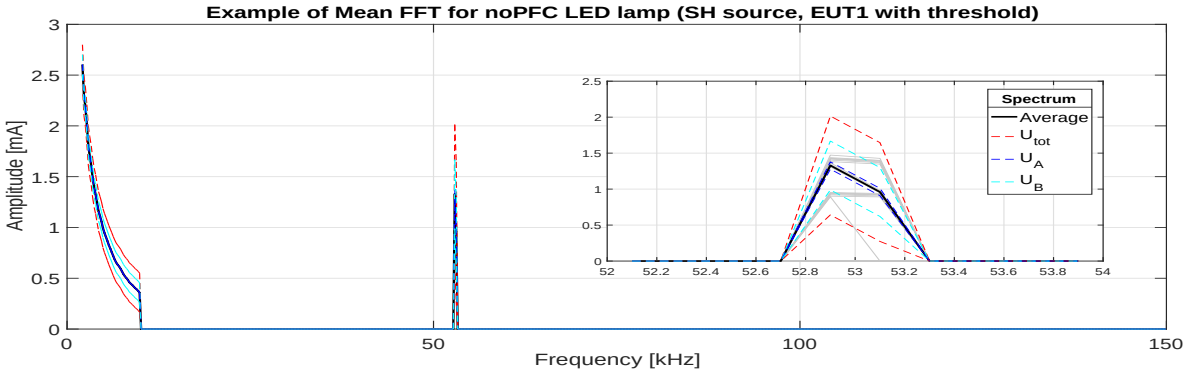

(a) Current emissions from a no PFC LED lamp in single operation

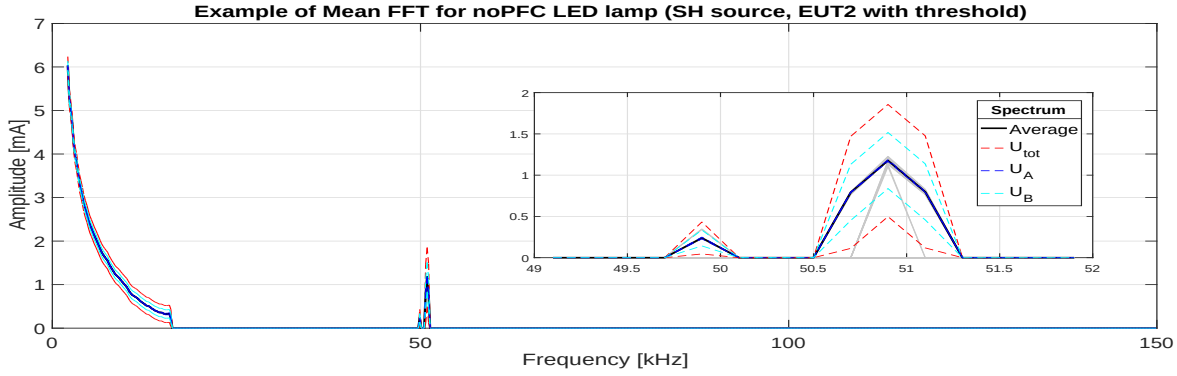

(b) Current emissions from a no PFC LED lamp in single operation

Figure 5-3.: Mean FFT for single operation of two different no PFC LED lamps

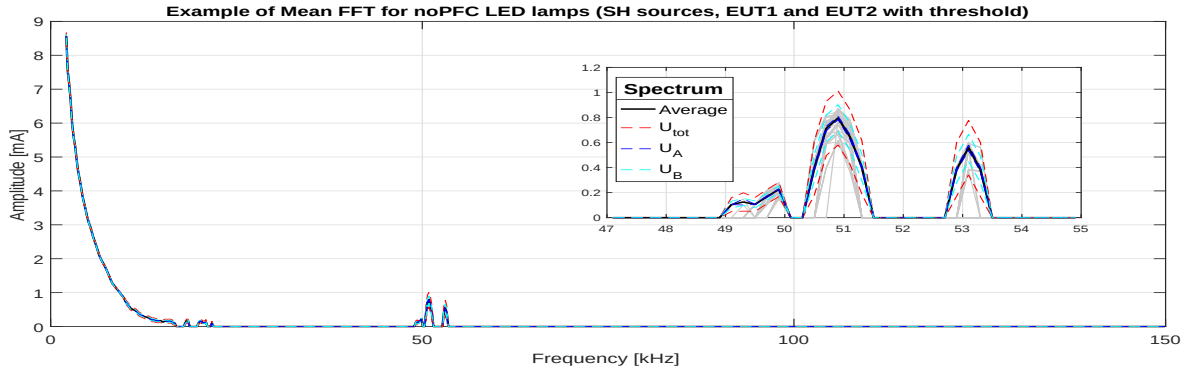

(a) Current emissions from two different no PFC LED lamps in simultaneous operation (Current at source, i_s)

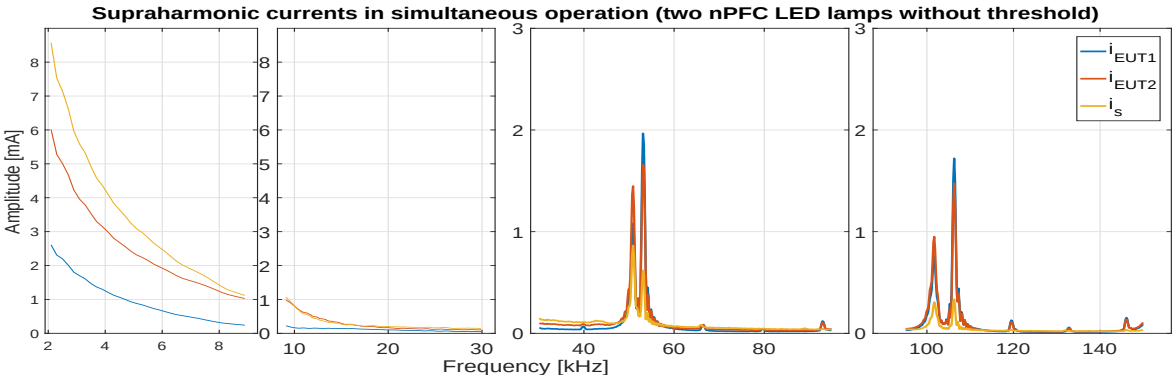

(b) Current emissions from two different no PFC LED lamps in simultaneous operation (i_s, i_{EUT1}, i_{EUT2})

Figure 5-4.: Mean FFT for simultaneous operation of two different no PFC LED lamps

For the assessment of the supraharmonic emissions in base case, i.e. using a pure sinusoidal voltage source and none network impedance between voltage source and EUT, the "source-sink" approach is used to describe the behaviour of selected EUT under simultaneous operation. Table **5-3** summarizes the set of EUT combinations.

Table 5-3.: Equipment Under Test (EUT)

Combination	PFC approach		Source-Sink approach	
	EUT1	EUT2	EUT1	EUT2
1	no PFC	no PFC	source	source
2	noPFC	capacitive	source	sink
3	aPFC	noPFC	source	source
4	aPFC	aPFC	source	source

5.2.2. Variations in the interaction of supraharmonic emissions

Analogous to the set of combinations of Chapter 4, Table **5-4** lists the considered deviations from base case for the assessment of the variation of supraharmonics emissions for simultaneous operation of EUT.

Table 5-4.: Variations of experimental setup base case

Experiment	Description	
	Voltage source	Network impedance
1	Sinusoidal	-
2		LISN (Z2)
3	Distorted	-
4		LISN (Z2)
5	Grid	

The three-steps methodology for supraharmonics emission processing were the same mentioned in Chapter 4 and rewritten here for completeness:

Table 5-5.: Summary of methodology for assessing supraharmonic emissions in simultaneous operation

Parameter	**Magnitude**	**Angle**
Spectrum	Scaled single-sided FFT	Artificially assigned
Frequency aggregation	RMS value of each 200 Hz frequency band	The angle of highest emission within each 200 Hz frequency band
Time aggregation	Mean value using 40 signal blocks	Mean value using 40 signal blocks

5.3. Results

Since magnitude thresholds were not used in this chapter in order to better describe the behaviour of emissions, hypothesis test were used instead of coherence function. These tests were used for the assessment of emissions magnitude variation when different network impedances were considered according to Table **5-4**. Hypothesis test are basically defined as follows [2]:

$$\begin{cases} H0: & \text{magnitude did not changed in average (null hypothesis)} & \text{(5-1a)} \\ H1: & \text{magnitude was different in average (not null hypothesis)} & \text{(5-1b)} \end{cases}$$

Equation 5-2 was therefore intended to show an "averaged" value of hypothesis test when it is evaluated within a frequency band. The hypothesis test is performed at each frequency component assuming that population values were obtained from one spectrum (i.e. reference spectrum) and the sampling values were obtained from another spectrum (i.e. tested spectrum) .

$$H_{xy|_{a-b}} = \frac{1}{(b-a)} \sum_{f=a}^{f=b} H_{xy,f_i} \tag{5-2}$$

Where:

- $H_{xy|_{a-b}}$: Averaged value of hypothesis test between signals x and y
- a, b: Lower and upper frequencies defining a frequency band

This average value took into account the result of hypothesis test (0 or 1) for the currents magnitudes at each frequency band. An averaged hypothesis test result close to 1 means that the null hypothesis can be rejected at the selected significance level (magnitudes are different at 95% level of confidence), whilst an averaged hypothesis test result close to 0 means the null hypothesis cannot be rejected at the selected significance level (magnitudes cannot be said to be different at 95% level of confidence).

In order to show the frequency bands having higher averaged hypothesis test results, values equal or above 0.5 were highlighted. Although values lower than 0.5 are not highlighted, they do not mean the variation in emissions magnitude were completely negligible: since averaged hypotehsis test results took into account frequency bands, narrow band emissions can represent a short amount of frequencies within the assessed frequency band.

5.3.1. Interactions in base case: sinusoidal voltage source and no network impedance

A set of four LED lamps were combined as listed in Table **5-3** for the assessment of supraharmonic emissions in EUT simultaneous operation. Although selected noPFC LED lamps in Chapter 4 did not have significant emissions, other set of same topology devices did show current emissions at supraharmonic range. Figures **5-5**a to **5-5**d show current emissions for the proposed combinations using the "source - sink" approach.

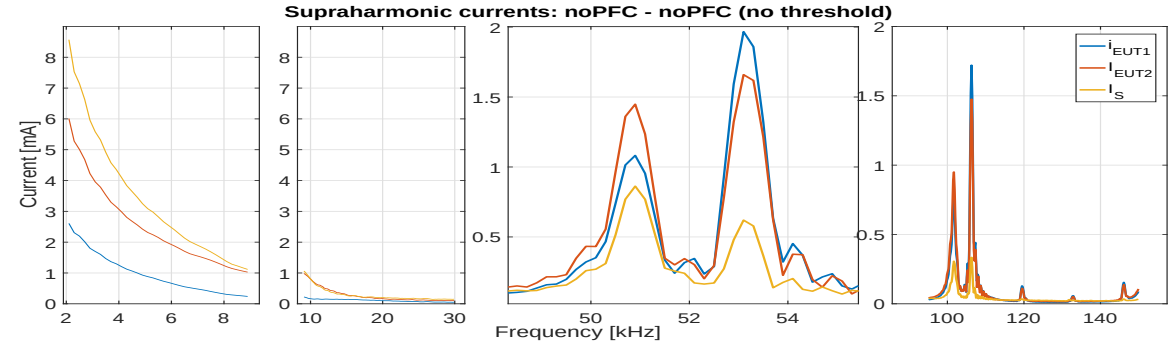

(a) noPFC - noPFC (source - source)

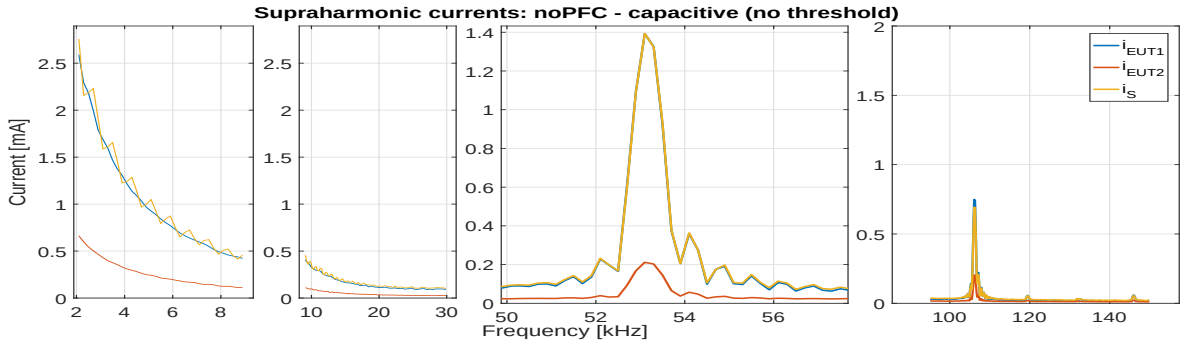

(b) noPFC - capacitive (source - sink)

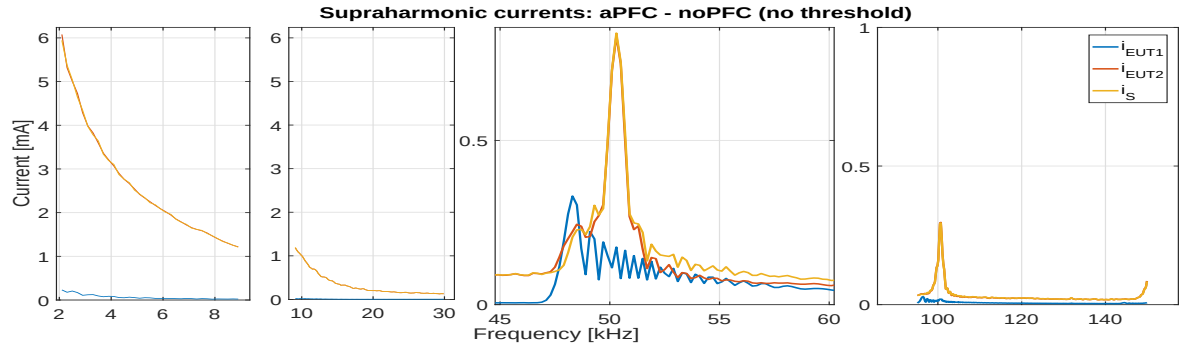

(c) aPFC - noPFC (source - source)

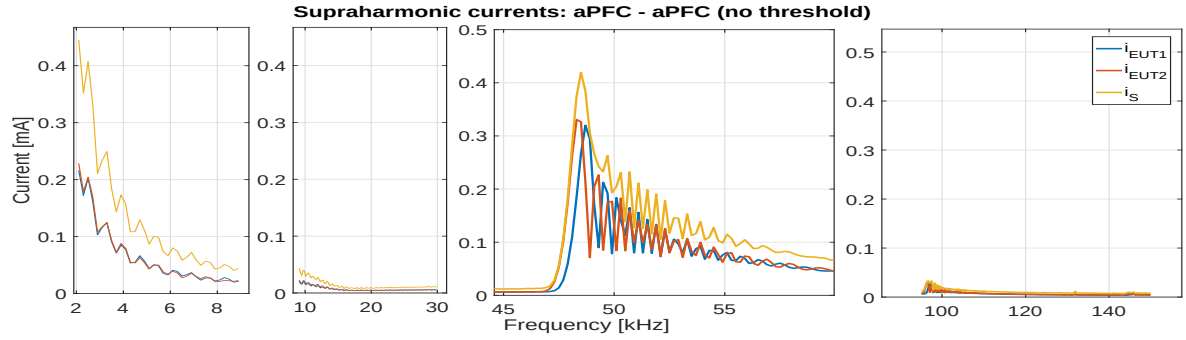

(d) aPFC - aPFC (source - source)

Figure 5-5.: Supraharmonic currents for different combination of LED topologies (sources and sinks) using pure sinusoidal voltage source and no network impedance.

Because most of the interaction features can be imperceptible after using the thresholds proposed in Chapter 3, no thresholds were used for interactions description. Hence, the description of current emissions in this chapter is more qualitative: the purpose is not to report a certain value of amplitude but rather to perceive the behaviour of emissions. Because of the same reason, most supraharmonic voltages are below the thresholds and the corresponding analysis in simultaneous operation might lead to erroneous results without using thresholds. In summary, only current supraharmonics are analyzed in this section using no amplitude threshold.

5.3.1.1. Current interaction

Figure **5-5**a shows the supraharmonic emissions from two noPFC LED lamps in simultaneous operation. The current emissions around 51 kHz and 53 kHz are produced by each LED lamp respectively, see Figures **5-3**a and **5-3**b. In simultaneous operation the total supraharmonic current from voltage source (i_s, yellow color) is lower than the currents i_{EUT1} and i_{EUT2} at 53 kHz and 51 kHz respectively. As discussed in different previous works (e.g. [3],[4],[5]), supraharmonic currents mainly flows between appliances rather than towards the grid because of the low impedance of the neighboring devices. The primary emission related to each EUT in single operation remains dominant in simultaneous operation (blue current is related to EUT1 primary emission; red current is related to EUT2 primary emission). Both primary current emissions lead to a corresponding secondary current emission at neighboring EUT around 51 kHz and 53 kHz correspondingly. Nevertheless, the behaviour of surpaharmonic currents between 45 kHz and 55 kHz is different from that below 10 kHz, where current magnitude from voltage source i_S is higher than currents i_{EUT1} and i_{EUT2}.

The interaction of current emissions in supraharmonic range depicted in Figure **5-5**b was rather different to the previous case: when using a source-sink combination in simultaneous operation (passive PFC and a capacitive LED lamps), the current from the EUT acting as supraharmonic source (i_{EUT1}) is mainly perceived at source current (i_S) rather than at EUT acting as supraharmonic sink (i_{EUT2}). That to say, in this case the main interaction in terms of currents was between EUT1 and voltage source.

For the case aPFC - noPFC (source-source) combination the situation is similar to the previous case: the magnitude of supraharmonic current from active PFC LED lamp (i_{EUT1}) was not notably affected by current from noPFC LED lamp (i_{EUT2}). Indeed, total current (i_S) around 50 kHz mainly contains emissions from noPFC LED lamp (i_{EUT2}).

Finally, the interaction between aPFC - aPFC LED lamps are depicted in Figure **5-5**d. The influence of current i_{EUT2} over current i_{EUT1} and vice versa was negligible. Therefore, the interaction of supraharmonic currents between these EUT was negligible between 55 kHz and

60 kHz. The total current i_S showed the aggregation of both current emissions, therefore each of the EUT interacted mainly with the voltage source.

From the previous results, it can be stated that the interaction of supraharmonic currents strongly depends on the input impedance of neighboring EUT. Although some noPFC and active PFC LED lamps may act as supraharmonic sources, the current that is perceived on other EUT (i_{EUT1}, i_{EUT2}) or in the total current from voltage source (i_S) depends on the input impedance of devices. In this sense, the topology of EMI filters, Power Factor Corrector and other interacting stages at the frontier between EUT and voltage source (the grid in real life cases) will determine the interaction of emissions in simultaneous operation. For selected EUT in this thesis the interaction of noPFC LED lamps acting as supraharmonic sources was stronger than the interaction of these EUT with other topologies such as capacitive, passive or active PFC LED lamps. The EUT classification according to current waveform distortion below 2 kHz might be improved if supraharmonic range is also considered. The latter would provide a more comprehensive classification not only in terms of PFC topologies (therefore input impedances) but also the emissions produced by such EUT in supraharmonic range.

5.3.1.2. Emissions using different wires length

Figures **5-6**a to **5-6**d show subtle changes when connection wires of EUT2 were lengthen, see Figure **5-1**. There were two main differences in the considered cases: the supraharmonic current magnitude and the frequency of emissions. For the case noPFC - noPFC (source-source) the changes in magnitude were rather small, but the changes in emissions frequency were perceptible. After increasing length of EUT2 connection wires, the original supraharmonic shifted from 50.9 kHz to 50.7 kHz (about 200 Hz). Since emissions are grouped into 200Hz frequency bands as explained in Chapter 3, this means that the frequency of average emission might be shifted to a lower 200-Hz frequency band.

For the case noPFC - capacitive LED lamps (source-sink) the magnitude of supraharmonic current was decreased about 20% in both EUT1 and EUT2 after lengthening connection wires of EUT2 (capacitive LED lamp), see Figure **5-6**b. The frequency of main emissions was shifted from 53.1 kHz to 52.9 kHz. Main interaction using original and longer connection wires was still between noPFC LED lamp acting as supraharmonic source and voltage source.

Figure **5-6**c shows a different behaviour compared to the two last cases. When noPFC LED lamp (EUT2) is electrically further from active PFC LED lamp (EUT1) and voltage source, the original supraharmonic current i_{EUT2} is increased in magnitude about 50% and shifted up to 50.9 kHz (600 Hz increase). On the contrary, current from EUT1 i_{EUT1} remained virtually unmodified. It is clear that current i_{EUT2} mainly interacts with the total current from voltage source i_S.

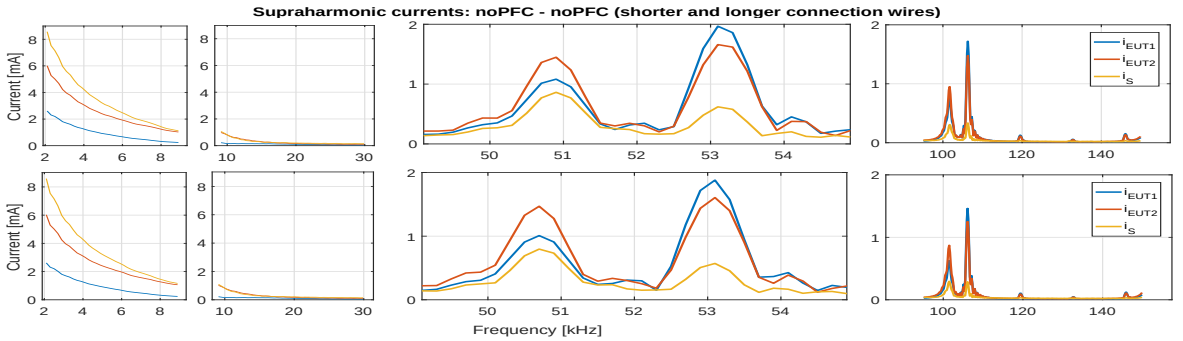

(a) noPFC - noPFC (source - source)

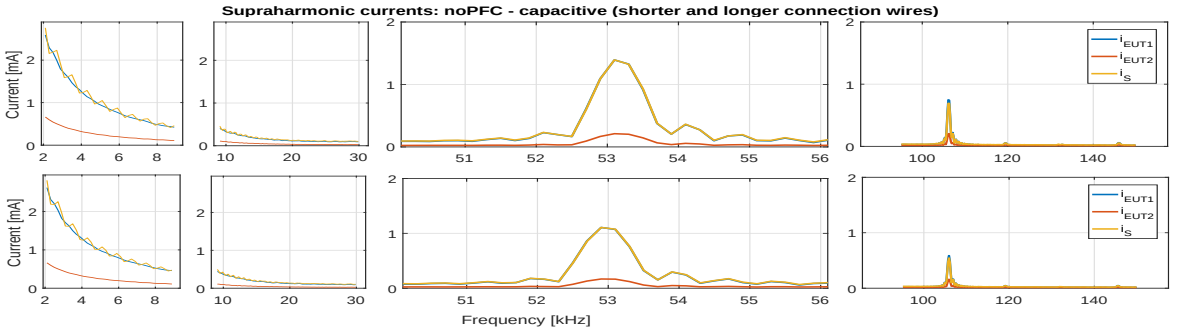

(b) noPFC - capacitive (source - sink)

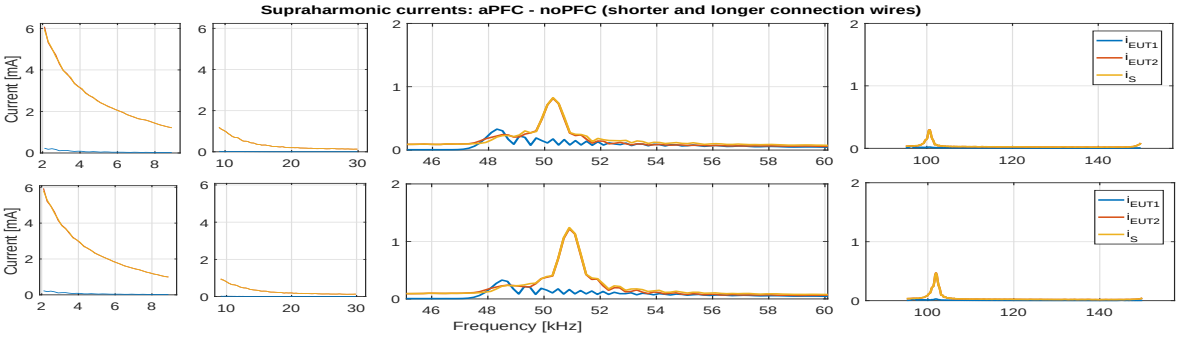

(c) aPFC - noPFC (source - source)

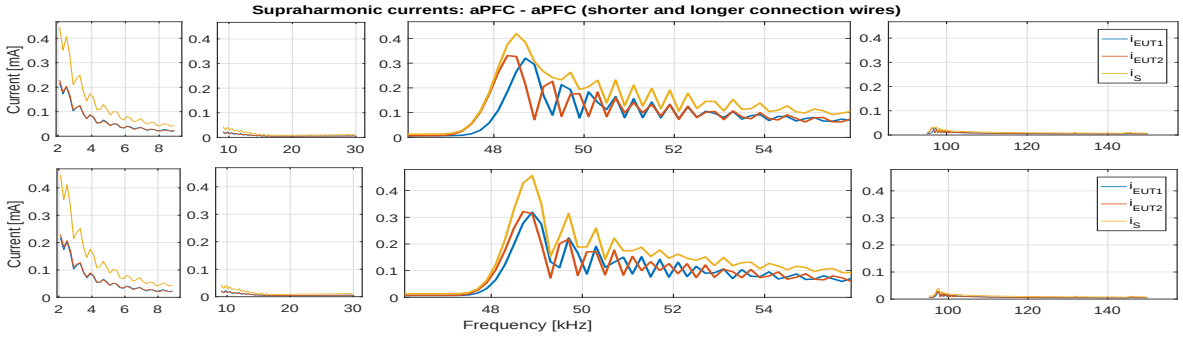

(d) aPFC - aPFC (source - source)

Figure 5-6.: Supraharmonic currents for different combination of LED topologies (sources and sinks) using sinusoidal voltage source, no network impedance and two different lengths for connection wires.

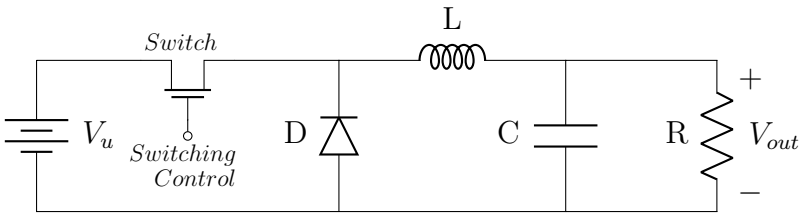

Figure 5-7.: Circuit model for Buck Converter [5].

Finally, Figure **5-6**d depicted a similar behaviour of that of aPFC-noPFC (source-source) case. The changes in the interaction of two active PFC LED lamps were mainly perceived in a frequency shift of emissions. In general terms, all supraharmonic currents were shifted 400 Hz from the original frequency 48.5 kHz. Changes in supraharmonic magnitudes were rather negligible and the total current i_S contained both spectra from i_{EUT1} and i_{EUT2}.

From the point of view of DC-DC converters' control loop, the average output voltage (V_{out} in Figure **5-7**) is controlled by methods modifying the switch on and off duration (t_{on} and t_{off}) [6]. One of such methods employs switching at a constant frequency (Continous Conduction Mode, CCM) and adjusts the t_{on} duration of the switch to control the average output voltage (pulse-width modulation switching PWM) [6]. Other methods are based on the variation of both switching frequency and t_{on} duration [6][7]. The Boundary Conduction Mode (BCM) is used to achieve a lower PFC inductor size, continuously varying the switching frequency to keep this mode over the entire power cycle [7]. With either methods an increase in the connection wires might lead to a reduction in converter's input voltage (V_u in Figure **5-7**) and therefore, the control loop will act over transistor commutation (*Switch* in Figure **5-7**) [5]. This can be perceived in Figures from **5-6**a to **5-6**d, where EUT changed both their current supraharmonic magnitudes and switching frequencies when connection wires were lengthen. Once again, EUT equivalent input impedances govern the behaviour of converters' built-in circuits and therefore, the interaction of supraharmonic current emissions among EUT and voltage source.

5.3.2. Variations in the interaction: distorted voltage source and different networks impedances

The last section described the interaction of current supraharmonics in simultaneous operation using pure sinusoidal voltage source and no additional network impedance. This set of "controlled" conditions are not likely to be found in real low voltage grid though. Similar to the variations presented in Chapter 4: *Referencesch:Identification*, next subsections describe the results from varying the base case setup according to the experiments listed in Table **5-4**.

5.3.2.1. Variation in voltage source distortion

Supraharmonic emissions from a distorted voltage source will also interact with emissions from EUT. Figures **5-8**a to **5-8**d show the interaction of such emissions when no additional network impedance is used between voltage source and EUT. Although the voltage distortion was kept the same as in Chapter 4, i.e. at 1V and 20 kHz (usual value for switching frequency of PV inverters [8][9][10]), interactions were different using different PFC topologies for LED lamps.

Figures **5-8**a and **5-8**b show the effect over current primary emissions when voltage secondary emission is present at voltage source. This behaviour mostly corresponds to amplitude modulation, in the sense that a time-varying signal is acting as a modulating signal over another time-varying signal acting as base-band signal[11]. According to amplitude modulation theory using continuous waves, a carrier signal can be represented as an impulse function in frequency domain which shifts the base-band signal (in communication systems, the message) to another frequency range [11]. The general form for an amplitude-modulated signal in time domain can be expressed as [11]:

$$s(t) = [A_c + A_c K_a m(t)]\, cos(2\pi f_c t)$$

Where:

- $s(t)$: Modulated signal.
- A_c: Carrier amplitude.
- K_a: Amplitude sensitivity (normalization factor, relevant in communication systems).
- . $m(t)$: Modulating signal.

For such modulation in time, the corresponiding Fourier transform is given by [11]:

$$S(f) = \frac{A_c}{2}\left[\delta(f - f_c)\delta(f + f_c)\right] + \frac{K_a A_c}{2}\left[M(f - f_c) + M(f + f_c)\right] \tag{5-3}$$

Interaction of voltage disturbance at 20 kHz and current primary emissions around 50 kHz are depicted in Figure **5-8**a. Primary current emissions in the noPFC - noPFC (source-source) case produced supraharmonic currents at 51 kHz and 53 kHz, see Figure **5-5**a. This current emissions also appeared around 50 kHz, but in this case, two additional current emissions at ± 20 kHz appeared keeping same structure of original current emissions. This behaviour is similar to that known as of Double-Side Band Long-Carrier (DSB-LC), the simplest AM modulation technique [11]. The other perceptible, non-linear behaviour perceived in cases noPFC - noPFC (source-source) and noPFC - capacitive (source-sink) cases, Figures **5-8**a and **5-8**b respectively, corresponds to the harmonics of voltage distortion at $\pm 20n$ kHz, where n is an integer number. The case activePFC - noPFC (source-source) shows a subtle but similar behaviour form previous two cases.

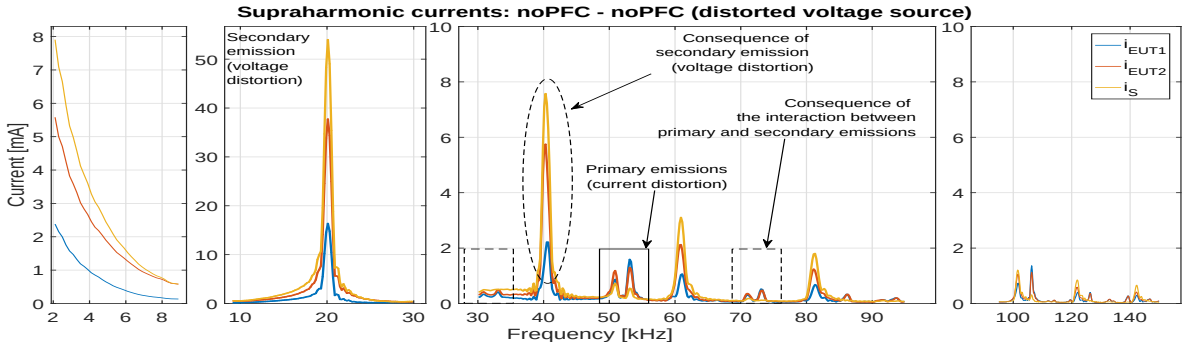

(a) noPFC - noPFC (source - source)

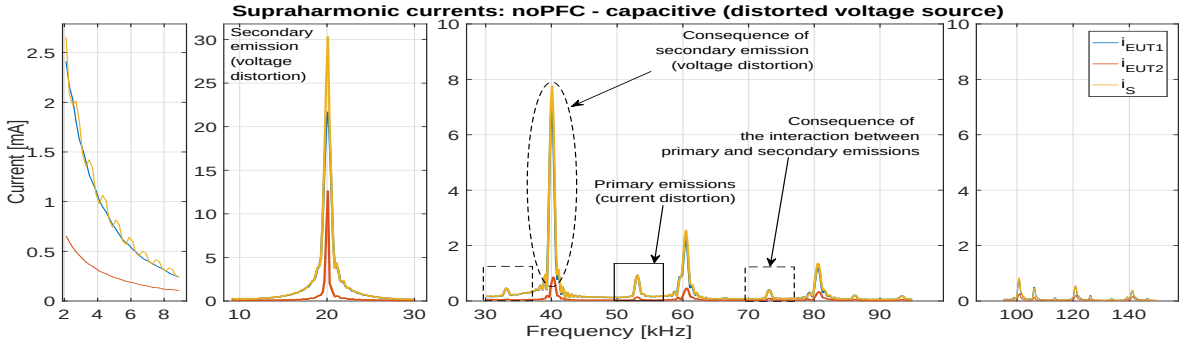

(b) noPFC - capacitive (source - sink)

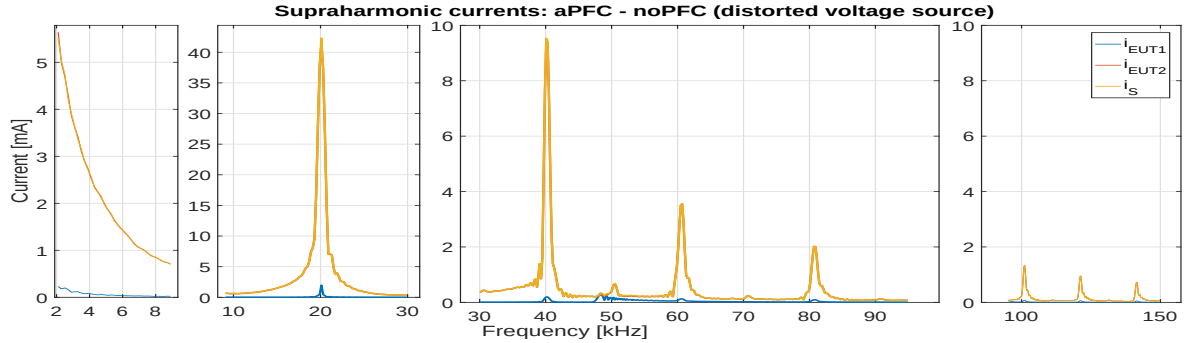

(c) aPFC - noPFC (source - source)

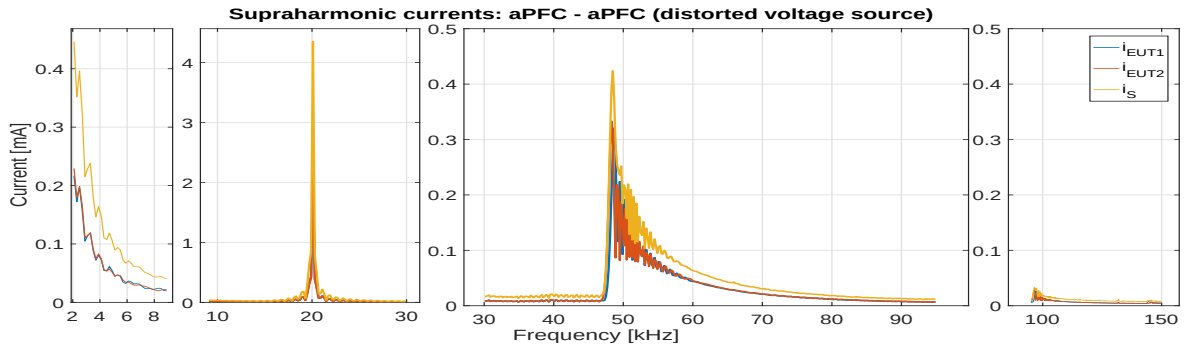

(d) aPFC - aPFC (source - source)

Figure 5-8.: Supraharmonic currents for different combination of LED topologies (sources and sinks) using a distorted voltage source and none external nework impedance.

Finally, active PFC LED lamp did not show a significant change in current emission when exposed to voltage distortion. Figure **5-8**c showed that most of the interaction between voltage supraharmonic distortion and current emissions are developed between noPFC and voltage source. Figure **5-8**d showed that supraharmonic currents from active PFC LED lamps were not influenced by voltage distortion, that to say no secondary emissions were produced when these lamps were exposed to supraharmonic voltages.

5.3.2.2. Variation in network impedance

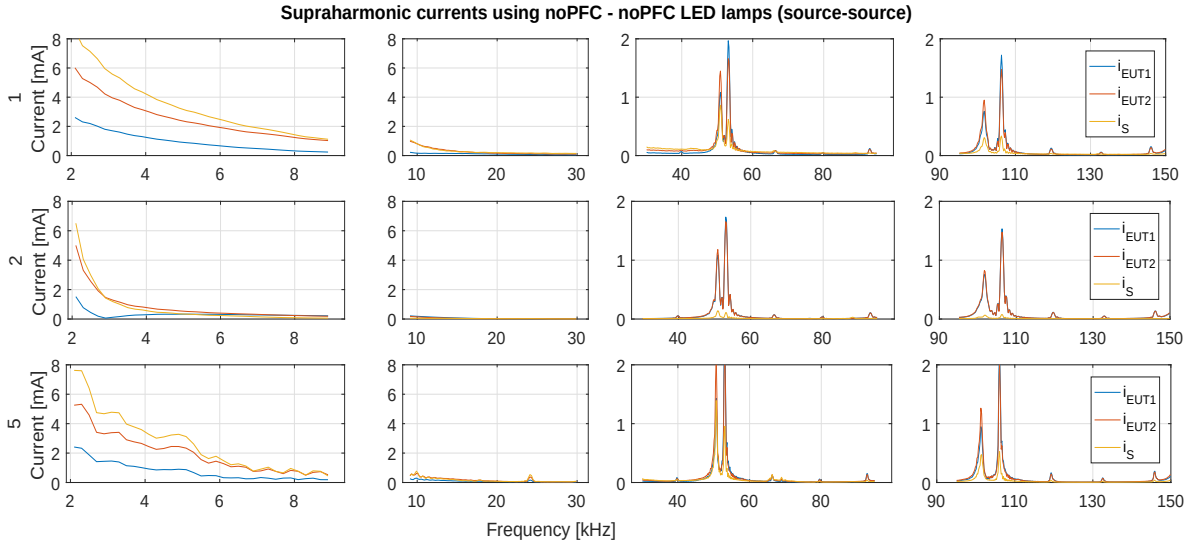

(a) noPFC - noPFC (source - source)

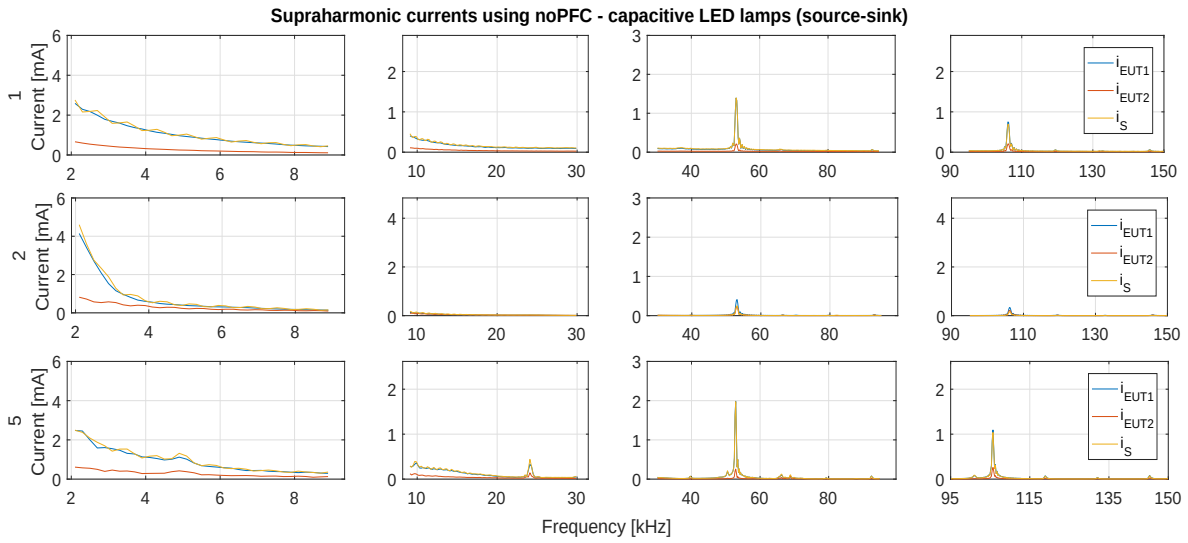

(b) noPFC - capacitive (source - sink)

Figure 5-9.: Supraharmonic currents for noPFC-noPFC and noPFC-Capacitive LED lamps using sinusoidal voltage source and different network impedances.

Figures **5-9**a to **5-10**b show the spectrum for EUT combinations described in Table **5-3**. Experiments 1 and 2 corresponds to Z1 (no network impedance) and Z2 (LISN impedance), whilst experiment 5 corresponds to grid measurements. Similar to the situation in single operation, the variation in supraharmonic current emissions showed strong dependency on the EUT input impedances. For combination noPFC - noPFC (source-source), experiment 2 (Z2 impedance) showed a reduction in emissions magnitude compared to experiment 1 (Z1), see Figure **5-9**a, in all four frequency bands (2-8.9, 9.1-29.9, 30.1-94.9, 95.1-150 kHz). This was also found in Chapter 4 for current emissions. All three currents were reduced in magnitude when using Z2 impedance compared to emissions using Z1 impedance at first frequency band. Grid measurements (experiment 5) shows that supraharmonic primary currents appeared at same frequencies (third frequency band) that experiments 1 and 2 but had different magnitudes though. The highest magnitude variation between 29.9 kHz and 94.9 kHz was perceived in source current when using Z2 network impedance compared to the other two cases.

Table **5-6** summarizes the average results of hypothesis test performed over the whole supraharmonic range 2-150 kHz for i_{EUT1}, i_{EUT2} and i_S in combination noPFC - noPFC (source-source) LED lamps. This average value took into account the result of hypothesis test (0 or 1) for the currents magnitudes at each frequency band. An averaged hypothesis test result close to 1 means the null hypothesis can be rejected at the selected significance level (magnitudes are different at 95% level of confidence), whilst an averaged hypothesis test result close to 0 means the null hypothesis cannot be rejected at the selected significance level (magnitudes cannot be said to be different at 95% level of confidence).

Table 5-6.: Hypothesis test average results for supraharmonic current magnitude using noPFC - noPFC LED lamps

Hypothesis test: average results												
COMPARISON	noPFC - noPFC (source - source)											
	i_{EUT1}				i_{EUT2}				i_S			
	2.1-8.9	9.1-29.9	30.1-94.9	95.1-149.9	2.1-8.9	9.1-29.9	30.1-94.9	95.1-149.9	2.1-8.9	9.1-29.9	30.1-94.9	95.1-149.9
1-2	0.8	0.1	0.0	0.1	1.0	0.8	0.1	0.1	1.0	0.9	0.3	0.1
1-5	0.6	0.1	0.1	0.1	0.9	0.4	0.1	0.1	0.9	0.5	0.1	0.1

Similar to results from Figure **5-9**a, Table **5-6** shows the highest average variation of currents magnitude between 2 and 9 kHz for all three currents. The hypothesis test averaged value reported for currents i_{EUT2} and i_S between 9-30 kHz where higher than the results for current i_{EUT1}. That to say, currents i_{EUT2} and i_S had a higher variation when network impedance changed from Z1 to Z2 compared to changes in current i_{EUT1}.

The situation is similar for noPFC-capacitive (source-sink) EUT combination. Figure **5-9**b and Table **5-7** show an evident reduction in magnitude of currents i_{EUT1} and i_S between 2-8.9 kHz. Supraharmonic currents within third frequency band (30.1-94.9 kHz) appeared at same frequencies that the case in single operation, but again the use of Z2 led to a magnitude reduction compared to case of Z1. Grid measurements showed emissions at same frequencies within third frequency band, but again higher than the other two cases. The reduction of currents magnitude between 30.1-94.9 kHz is evident from Figure **5-9**b. However, these emissions can be considered as narrow-band signals and therefore, Table **5-7** shows a low average result for hypothesis test.

Table 5-7.: Hypothesis test average results for supraharmonic current magnitude using noPFC - capacitive LED lamps

Hypothesis test: average results												
COMPARISON	noPFC - capacitive (source - sink)											
	i_{EUT1}				i_{EUT2}				i_S			
	2.1-8.9	9.1-29.9	30.1-94.9	95.1-149.9	2.1-8.9	9.1-29.9	30.1-94.9	95.1-149.9	2.1-8.9	9.1-29.9	30.1-94.9	95.1-149.9
1-2	0.9	0.6	0.2	0.1	0.2	0.0	0.0	0.1	0.9	0.6	0.3	0.1
1-5	0.6	0.2	0.1	0.1	0.1	0.0	0.0	0.0	0.6	0.1	0.2	0.1

Table 5-8.: Hypothesis test average results for supraharmonic current magnitude using activePFC - noPFC LED lamps

Hypothesis test: average results												
COMPARISON	aPFC - noPFC (source - source)											
	i_{EUT1}				i_{EUT2}				i_S			
	2.1-8.9	9.1-29.9	30.1-94.9	95.1-149.9	2.1-8.9	9.1-29.9	30.1-94.9	95.1-149.9	2.1-8.9	9.1-29.9	30.1-94.9	95.1-149.9
1-2	0.0	0.0	0.0	0.0	0.9	0.9	0.2	0.1	1.0	0.9	0.2	0.1
1-5	0.0	0.0	0.0	0.0	1.0	0.5	0.2	0.1	1.0	0.5	0.2	0.0

Figure **5-10**a shows a slightly different behaviour for noPFC - aPFC (source-source) EUT combination. Emissions magnitude at first frequency band are also decreased when using Z2 network impedance compared to the other two cases. While primary emissions from noPFC LED lamp also decreased in magnitude like previous cases at third frequency band, the current emission for active PFC remained rather unmodified. This matches the results

from Chapter 4, where emissions magnitude depicted in Figure **4-15**a and Table **4-5** showed that current emissions remained rather unchanged for active PFC LED lamps when different network impedances were used. Figures **5-5**c-**5-5**d as well as **5-8**c-**5-8**d are also consistent with these findings. Table **5-8** also shows that current i_{EUT1} (aPFC)did not change at 95% level of confidence when using different network impedances. On the other hand, the changes in i_{EUT2} (noPFC) and consequently in i_S were evident at 95% level of confidence.

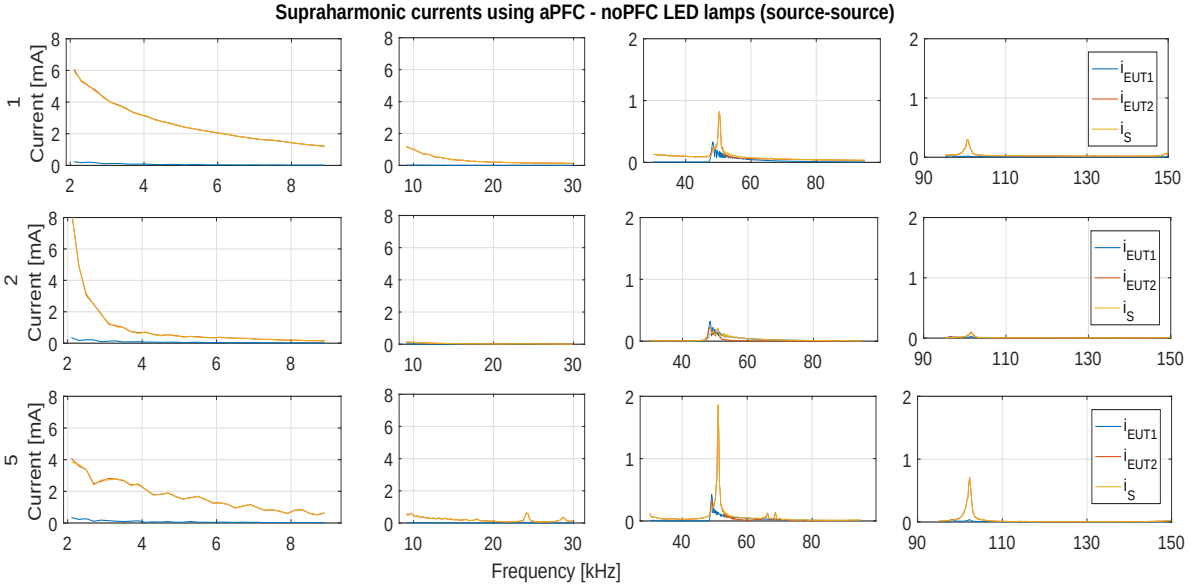

(a) aPFC - noPFC (source - source)

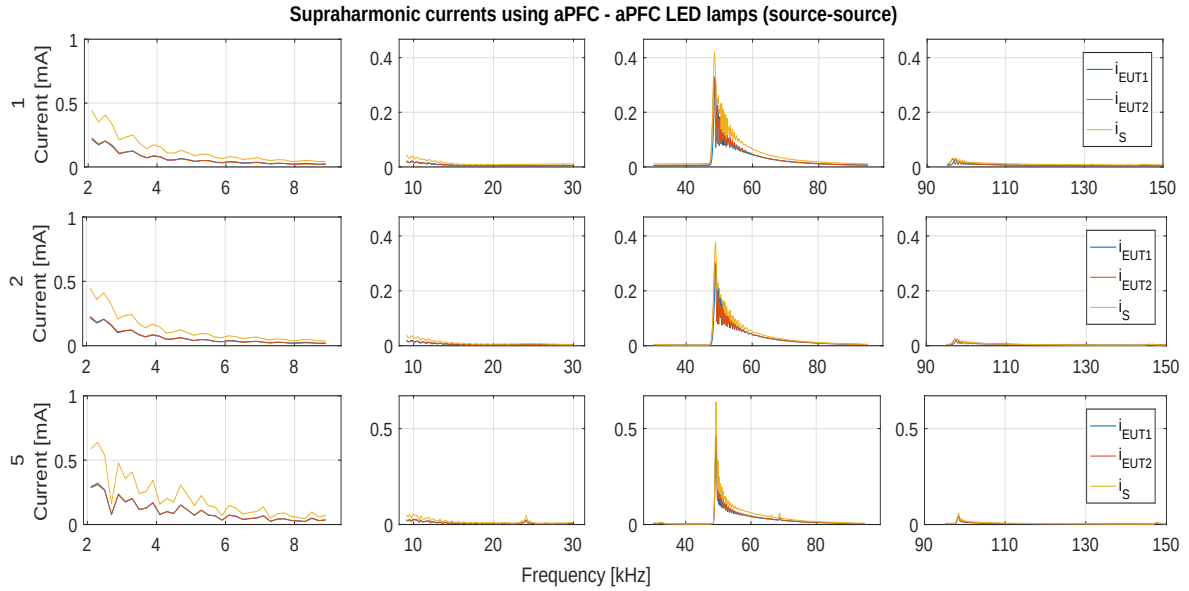

(b) aPFC - aPFC (source - source)

Figure 5-10.: Supraharmonic currents for activePFC-noPFC and activePFC-activePFC LED lamps using sinusoidal voltage source and different network impedances.

Finally, Figure **5-10**b shows the variation of supraharmonic currents when different network impedances are used for aPFC - aPFC (source-source) EUT combination. Similar to the previous combination, the current emissions remained rather unchanged when Z1 and Z2 network imepdances were used. The same described in the latter chapter, the input impedance of selected active PFC LED lamps showed a different behaviour in terms of supraharmonic current interactions compared to noPFC and capacitive LED lamps topologies. Results from averaged hypothesis thesis also showed that most of the emissions remained unchanged at 95% level of confidence, as can be seen in Table **5-9**. The highest variation was for the comparison between Z1 and Grid measurements.

Table 5-9.: Hypothesis test average results for supraharmonic current magnitude using activePFC - activePFC LED lamps

Hypothesis test: average results												
COMPARISON	aPFC - aPFC (source - source)											
	i_{EUT1}				i_{EUT2}				i_S			
	2.1-8.9	9.1-29.9	30.1-94.9	95.1-149.9	2.1-8.9	9.1-29.9	30.1-94.9	95.1-149.9	2.1-8.9	9.1-29.9	30.1-94.9	95.1-149.9
1-2	0.0	0.0	0.0	0.0	0.0	0.0	0.1	0.0	0.1	0.0	0.0	0.0
1-5	0.1	0.0	0.1	0.0	0.1	0.0	0.1	0.0	0.3	0.0	0.1	0.0

From these results, it can be stated that most of the interactions between considered EUT at supraharmonic range strongly depend on input impedances. Different LED lamps led to different interactions between supraharmonic currents. Network impedance also influences the magnitude of emissions and therefore, the measurement setup must be carefully selected in order to represent real, likely conducted supraharmonic emissions in an electrical installation.

5.4. Conclusions

This chapter presented an assessment of supraharmonic emissions using EUT in simultaneous operation. From the use of the spectrogram and mean FFT, it could be perceived the time-varying behaviour of supraharmonic current emissions. These emissions were perceptible at grid current during the conduction of rectifier diodes and therefore, they appear during a time shorter than a single power cycle. Because most of the interaction features were imperceptible after using the thresholds proposed in Chapter 3, no thresholds were used for interactions description. Because of the same reason, most supraharmonic voltages were below the proposed thresholds and were threfore not analyzed in the interaction assessment. As discussed in different previous works, supraharmonic currents mainly flows between appliances rather than towards the grid because of the low impedance of the neighboring devices.

Because of this, a “source and sink” approach was used to describe the interactions. The primary emission related to each EUT in single operation remains dominant in simultaneous operation. Both primary current emissions lead to a corresponding secondary current emission at neighboring EUT. It could be stated that the interaction of supraharmonic currents strongly depends on the input impedance of neighboring EUT.

REFERENCES

[1] Ana Maria Blanco, Manish Gupta, Aurora Gil de Castro, Sarah Ronnberg, and Jan Meyer. Impact of flat-top voltage waveform distortion on harmonic current emission and summation of electronic household appliances. *Renewable Energy and Power Quality Journal*, 1:698–703, Apr 2018. doi: 10.24084/repqj16.437.

[2] Roy D. Yates and David J. Goodman. *Probability and Stochastic Processes: A Friendly Introduction for Electrical and Computer Engineers*. Wiley, 2004. ISBN 0471272140.

[3] Sarah K. Rönnberg, Math H.J. Bollen, Hortensia Amaris, Gary W. Chang, Irene Y.H. Gu, Łukasz H. Kocewiak, Jan Meyer, Magnus Olofsson, Paulo F. Ribeiro, and Jan Desmet. On waveform distortion in the frequency range of 2 khz–150 khz—review and research challenges. *Electric Power Systems Research*, 150:1–10, Sep 2017. doi: 10.1016/j.epsr.2017.04.032.

[4] Sarah Rönnberg, Math Bollen. Propagation of Supraharmonics in the Low Voltage Grid. Report, Energiforsk, Stockholm, Sweden, 2017.

[5] Daniel Agudelo-Martinez, Fabian Rios, and Andres Pavas. Interaction of some low power led lamps within 2–150 khz (supraharmonics). In *2018 18th International Conference on Harmonics and Quality of Power (ICHQP)*. IEEE, May 2018. doi: 10.1109/ichqp.2018.8378815.

[6] Ned Mohan, Tore M. Undeland, and William P. Robbins. *Power Electronics: Converters, Applications, and Design*. Wiley, 2002. ISBN 9780471226932.

[7] Christian Waniek, Thomas Wohlfahrt, Johanna M.A. Myrzik, Jan Meyer, Matthias Klatt, and Peter Schegner. Supraharmonics: Root causes and interactions between multiple devices and the low voltage grid. In *2017 IEEE PES Innovative Smart Grid Technologies Conference Europe (ISGT-Europe)*. IEEE, Sep 2017. doi: 10.1109/isgteurope.2017.8260267.

[8] Sarah K. Ronnberg, Aurora Gil de Castro, Antonio Moreno-Munoz, Math H.J. Bollen, and Joaquin Garrido. Solar PV inverter supraharmonics reduction with random PWM. In *2017 11th IEEE International Conference on Compatibility, Power Electronics and Power Engineering (CPE-POWERENG)*. IEEE, 2017. doi: 10.1109/cpe.2017.7915248.

[9] Dilini Darmawardana, Sarath Perera, Duane Robinson, Philip Ciufo, Jan Meyer, Matthias Klatt, and Upuli Jayatunga. Investigation of high frequency emissions (supra-harmonics) from small, grid-tied, photovoltaic inverters of different topologies. In *2018 18th International Conference on Harmonics and Quality of Power (ICHQP)*. IEEE, May 2018. doi: 10.1109/ichqp.2018.8378926.

[10] Andras Mohos and Jozsef Ladanyi. Emission measurement of a solar park in the frequency range of 2 to 150 kHz. In *2018 International Symposium on Electromagnetic Compatibility (EMC EUROPE)*. IEEE, August 2018. doi: 10.1109/emceurope.2018.8485049.

[11] Simon Haykin and Michael Moher. *Communication Systems*. Wiley, 2009. ISBN 9780471697909.

6. Conclusions

Supraharmonic emissions are currently understood as a type of permanent Power Quality deviation (conducted phenomena) from the idealized voltage and current waveforms: sinusoidal, constant amplitude and single frequency, neither frequency nor angle difference between them, zero-phase difference between them. These waveform disturbances, mainly caused by the operation of non-linear loads, might be able to produce interference on susceptible equipment exposed to them.

This research identified the unintentional supraharmonic emissions from a selected set of low power LED lamps acting as household appliances, used in the customer side (low voltage) of the distribution grid. The assessed LED lamps mainly use non-linear circuits, i.e. rectifiers, filters, converters, and other stages based on power electronics circuits. These non-linear circuits allow to reduce equipment size and/or increase their energy efficiency (energy-savings devices). The following paragraphs describe the conclusions derived from the achievement of general and specific objectives of this research stated in Chapter 1.

6.1. Measurement challenges

A measurement system, an experimental setup and their related metrological parameters were successfully proposed and implemented in the development of this research to measure narrowband and boradband supraharmonic emissions in a single-phase, low voltage test network. Measurements showed that laboratory (partially controlled) and grid (uncontrolled) measurements of supraharmonic emissions may differ significantly regardless the Equipment Under Test (EUT) considered. Supraharmonic emissions produced by the operation of different LED low power lamps strongly depend on the voltage source, equivalent network impedance, sensors used in the measurement setup, and on the input impedance of selected lamps as shown in Chapter 3. 50% was used as the maximum percentage for the proposed metrological threshold, below which supraharmonic emissions were not taken into account for further analysis. However, this percentage is a tuning parameter prone to changes in future works. Realistic network impedances led to different current and voltage supraharmonic emissions compared to laboratory measurement setups; discrepancies are therefore expected between laboratory and real grid measurements. That to say, voltage source and network impedance strongly influence the supraharmonic current and voltage emissions from the assessed LED lamps.

6.2. Emissions in EUT single operation

For the identification of supraharmonic emissions from low power LED lamps in a low voltage test network under controlled conditions of voltage source and network impedance topology, different combinations of voltage source, network impedance and LED lamps were considered. Although different emissions were identified from devices classified as same PFC topology, the classification according to Power Factor Corrector topology helped organize some common behaviour of selected EUT as shown in Chapter 4. Using a sinusoidal voltage source, all EUT reported current emissions between 2-9 kHz, and only selected active PFC LED lamps had current emissions between 30-95 kHz. Using a voltage source with a controlled supraharmonic distortion, most of the selected LED lamps showed supraharmonic current emissions at the same frequency of that supraharmonic voltage emission, as well as its entire multiples (harmonics of supraharmonic distortion). Because of the metrological restrictions imposed by the measurement system used, most of the voltage supraharmonics presented amplitudes that lied below the proposed metrological thresholds and therefore an accurate value for such emissions was rather difficult to report. Compared to the other topologies, capacitive topology was more susceptible to have current harmonics as consequence of the intentional, controlled supraharmonic voltage emission.

In general terms, the selected LED lamps had a very different spectrum when comparing laboratory and grid measurements. Based on literature review and other works carried out by the author before and during the development of this research, it has been identified that supraharmonic emissions can be in general considered as a highly time-varying phenomena. Because of the supraharmonic emission pattern could change even within a single power cycle, an appropriate identification of supraharmonic voltages and currents should be performed in both frequency and time domains. Results from the use of the measurement system and experimental setup used in this research, showed that no supraharmonic emissions were identified from selected low power LED lamps between 95 and 150 kHz neither from laboratory nor from grid measurements. However, from the identification of supraharmonic emissions, EUT input impedance (i.e. the impedance seen from the Point of Common Connection towards the load) showed to be determinant for the understanding of supraharmonic emissions.

6.3. Interactions in EUT simultaneous operation

Chapter 5 was aimed to describe the interaction between supraharmonic sources in a low voltage test network. The lack of supraharmonic emissions from noPFC LED lamps used in Chapter 4 was the main reason to select a different set of noPFC LED lamps in Chapter 5 for the assessment of simultaneous operation of LED lamps. From this perspective, the "source and sink" approach served as a complement of the "primary and secondary emis-

sions" approach for the analysis of the interaction of supraharmonic currents. Similar to the assessment of supraharmonic voltages in single operation of EUT, an accurate value for the voltage distortions between 2-150 kHz under EUT in simultaneous operation was rather difficult to report as consequence of the metrological restrictions of measurement system used in this research. Selected active PFC LED lamps were less susceptible to network impedance changes and secondary supraharmonic emissions compared to no PFC, capacitive and passive PFC LED lamps. An increment of the length of connection wires slightly changed the amplitude and frequency of current emissions between 2-150 kHz in all selected low power LED lamps.

The interaction of surpaharmonic emissions in simultaneous operation showed to depend strongly on the input impedances of neighboring EUT. Similar to the case of EUT in single operation, different network impedances led to different supraharmonic current emissions. Therefore a discrepancy is expected between laboratory and grid measurements if a reference network impedance is not used. However, lower supraharmonic currents were measured by using LISN reference impedance when compared to more realistic, measured-based network impedances. Amplitude modulation was also perceptible when no PFC LED lamps were supplied simultaneously by a voltage source with an intentional supraharmonic emission. In general terms, the assessment of supraharmonic current interactions between 2-9 kHz might be different from the interactions perceived between 9-150 kHz.

6.4. Contributions

Some of the most relevant contributions from the development of this research are listed as follows:

- Metrological thresholds for analysis of supraharmonic emissions.
- Influence of a selected measurement setup on the emission of supraharmonics.
- Identification of supraharmonic emissions considering different network impedances and different topologies of LED lamps in single operation.
- Description of the interaction of supraharmonic emissions using different network imepdances and different topologies of LED lamps in single operation.

6.5. Publications

The following are the publications carried out during the development of this research:

D. Agudelo-Martínez, M. Limas, A. Pavas and J. Bacca,"Supraharmonic bands detection for low voltage devices," 2016 17th International Conference on Harmonics and Quality of Power (ICHQP), Belo Horizonte, 2016, pp. 1003-1009. doi: 10.1109/ICHQP.2016.7783327

D. Agudelo-Martínez and A. Pavas, "Simulation of supraharmonics: A Compact Fluorescent Lamp (CFL) in single operation," 2017 IEEE Workshop on Power Electronics and Power Quality Applications (PEPQA), Bogota, 2017, pp. 1-6. doi: 10.1109/PEPQA.2017.7981682

D. Agudelo-Martínez, C. Garzón and A. Pavas, "Interaction of power quality disturbances within 2–150 kHz (supraharmonics): Analytical framework," 2018 18th International Conference on Harmonics and Quality of Power (ICHQP), Ljubljana, 2018, pp. 1-7. doi: 10.1109/ICHQP.2018.8378859

D. Agudelo-Martínez and A. Pavas, "Measurement and simulation of power quality disturbances between 2–150 kHz from compact fluorescent lamps," 2018 18th International Conference on Harmonics and Quality of Power (ICHQP), Ljubljana, 2018, pp. 1-6. doi: 10.1109/ICHQP.2018.8378816

M. Limas, D. Agudelo-Martinez, J. B. Rodríguez and A. Pavas, "Conducted emission variations using low power LED lamps connected to other devices," 2018 18th International Conference on Harmonics and Quality of Power (ICHQP), Ljubljana, 2018, pp. 1-6. doi: 10.1109/ICHQP.2018.8378817

D. Agudelo-Martínez, F. Ríos and A. Pavas, "Interaction of some low power LED lamps within 2–150 kHz (supraharmonics)," 2018 18th International Conference on Harmonics and Quality of Power (ICHQP), Ljubljana, 2018, pp. 1-7. doi: 10.1109/ICHQP.2018.8378815

V. Khokhlov, J. Meyer, P. Schegner, D. AgudeloMartinez, A. Pavas: "Immunity assessment of household appliances in the frequency range from 2 to 150 kHz," 25th International Conference on Electricity Distribution, CIRED, Madrid, 2019. ISBN: 978-2-9602415-0-1

D. Agudelo-Martinez, A. Pavas, A. M. Blanco, R. Stiegler and J. Meyer, "Influence of Measurement Setup on the Emission of Devices in the Frequency Range 2-150 KHz," 2019 IEEE Milan PowerTech, Milan, Italy, 2019, pp. 1-6. doi: 10.1109/PTC.2019.8810991

6.6. Future work

In the case of the metrological thresholds proposed in this research, Author would like to test this methodology in the future with more devices in order to validate its usefulness and limitations. As suggested in current research works around the world, supraharmonic identification in single and simultaneous operation of devices should also be performed over other low voltage equipment commonly used in current and future distribution grid (Photovoltaic inverters, electric vehicle chargers, household appliances, etc). Finally, impedance showed to also be very influential on the behaviour of supraharmonic emissions. Authors strongly suggest to consider the impedance of equipment involved in the emissions assessment for future works.

The $TSH_{C;V}$ was an useful tool for the assessment of the surpaharmonic emissions in both single and simultaneous operation. The coherence function was also used in single operation assessment, and the hypothesis test in the simultaneous operation assessment. These analysis tools were useful for the assessment of supraharmonic emissions. However, because of the time-varying nature of supraharmonic emissions, the coherence function presented some limitations when emissions were grouped into the four frequency bands (2-8.9,9.1-29.9, 30.1-94.9, 95.1-150 kHz). In the case of simultaneous operation, the hypothesis test had also some limitations when narrow-band emissions were grouped into the same four frequency bands. Authors suggest that future work might be also focused on both grouping techniques in frequency domain as well as more indices for the supraharmonic range, in order to accurately assess the behaviour of supraharmonic emissions.

Last but most important, it is suggested that most of the future work in supraharmonic emissions should be oriented to show how these disturbances eventually could or could not represent a thread for the electromagnetic compatibility of the current and future distribution grid, considering a scenario with distributed generation, customer (auto) generation and communication between grid devices (smart grids). The knowledge about the interferences produced by supraharmonic emissions will be the main argument for determining their relevance in the current and future distribution grid.

Appendices

A. ADC Effective Resolution

The Signal-to-Noise ratio is related to the amount of ADC bits in the following way [1][2][3]:

$$SNR\,[dB] = 10log\left(\frac{Power_{signal}}{Power_{noise}}\right)$$

Assuming an impedance Z equals to 1Ω, the equation yields:

$$SNR\,[dB] = 10log\left(\frac{v^2_{RMS_{signal}}}{v^2_{RMS_{noise}}}\right)$$
$$SNR\,[dB] = 20log\left(\frac{v_{RMS_{signal}}}{v_{RMS_{noise}}}\right)$$

Theoretical resolution from ADC equals the lowest analogue value that ADC can successfully convert to a digital value. This value is also known as Less Significant Bit, LSB. It can be expressed as follows:

$$ADC_{resolution} = LSB = \frac{FS}{2^N} \tag{A-1}$$

. FS: Full Scale range

. N: ADC bits

The maximum error an ideal converter makes when digitalizing a signal is half of the resolution, i.e. $\pm\frac{LSB}{2}$. The quantization error can be approximated by an uncorrelated sawtooth waveform having a peak-to-peak value of $\approx LSB$.

$$FS = LSB * 2^N \tag{A-2}$$

This approximation is used to compute the RMS value of quantization error, or in other words, the RMS value for the minimum amplitude the ADC can successfully convert. Recall that the RMS value for sawtooth signal can be expressed as the amplitude divided $\sqrt{3}$. When an ac signal is processed with ADC, the Full Scale amplitude is reduced to the half of the corresponding DC Full Scale value. The equation for SNR in dB for AC signals, using

Equation A-2, is transformed as follows:

$$SNR\,[dB] = 20log\left(\frac{\frac{\left(\frac{FS}{2}\right)}{\sqrt{2}}}{\frac{\left(\frac{FS}{2^N}\right)}{\sqrt{3}}}\right) = 20log\left(\frac{\frac{\left(\frac{LSB*2^N}{2}\right)}{\sqrt{2}}}{\frac{\left(\frac{LSB}{2}\right)}{\sqrt{3}}}\right) = 20log\left(\frac{\frac{2^N}{\sqrt{2}}}{\frac{1}{\sqrt{3}}}\right) = 20log\left(\sqrt{\frac{3}{2}}2^N\right)$$

$$SNR\,[dB] = 20log\left(\sqrt{\frac{3}{2}}\right) + 20log\left(2^N\right) = 10log\left(\frac{3}{2}\right) + N20log\,(2)$$

$$SNR\,[dB] \approx 1.76 + 6.02N$$

Using a 16-bit ADC, the theoretical SNR is then:

$$SNR\,[dB] \approx 99dB$$

The SNR reported in reference manual is however different from the theoretical [4]. The Effective Number of Bits ENOB can be then computed as follows:

$$ENOB\,[bits] \approx \frac{SNR_{manual}\,[db] - 1.76}{6.02} \tag{A-3}$$

Different SNR values are reported in reference manual for different frequency ranges. Taking into account the lowest SNR (worst cases) for each frequency range, the following results are obtained for ENOBs of HSI-LV and HSI-HV DAQ modules:

$$ENOB_i\,[bits] \approx \begin{cases} 13 & \leq 10 \text{ kHz} \quad \text{(A-4a)} \\ 12 & 10 \text{ kHz} \leq 100 \text{ kHz} \quad \text{(A-4b)} \\ 10 & 100 \text{ kHz} \leq 1 \text{ MHz} \quad \text{(A-4c)} \end{cases}$$

$$ENOB_v\,[bits] \approx \begin{cases} 15 & \leq 10 \text{ kHz} \quad \text{(A-5a)} \\ 14 & 10 \text{ kHz} \leq 100 \text{ kHz} \quad \text{(A-5b)} \\ 13 & 100 \text{ kHz} \leq 1 \text{ MHz} \quad \text{(A-5c)} \end{cases}$$

Now the resolution can be recomputed using the Equation A-1:

$$ADC_{eff_{resolution}} = \frac{FS}{2^{ENOB}} \tag{A-6}$$

Finally, the corresponding effective resolution LSB_{eff} for current (HSI-LV and e.g a sensor current of sensitivity 0.1 V/A) and voltage (HSI-HV) modules are given by the following RMS values:

$$Res_i \approx \begin{cases} 24\mu A & \leq 10 \text{ kHz} \quad \text{(A-7a)} \\ 49\mu A & 10 \text{ kHz} \leq 100 \text{ kHz} \quad \text{(A-7b)} \\ 195\mu A & 100 \text{ kHz} \leq 1 \text{ MHz} \quad \text{(A-7c)} \end{cases}$$

$$Res_v \approx \begin{cases} 1.5mV & \leq 10 \text{ kHz} \quad \text{(A-8a)} \\ 3.1mV & 10 \text{ kHz} \leq 100 \text{ kHz} \quad \text{(A-8b)} \\ 6.1mV & 100 \text{ kHz} \leq 1 \text{ MHz} \quad \text{(A-8c)} \end{cases}$$

Equations A-4 to A-8 are used to limit the amount of decimal figures for the measurement results. After all, measurement values cannot have a better resolution (lower value) than that given by the ADC.

REFERENCES

[1] W. Kester, *Taking the Mystery out of the Infamous Formula, "SNR = 6.02N + 1.76dB," and Why You Should Care.* Analog Devices, Inc.

[2] W. Kester, *Understand SINAD, ENOB, SNR, THD, THD + N, and SFDR so You Don't Get Lost in the Noise Floor.* Analog Devices, Inc.

[3] S. Labs, *Improving ADC resolution by oversampling and averaging.* Silicon Laboratories, Inc.

[4] D. Inc, *DEWE-3040 Data Acquisition System, Owner's Guide.* Dewetron Inc.

B. Spectral Coherence function

Let be $x(t)$ current and $y(t)$ voltage signals in time domain. If the current $x(t)$ through a resistor produced a voltage drop $y(t)$, the energy dissipated in such resistance is given by [1][2][3][4]:

$$E = \int_{-\infty}^{\infty} x(t)y(t)dt \tag{B-1}$$

According to Parseval's theorem [5][6]:

$$\int_{-\infty}^{\infty} x(t)y(t)dt = \frac{1}{2\pi}\int_{-\infty}^{\infty} X(\omega)Y(-\omega)d\omega = \frac{1}{2\pi}\int_{-\infty}^{\infty} X(\omega)Y^*(\omega)d\omega \tag{B-2}$$

Let $x(t)$ and $y(t)$ be periodic signals. These signals have infinite energy and finite average power. Therefore, a truncated version of $x(t)$ and $y(t)$ are required for Fourier Transform existence [5][6][7]:

$$x_T(t) \quad , \quad y_T(t) = \begin{cases} x(t) & |t| \leq \mathrm{T} \\ 0 & |t| > \mathrm{T} \end{cases} \tag{B-3a}$$
(B-3b)

$$x(t) = \lim_{T\to\infty} x_T(t) \quad , \quad y(t) = \lim_{T\to\infty} y_T(t) \tag{B-4}$$

$$P_{avg} = \lim_{T\to\infty} \frac{1}{T}\int_{-T/2}^{T/2} x_T(t)y_T(t)dt = \lim_{T\to\infty} \frac{1}{2\pi}\int_{-\infty}^{\infty} X_T(\omega)Y_T^*(\omega)d\omega \tag{B-5}$$

In case $x_T(t)$ and $y_T(t)$ are measured over a 1 Ω resistance and using Parseval's theorem, the equation yields [5][6][7]:

$$P_{avg} = \lim_{T\to\infty} \frac{1}{T}\int_{-T/2}^{T/2} x_T^2(t)dt = \lim_{T\to\infty} \frac{1}{T}\frac{1}{2\pi}\int_{-\infty}^{\infty} X_T(\omega)X_T^*(\omega)d\omega$$
$$P_{avg} = \frac{1}{2\pi}\int_{-\infty}^{\infty} \lim_{T\to\infty} \frac{|X_T^2(\omega)|}{T}d\omega = \frac{1}{2\pi}\int_{-\infty}^{\infty} S_{xx}(\omega)(d\omega)$$

According to Wiener-Khinchin theorem, the Power Spectral Density is also the Fourier Transform of the autocorrelation function [5][6][7]:

$$S_{xx}(\omega) = \int_{-\infty}^{\infty} \left[\lim_{T\to\infty} \frac{1}{T} \int_{-T/2}^{T/2} x_T(t) x_T(t+\tau) dt \right] e^{-j\omega\tau} d\tau \tag{B-6}$$

$$S_{xx}(\omega) = \int_{-\infty}^{\infty} r_{xx} e^{-j\omega\tau} d\tau \tag{B-7}$$

S_{xx} represents the Power Spectral Density (PSD) of signal $x(t)$, in other words, the Fourier Transform of the autocorrelation of $x(t)$. The Cross-Power Spectral Density (CPSD) is deduced in the same way when $x(t) \neq y(t)$, that to say, S_{xy} is the Fourier Transform of the cross-correlation between $x(t)$ and $y(t)$:

$$S_{xy}(\omega) = \int_{-\infty}^{\infty} \left[\lim_{T\to\infty} \frac{1}{T} \int_{-T/2}^{T/2} x_T(t) y_T(t+\tau) dt \right] e^{-j\omega\tau} d\tau \tag{B-8}$$

$$S_{xy}(\omega) = \int_{-\infty}^{\infty} r_{xy} e^{-j\omega\tau} d\tau \tag{B-9}$$

For random signals, the Power Spectral Density is expressed as [6][7]:

$$S_{xx} = \lim_{T\to\infty} \frac{E\left[|X_T(\omega) X_T^*(\omega)|\right]}{T} \quad , \quad S_{xy} = \lim_{T\to\infty} \frac{E\left[|X_T(\omega) Y_T^*(\omega)|\right]}{T} \tag{B-10}$$

Where $E[\ \ ]$ is the expectation operator. Finally, the coherence function is defined as [3]:

$$C_{xy}^2(f) = \frac{|E[S_{xy}]|^2}{E[S_{xx}]E[S_{yy}]} \tag{B-11}$$

$$C_{xy}(f) = \frac{|E[S_{xy}]|}{\sqrt{E[S_{xx}]E[S_{yy}]}} = \frac{|\left(\frac{1}{N}\sum^n [X_n(f) Y_n^*(f)]\right)|}{\sqrt{\left(\frac{1}{N}\sum^n [X_n(f) X_n^*(f)]\right)\left(\frac{1}{N}\sum^n [Y_n(f) Y_n^*(f)]\right)}}$$

REFERENCES

[1] P. Stoica, *Spectral Analysis of Signals*. Prentice Hall, 2005.

[2] M. A. Kramer, *An Introduction to Field Analysis Techniques: The Power Spectrum and Coherence*. Boston University, 1 ed., 2013.

[3] S. Malekpour, J. A. Gubner, and W. A. Sethares, "Measures of generalized magnitude-squared coherence: Differences and similarities," *Journal of the Franklin Institute*, vol. 355, no. 5, p. 2932–2950, 2018.

[4] J. C. Shaw, "An introduction to the coherence function and its use in eeg signal analysis.," *Journal of medical engineering & technology*, vol. 5, pp. 279–88, Nov 1981.

[5] A. V. Oppenheim, R. W. Schafer, and J. R. Buck, *Discrete-Time Signal Processing (2nd Edition) (Prentice-hall Signal Processing Series)*. Prentice Hall, 1999.

[6] M. Corinthios, *Signals, Systems, Transforms, and Digital Signal Processing with MATLAB*. CRC Press, 2009.

[7] National Semiconductor, *Power Spectra Estimation*, November 1980.

C. Emissions in Single Operation

The following tables show numerical results from experiments carried out in Chapter 4: Emissions in single operation. Table **4-2** summarizes these experiments, rewritten here for visualization purposes.

Table C-1.: Variations of experimental setup base case.

Experiment	Description	
	Voltage source	Network impedance
1	Sinusoidal	-
2		LISN (Z2)
3		Measured (Z3)
4	Distorted	-
5		LISN (Z2)
6		Measured (Z3)
7	Grid	

Tables **C-2** to **C-7** and **4-5** to **4-6** show numerical results for $THS_{C;V}$ index. This index was computed from emissions magnitude between 2-150 kHz after applying metrological threshold deduced in Chapter 3. All uncertainties were less than measured value. Because of figures rounding process, however, some of them increased.

Note: Green color: originated inside the EUT (primary emissions); yellow color: originated outside the EUT (secondary emissions); bold: combination of primary and secondary emissions.

Table C-2.: Supraharmonic current from LED lamps with no PFC (first group)

Total Supraharmonic Current [mA]												
EXPERIMENT	no PFC											
	n003				n005				n039			
	2.1-8.9	9.1-29.9	30.1-94.9	95.1-149.9	2.1-8.9	9.1-29.9	30.1-94.9	95.1-149.9	2.1-8.9	9.1-29.9	30.1-94.9	95.1-149.9
1	5.9± 0.1	0.0	0.0	0.0	1.3± 0.1	0.0	0.0	0.0	5.2± 0.1	0.0	0.0	0.0
2	4.6± 0.1	0.0	0.0	0.0	1.2± 0.1	0.0	0.0	0.0	3.9± 0.1	0.0	0.0	0.0
3	5.7± 0.1	0.0	0.0	0.0	1.3± 0.1	0.0	0.0	0.0	4.9± 0.1	0.0	0.0	0.0
4	5.8± 0.1	11.3± 0.1	0.0	0.0	1.3± 0.1	11.0± 0.1	0.0	0.0	5.1± 0.1	1.5± 0.1	0.0	0.0
5	4.6± 0.1	4.5± 0.1	0.0	0.0	1.2± 0.1	4.2± 0.1	0.1± 0.1	0.0	3.9± 0.1	0.5± 0.1	0.0	0.0
6	5.7± 0.1	2.9± 0.1	0.0	0.0	1.3± 0.1	2.8± 0.1	0.0	0.0	4.9± 0.1	0.4± 0.1	0.0	0.0
7	**4.8**± 0.1	0.0	0.0	0.0	**1.7**± 0.1	0.1	0.0	0.0	**5.5**± 0.1	0.0	0.0	0.0

Table C-3.: Supraharmonic voltage from LED lamps with no PFC

Total Supraharmonic Voltage [V]												
EXPERIMENT	no PFC											
	n003				n005				n039			
	2.1-8.9	9.1-29.9	30.1-94.9	95.1-149.9	2.1-8.9	9.1-29.9	30.1-94.9	95.1-149.9	2.1-8.9	9.1-29.9	30.1-94.9	95.1-149.9
1	0.00	0.00	0.00	0.00	0.00	0.00	0.00	0.00	0.00	0.00	0.00	0.00
2	0.05±0.03	0.00	0.00	0.00	0.00	0.00	0.00	0.00	0.04±0.03	0.00	0.00	0.00
3	0.00	0.00	0.00	0.00	0.00	0.00	0.00	0.00	0.00	0.00	0.00	0.00
4	0.00	1.00±0.01	0.00	0.00	0.00	1.00±0.02	0.00	0.00	0.00	0.97±0.02	0.00	0.00
5	0.05±0.03	0.41±0.01	0.00	0.00	0.00	0.39±0.01	0.00	0.00	0.04±0.03	0.36±0.01	0.00	0.00
6	0.00	0.26±0.01	0.00	0.00	0.00	0.26±0.01	0.00	0.00	0.00	0.26±0.01	0.00	0.00
7	**0.07**±0.04	0.01±0.01	0.01±0.01	0.00	**0.06**	0.01±0.01	0.02±0.01	0.00	**0.12**±0.03	0.01±0.01	0.00	0.00

Table C-4.: Supraharmonic current from LED lamps with capacitive topology

EXPERIMENT	Total Supraharmonic Current [mA]											
	capacitive											
	c022				c026				c027			
	2.1-8.9	9.1-29.9	30.1-94.9	95.1-149.9	2.1-8.9	9.1-29.9	30.1-94.9	95.1-149.9	2.1-8.9	9.1-29.9	30.1-94.9	95.1-149.9
1	0.8±0.1	0.0	0.0	0.0	1.8±0.1	0.0	0.0	0.0	1.8±0.1	0.0	0.0	0.0
2	0.8±0.1	0.0	0.0	0.0	1.8±0.1	0.0	0.0	0.0	1.8±0.1	0.0	0.0	0.0
3	0.8±0.1	0.0	0.0	0.0	1.8±0.1	0.0	0.0	0.0	1.8±0.1	0.0	0.0	0.0
4	0.8±0.1	3.6±0.1	0.0	0.0	1.7±0.1	15.8±0.1	1.6±0.1	0.0	1.7±0.1	15.8±0.1	1.6±0.1	0.0
5	0.8±0.1	1.2±0.1	0.0	0.0	1.8±0.1	5.1±0.1	0.2±0.1	0.0	1.8±0.1	5.1±0.1	0.2±0.1	0.0
6	0.8±0.1	0.9±0.1	0.0	0.0	1,8±0.1	4.2±0.1	0.0	0.0	1.8±0.1	4.2±0.1	0.0	0.0
7	**1.0**±0.1	0.0	0.0	0.0	**1.6**±0.1	0.2±0.1	0.0	0.0	**1.7**±0.1	0.3±0.1	0.0	0.0

Table C-5.: Supraharmonic voltage from LED lamps with capacitive topology

EXPERIMENT	Total Supraharmonic Voltage [V]											
	capacitive											
	c022				c026				c027			
	2.1-8.9	9.1-29.9	30.1-94.9	95.1-149.9	2.1-8.9	9.1-29.9	30.1-94.9	95.1-149.9	2.1-8.9	9.1-29.9	30.1-94.9	95.1-149.9
1	0.00	0.00	0.00	0.00	0.00	0.00	0.00	0.00	0.00	0.00	0.00	0.00
2	0.00	0.00	0.00	0.00	0.00	0.00	0.00	0.00	0.00	0.00	0.00	0.00
3	0.00	0.00	0.00	0.00	0.00	0.00	0.00	0.00	0.00	0.00	0.00	0.00
4	0.00	0.98±0.02	0.00	0.00	0.00	0.99±0.01	0.00	0.00	0.00	0.99±0.01	0.00	0.00
5	0.00	0.36±0.01	0.00	0.00	0.00	0.34±0.01	0.00	0.00	0.00	0.34±0.01	0.00	0.00
6	0.00	0.26±0.01	0.00	0.00	0.00	0.25±0.01	0.00	0.00	0.00	0.25±0.01	0.00	0.00
7	**0.07**±0.03	0.01±0.03	0.00	0.00	**0.12**±0.08	0.01±0.03	0.00	0.00	**0.07**±0.05	0.01±0.01	0.00	0.00

Table C-6.: Supraharmonic current from LED lamps with passive PFC

Total Supraharmonic Current [mA]												
EXPERIMENT	passive PFC											
	p058				p059				p061			
	2.1-8.9	9.1-29.9	30.1-94.9	95.1-149.9	2.1-8.9	9.1-29.9	30.1-94.9	95.1-149.9	2.1-8.9	9.1-29.9	30.1-94.9	95.1-149.9
1	2.2±0.1	0.0	0.0	0.0	2.3±0.1	0.0	0.0	0.0	2.5±0.1	0.0	0.0	0.0
2	1.7±0.1	0.0	0.0	0.0	1.8±0.1	0.0	0.0	0.0	1.9±0.1	0.0	0.0	0.0
3	2.1±0.1	0.0	0.0	0.0	2.3±0.1	0.0	0.0	0.0	2.4±0.1	0.0	0.0	0.0
4	2.0±0.1	17.7±0.1	0.0	0.0	2.1±0.1	17.6±0.1	0.0	0.0	2.2±0.1	15.8±0.1	0.0	0.0
5	1.7±0.1	6.1±0.1	0.0	0.0	1.8±0.1	6.1±0.1	0.0	0.0	1.9±0.1	4.9±0.1	0.0	0.0
6	2.1±0.1	4.5±0.1	0.0	0.0	2.2±0.1	4.4±0.1	0.0	0.0	2.4±0.1	4.0±0.1	0.0	0.0
7	**2.3**±0.1	0.0	1.6±0.1	0.0	**2.1**±0.1	0.3±0.1	0.0	0.0	**2.1**±0.1	0.0	0.0	0.0

Table C-7.: Supraharmonic voltage from LED lamps with passive PFC

Total Supraharmonic Voltage [V]												
EXPERIMENT	passive PFC											
	p058				p059				p061			
	2.1-8.9	9.1-29.9	30.1-94.9	95.1-149.9	2.1-8.9	9.1-29.9	30.1-94.9	95.1-149.9	2.1-8.9	9.1-29.9	30.1-94.9	95.1-149.9
1	0.00	0.00	0.00	0.00	0.00	0.00	0.00	0.00	0.00	0.00	0.00	0.00
2	0.01±0.01	0.00	0.00	0.00	0.02±0.01	0.00	0.00	0.00	0.02±0.01	0.00	0.00	0.00
3	0.00	0.00	0.00	0.00	0.00	0.00	0.00	0.00	0.00	0.00	0.00	0.00
4	0.00	1.00±0.03	0.00	0.00	0.00	1.00±0.03	0.00	0.00	0.00	0.98±0.03	0.00	0.00
5	0.01±0.01	0.36±0.01	0.00	0.00	0.01±0.01	0.37±0.01	0.00	0.00	0.02±0.01	0.34±0.01	0.00	0.00
6	0.00	0.26±0.01	0.00	0.00	0.00	0.26±0.01	0.00	0.00	0.00	0.26±0.01	0.00	0.00
7	**0.15**±0.07	0.01±0.03	0.07±0.03	0.00	**0.07**±0.03	0.02±0.01	0.00	0.00	**0.09**±0.03	0.01±0.01	0.00	0.00

Tables **C-8** to **C-13** and **4-7** to **4-8** show numerical results for $C_{xy|_{band}}$ index explained in Equation 4-10. This index was computed from the spectral coherence of emissions magnitude between 2-150 kHz after applying metrological threshold deduced in Chapter 3.

Note: Blue color: coherence is different from zero between selected signals.

Table C-8.: Supraharmonic current coherence from LED lamps with no PFC(first group)

Total Supraharmonic Current [mA]												
COMPARISON	no PFC											
	n003				n005				n039			
	2.1-8.9	9.1-29.9	30.1-94.9	95.1-149.9	2.1-8.9	9.1-29.9	30.1-94.9	95.1-149.9	2.1-8.9	9.1-29.9	30.1-94.9	95.1-149.9
1-2	0.9	0.0	0.0	0.0	1.0	0.0	0.0	0.00	0.9	0.0	0.0	0.00
1-3	1.0	0.0	0.0	0.0	1.0	0.0	0.0	0.0	1.0	0.0	0.0	0.0
1-7	0.8	0.0	0.0	0.0	0.9	0.0	0.0	0.0	1.0	0.0	0.0	0.0
4-5	0.9	0.8	0.0	0.0	1.0	0.7	0.0	0.0	0.9	1.0	0.0	0.0
4-6	1.0	0.4	0.0	0.0	1.0	0.5	0.0	0.0	1.0	1.0	0.0	0.0

Table C-9.: Supraharmonic voltage coherence from LED lamps with no PFC (first group)

Total Supraharmonic Voltage [V]												
COMPARISON	no PFC											
	n003				n005				n039			
	2.1-8.9	9.1-29.9	30.1-94.9	95.1-149.9	2.1-8.9	9.1-29.9	30.1-94.9	95.1-149.9	2.1-8.9	9.1-29.9	30.1-94.9	95.1-149.9
1-2	0.0	0.0	0.0	0.0	0.0	0.0	0.0	0.0	0.0	0.0	0.0	0.0
1-3	0.0	0.0	0.0	0.0	0.0	0.0	0.0	0.0	0.0	0.0	0.0	0.0
1-7	0.0	0.0	0.0	0.0	0.0	0.0	0.0	0.0	0.0	0.0	0.0	0.0
4-5	0.0	1.0	0.0	0.0	0.0	1.0	0.0	0.0	0.0	1.0	0.0	0.0
4-6	0.0	1.0	0.0	0.0	0.0	1.0	0.0	0.0	0.0	1.0	0.0	0.0

Table C-10.: Supraharmonic current coherence from LED lamps with capacitive topology

Total Supraharmonic Current [mA]												
COMPARISON	capacitive											
	c022				c026				c027			
	2.1-8.9	9.1-29.9	30.1-94.9	95.1-149.9	2.1-8.9	9.1-29.9	30.1-94.9	95.1-149.9	2.1-8.9	9.1-29.9	30.1-94.9	95.1-149.9
1-2	0.9	0.0	0.0	0.0	0.7	0.0	0.0	0.00	0.7	0.0	0.0	0.00
1-3	0.9	0.0	0.0	0.0	0.7	0.0	0.0	0.00	0.7	0.00	0.0	0.0
1-7	0.8	0.0	0.0	0.0	0.7	0.0	0.0	0.0	0.6	0.0	0.0	0.0
4-5	1.0	0.6	0.0	0.0	0.8	0.6	0.5	0.0	0.8	0.5	0.6	0.00
4-6	1.0	0.6	0.0	0.0	0.7	0.6	0.0	0.0	0.7	0.6	0.0	0.0

Table C-11.: Supraharmonic voltage coherence from LED lamps with capacitive topology

Total Supraharmonic Voltage [V]												
COMPARISON	capacitive											
	c022				c026				c027			
	2.1-8.9	9.1-29.9	30.1-94.9	95.1-149.9	2.1-8.9	9.1-29.9	30.1-94.9	95.1-149.9	2.1-8.9	9.1-29.9	30.1-94.9	95.1-149.9
1-2	0.0	0.0	0.0	0.0	0.0	0.0	0.0	0.0	0.0	0.0	0.0	0.0
1-3	0.0	0.0	0.0	0.0	0.0	0.0	0.0	0.0	0.0	0.0	0.0	0.0
1-7	0.0	0.0	0.0	0.0	0.0	0.0	0.0	0.0	0.0	0.0	0.0	0.0
4-5	0.0	1.0	0.0	0.0	0.0	1.0	0.0	0.0	0.0	1.0	0.0	0.0
4-6	0.0	1.0	0.0	0.0	0.0	1.0	0.0	0.0	0.0	1.0	0.0	0.0

Table C-12.: Supraharmonic current coherence from LED lamps with passive PFC topology

Total Supraharmonic Current [mA]												
COMPARISON	passive PFC											
	p058				p059				p061			
	2.1-8.9	9.1-29.9	30.1-94.9	95.1-149.9	2.1-8.9	9.1-29.9	30.1-94.9	95.1-149.9	2.1-8.9	9.1-29.9	30.1-94.9	95.1-149.9
1-2	0.8	0.0	0.0	0.0	0.8	0.0	0.0	0.00	0.9	0.0	0.0	0.00
1-3	0.9	0.0	0.0	0.0	0.9	0.0	0.0	0.0	1.0	0.0	0.0	0.0
1-7	0.9	0.0	0.0	0.0	0.8	0.0	0.0	0.0	0.8	0.0	0.0	0.0
4-5	0.9	0.7	0.0	0.0	0.9	0.7	0.0	0.0	0.9	0.7	0.0	0.0
4-6	1.0	0.6	0.0	0.0	1.0	0.6	0.0	0.0	1.0	0.6	0.0	0.0

Table C-13.: Supraharmonic voltage coherence from LED lamps with passive PFC topology

Total Supraharmonic Voltage [V]												
COMPARISON	passive PFC											
	p058				p059				p061			
	2.1-8.9	9.1-29.9	30.1-94.9	95.1-149.9	2.1-8.9	9.1-29.9	30.1-94.9	95.1-149.9	2.1-8.9	9.1-29.9	30.1-94.9	95.1-149.9
1-2	0.0	0.0	0.0	0.0	0.0	0.0	0.0	0.0	0.0	0.0	0.0	0.0
1-3	0.0	0.0	0.0	0.0	0.0	0.0	0.0	0.0	0.0	0.0	0.0	0.0
1-7	0.0	0.0	0.0	0.0	0.0	0.0	0.0	0.0	0.0	0.0	0.0	0.0
4-5	0.0	1.0	0.0	0.0	0.0	1.0	0.0	0.0	0.0	1.0	0.0	0.0
4-6	0.0	1.0	0.0	0.0	0.0	1.0	0.0	0.0	0.0	1.0	0.0	0.0